arXiv:hep-ph/0112211 v1 14 Dec 2001

Coherent $\gamma\gamma$ and γA interactions in very peripheral collisions at relativistic ion colliders.

Gerhard Baur [a] Kai Hencken [b] Dirk Trautmann [b]
Serguei Sadovsky [c] Yuri Kharlov [c]

[a] *Forschungszentrum Jülich, Jülich, Germany*
[b] *Universität Basel, Basel, Switzerland*
[c] *IHEP, Protvino, Russia*

Abstract

Due to coherence, there are strong electromagnetic fields of short duration in very peripheral collisions. They give rise to photon-photon and photon-nucleus collisions with a high flux up to an invariant mass region hitherto unexplored experimentally. After a general survey of the field equivalent photon numbers and photon-photon luminosities, especially for relativistic heavy ion collisions, are discussed. Special care needs to be taken to include the effects of the strong interaction and nuclear size in this case. Photon-photon and photon-hadron physics at various invariant mass scales are then discussed. The maximum equivalent photon energy in the lab-system (collider frame) are typically of the order of 3 GeV for RHIC and 100 GeV for LHC. Diffractive processes are an important background process. Lepton-pair, especially electron-positron pair production is copious. Due to the strong fields there will be new phenomena, like multiple e^+e^- pair production. The experimental techniques to select $\gamma\gamma$-processes are finally discussed together with important background processes.

Key words: photon-photon processes, photon-hadron processes, relativistic heavy ion collisions.

Contents

1 Introduction and Purpose 4

1.1 A Short History of Very Peripheral Collisions 8

2 From Impact-Parameter Dependent Equivalent Photon Spectra to $\gamma\gamma$-Luminosities 11

2.1 Equivalent Photon Numbers 12

2.2 The Quantum Mechanical Plane Wave Formalism 15

2.3 Elastic Photon Emission 17

2.4 Inelastic Form Factors 19

2.5 Integrated Photon-Photon Luminosity 21

2.6 Semiclassical Impact Parameter Description 22

2.7 Effects of Strongly Interacting Particles 23

2.8 Effective $\gamma\gamma$-Luminosities and Perspectives for RHIC and LHC 27

3 $\gamma\gamma$ Physics at Hadron Colliders, General Considerations 29

3.1 The Photon at High Energy 30

3.2 Total $\gamma\gamma$ Cross Section 32

3.3 Charged Fermion Pair Production 33

3.4 W^+W^--Pair Production 35

3.5 Vector Meson Pair Production 37

3.6 Resonance Production 37

3.7 Exotic Mesons 42

4 Two-Photon Collisions as a Tool for the Search of New Physics 45

4.1 Supersymmetry Particle Pair Production 46

4.2 Higgs Search 48

4.3 Search for Extra Dimensions 49

4.4 Search for Heavy Point-like Dirac Monopoles 50

4.5 Tightly Bound States 50

5 Photon-Nucleus and Photon-Hadron Interactions 52

5.1 Photonuclear Processes: Giant Dipole Excitation, Beam Loss and Luminosity Monitor 52

5.2 Excitation of Nucleon Resonances 57

5.3 Photonuclear Reactions to the Continuum above the Nucleon Resonances 57

5.4 Coherent Vector Meson Production in Photon Diffraction 58

5.5 Incoherent Production of Vector Mesons 62

5.6 Photon-Gluon Fusion and the Gluon Structure Function in a Nuclear Environment 64

6 Diffractive Processes 66

7 Special Aspects of Dilepton Pair Production 72

7.1 Strong Field Effects in Electron Pair Production: Multiple Pair Production 73

7.2 Strong Field Effects in Electron Pair Production: Coulomb Corrections 78

7.3 Electromagnetic Production of Electron Pairs and Other Particles in Central Collisions 83

7.4 Electrons and Muons as Equivalent Particles, Equivalent Electron (Muon) Approximation 83

7.5 Radiation from e^+e^--Pairs 86

7.6 Bound-free Pair Production 88

7.7 Formation of Dilepton Bound States: Positronium and Muonium 93

8 Methods of Detecting Very Peripheral Collisions in Experiments at Heavy Ion Colliders 95

8.1 Signatures of $\gamma\gamma$-Processes in Heavy Ion Collisions 95

8.2 Background Processes 97

8.3 Detection of Some $\gamma\gamma$-Processes 103

8.4 Perspectives of ion experiments 108

9 Conclusion 109

9.1 Acknowledgments 110

References 111

1 Introduction and Purpose

With the first collisions at the relativistic heavy ion collider RHIC at Brookhaven (BNL) in June 2000 heavy ion physics has entered a new stage. The interaction of nuclei at such high energies has only been observed up to now in cosmic ray interactions. Many interesting physics topics can now be studied in the laboratory. The main aim is to study the violent central collisions. One is looking for the formation and the signature of a new state of hadronic matter, the Quark Gluon Plasma. The present status of this field is exposed in the Proceedings of Quark Matter QM2001 [1].

Relativistic heavy ions are also very important tools for other physics investigations. We mention here projects (sometimes referred to as *"non-QGP" physics*, a term which we will avoid in the following) like the search for new physics at very high rapidities in the CASTOR subproject at ALICE. This project is related to cosmic ray physics and searches for the so called Centauro events at the LHC [2]. Other "exotic" physics topics like the possible occurrence of CP violation or "disoriented chiral condensates" (DCC), see [3,4], have also been investigated in the past.

It is the purpose of this Report to review the physics of very peripheral [1] collisions. We put the main emphasis on the energy regions of the colliders RHIC (Relativistic Heavy Ion Collider) at Brookhaven and the forthcoming LHC (Large Hadron Collider) at CERN/Geneva. Due to the coherent action of all the protons in the nucleus, the electromagnetic field surrounding the ions is very strong. It acts for a very short time. According to Fermi [5] "*this time-dependent electromagnetic field can be replaced by the field of radiation with a corresponding frequency distribution*", see also Fig. 1. He called this "äquivalente Strahlung". The spectrum of these photons can be calculated from the kinematics of the process. The "equivalent photon method" (EPA) is often called also the "Weizsäcker-Williams method". For a more popular introduction see, e.g., [6], and also the corresponding remarks in [7].

A very useful view on the electromagnetic processes is the parton picture with the photons seen as the partons. We give the basic argument here in the introduction, a detailed explanation will then follow in Chap. 2. In this picture the scattering is described as an incoherent superposition of the scattering of the various constituents. For example, nuclei consist of nucleons which in turn consist of quarks and gluons, photons consist of lepton pairs, electrons consist

[1] In the following we will always use "very peripheral" to denote the distant collisions with $b > R_1 + R_2$ we are interested in. Here b denotes the impact parameter and R_1 and R_2 are the radii of the two nuclei. The term "ultraperipheral" collisions is also sometimes used for them. This is an attempt to distinguish it clearly from what is sometimes called "peripheral collisions", where $b \approx R_1 + R_2$.

of photons, etc.. Relativistic nuclei have photons as an important constituent, especially for low virtuality and a low ratio of the photon energy compared to the one of the ion (see below for quantitative arguments). This is due to the coherent action of all the charges in the nucleus: for these conditions the wavelength of the photon is larger than the size of the nucleus, therefore it does not resolve the individual nucleons but sees the coherent action of them. This has some similarity to the "low-x physics" and the Weizsäcker-Williams approach of [8] to gluons in the initial state of heavy ion collisions.

The coherence condition limits the virtuality $Q^2 = -q^2$ of the photon to very low values

$$Q^2 \lesssim 1/R^2, \tag{1}$$

where the radius of a nucleus is approximately $R = 1.2$ fm $A^{1/3}$ with A the nucleon number. This is due to the rapid decrease of the nuclear electromagnetic form factor for high Q^2 values. For most purposes these photons can therefore be considered as real ("quasireal"). From the kinematics of the process one has a photon four-momentum of $q^\mu = (\omega, \vec{q}_\perp, q_3 = \omega/v)$, where ω and $q_\perp$ are energy and transverse momentum of the quasireal photon in a given frame, where the projectile moves with velocity v. This leads to an invariant four-momentum transfer of

$$Q^2 = \frac{\omega^2}{\gamma^2} + q_\perp^2, \tag{2}$$

where the Lorentz factor is $\gamma = E/m = 1/\sqrt{1-v^2}$. The condition Eq. (1) limits the maximum energy of the quasireal photon to

$$\omega < \omega_{max} \approx \frac{\gamma}{R}, \tag{3}$$

and the perpendicular component of its momentum to

$$q_\perp \lesssim \frac{1}{R}. \tag{4}$$

At LHC energies this means a maximum photon energy of about 100 GeV in the laboratory system, at RHIC this number is about 3 GeV. We define the ratio $x = \omega/E$, where E denotes the energy of the nucleus $E = M_N \gamma A$ and M_N is the nucleon mass. It is therefore smaller than

$$x < x_{max} = \frac{1}{R M_N A} = \frac{\lambda_C(A)}{R}, \tag{5}$$

where $\lambda_C(A)$ is the Compton wavelength of the ion. x_{max} is 4×10^{-3}, 3×10^{-4}, 1.4×10^{-4} for O, Sn, Pb ions, respectively. Here and also throughout the rest of the paper we use natural units, i.e., $\hbar = c = 1$.

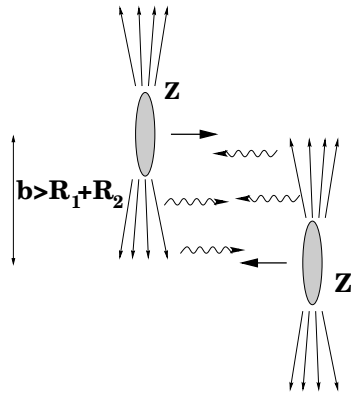

Fig. 1. A fast moving nucleus with charge Ze is surrounded by a strong electromagnetic field. This can be viewed as a cloud of virtual photons. These photons can often be considered as real. They are called "*equivalent*" or "*quasireal photons*". In the collision of two ions these quasireal photons can collide with each other and with the other nucleus. For very peripheral collisions with impact parameters $b > 2R$, this is useful for photon-photon as well as photon-nucleus collisions.

The collisions of e^+ and e^- has been the traditional way to study $\gamma\gamma$ collisions. Similarly photon-photon collisions can also be observed in hadron-hadron collisions, see Fig. 1. Since the photon number scales with Z^2 (Z being the charge number of the nucleus) such effects can be particularly large. This factor of $\gtrsim 6000$ (corresponding to Au, $Z = 79$) is the reason why the name "gold flashlight" [9] has been used to describe very peripheral (AuAu) collisions at RHIC.

Similarly the strong electromagnetic field can be used as a source of photons to induce electromagnetic reactions in the second ion, see Fig. 1. Since the ion, which is hit by these photons, is moving in the collider frame the photon-hadron invariant masses can become very high. In the rest frame of one of the ions (sometimes called the "target frame") the Lorentz factor of the other ion is given by $\gamma_{ion} = 2\gamma_{lab}^2 - 1$, where γ_{lab} is the Lorentz factor in the collider (cm) frame. The maximum photon energy in this frame is 500 TeV for the LHC and 600 GeV for RHIC.

This high equivalent photon flux has already found many useful applications in nuclear physics [10], nuclear astrophysics [11,12], particle physics [13] (sometimes called the "Primakoff effect"), as well as, atomic physics [14]. Previous reviews of the present topic can be found in [15–18].

The theoretical tool to analyze very peripheral collisions is the equivalent photon method. This method is described in Chap. 2. The equivalent photon

method is often used for high energy reactions, e.g., in the description of e^+e^- and ep collisions. We put most emphasis here on the peculiarities which arise due to the finite size and the strong interactions of the ions. These equivalent photons can collide with the other nucleus and with each other. This leads to the possibility of doing photon-hadron and photon-photon physics at relativistic heavy ion accelerators, with high fluxes of equivalent photons in hitherto inaccessible invariant mass regions.

Thus there will be new possibilities to study photon-hadron interactions at RHIC and LHC. It extends the γp interaction studies at HERA/DESY to γA interactions. The photon-hadron invariant mass range at RHIC will be somewhat below the one at HERA, whereas at LHC one will reach higher invariant masses than those possible at HERA. As was mentioned above, these photons can be regarded as quasireal and the freedom to vary the four-momentum transfer Q^2 is not given in the heavy ion case. According to [19,20] relativistic heavy ion colliders can be regarded as *"vector meson factories"*. This is discussed in detail in chapter 5.

This vector meson production is essentially a diffraction process: the (equivalent) photon emitted by one of the nuclei is diffractively excited to a vector meson on the other nucleus. This can be viewed as a photon-Pomeron interaction. In addition there are also Pomeron-Pomeron processes, which are interesting processes of their own [21]. Their importance as a possible background will be studied in chapter 6.

The physics potential of photon-photon collisions is discussed in chapters 3 and 4. These chapters extend our previous studies for the CMS Heavy Ion Programme [22,23], see also [24]. It ranges from studies in QCD (Chap. 3) like meson production and the total $\gamma\gamma \to$ hadron cross section to the search for new particles (Chap. 4) like a light Higgs particle.

Chapter 7 is devoted to lepton pair production. Due to their low mass especially the electrons have a special status and EPA is not always a good approximation. Effects of the strong fields manifest themselves essentially in multiple e^+e^- pair production. Besides the free pair production we also discuss some important related processes like bremsstrahlung from these leptons, the production of muons with a large transverse momenta and bound-free pair production.

Central collision events are characterized by a very high multiplicity. Therefore all major heavy ion detectors are tuned to deal with the large amount of data in this case. On the other hand, the multiplicity in very peripheral collisions is comparatively low (therefore the name *"silent collisions"* has been coined for them). The ions do not interact strongly with each other and move on essentially undisturbed in the beam direction. The only possible interactions

are due to the long range electromagnetic interaction and diffractive processes. Still some of these "silent events" are not so silent, e.g., quite a few particles will be produced in a 100 GeV on 100 GeV $\gamma\gamma$-interaction leading to a final hadron state. The background coming from especially grazing collisions needs to be taken into account. Also a way to trigger on very peripheral collisions is needed. This will be discussed in chap. 8.

1.1 A Short History of Very Peripheral Collisions

Relativistic heavy ion collisions have been suggested as a general tool for two-photon physics about twelve years ago and the field has grown rapidly since. Yet the study of a special case, the production of e^+e^- pairs in nucleus-nucleus collisions, goes back to Landau and Lifschitz in 1934 [25] and to Racah in 1937 [26]. In those days one thought more about high energy cosmic ray nuclei than about relativistic heavy ion colliders. The general possibilities and characteristic features of two-photon physics in relativistic heavy ion collisions have been discussed in [27]. The possibility to produce a Higgs boson via $\gamma\gamma$ fusion was suggested in [28,29]. In these papers the effect of strong absorption in heavy ion collisions was not taken into account. Absorption is a feature, which is quite different from the two-photon physics at e^+e^- colliders. The problem of taking strong interactions into account was solved by using impact parameter space methods in [30–32]. Thus the calculation of $\gamma\gamma$ luminosities in heavy ion collisions was put on a firm basis and rather definite conclusions were reached by many groups working in the field, as described, e.g., in [16,15]. This opens the way for many interesting applications.

Up to now hadron-hadron collisions have rarely been used for two-photon physics. The work of Vannucci et al. [33] in 1980 may be regarded as its beginning, see Fig. 2. In this work, the production of $\mu^+\mu^-$ pairs was studied at the ISR. The special class of events was selected, where no hadrons are seen associated with the muon pair in a large solid angle vertex detector. In this way one makes sure that the hadrons do not interact strongly with each other, i.e., one is dealing with very peripheral collisions; the photon-photon collisions manifest themselves as "silent events", that is, with only a relatively small multiplicity. It seems interesting to quote from Vannucci [33]: *"The topology of these events, their low transverse momentum, and the magnitude of the cross section can be most naturally be interpreted by the $\gamma\gamma$ process. This effect, which is still a small background at the ISR compared with the Drell-Yan mechanism, grows with energy and could trigger enough interest to be studied for itself, possibly at the* $\mathrm{p\bar{p}}$ *collider, probably at the ISABELLE machine."* Although ISABELLE has never been built, we have now the Relativistic Heavy Ion Collider (RHIC) in this ring, where $\gamma\gamma$ processes will be studied with the "gold flashlight" in this way. Another example is the search for a magnetic

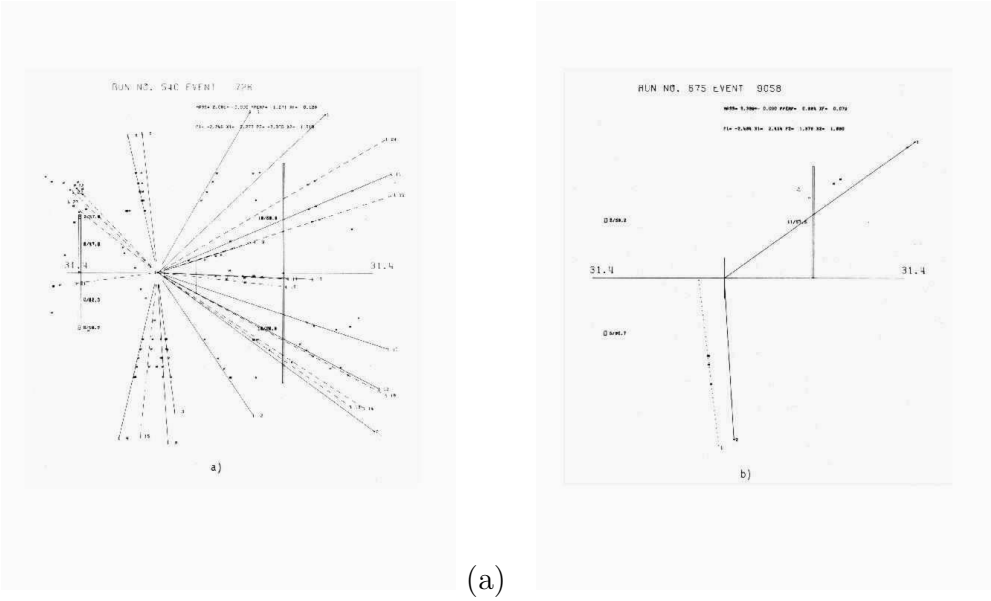

(a) (b)

Fig. 2. The production of a muon pair at the ISR with (a) and without the production of hadrons (b) is shown. Typical characteristics of very peripheral collisions are seen: low particle multiplicity and a small sum of transverse momenta. Reproduced from Fig. 2, p. 244 of [33] with kind permission of Springer-Verlag and the author.

monopole in photon-photon elastic scattering in $p\bar{p}$ collisions at the Tevatron following the idea in [34]. This is discussed in chapter 4. Dimuons with a very low sum of transverse momenta (i.e., coming from $\gamma\gamma$-interactions) are also considered as a luminosity monitor for the ATLAS detector at LHC [35]. A more recent discussion can also be found in [36].

The physics potential of relativistic heavy ion collisions for photon-hadron studies was gradually realized during the last decade. Nuclear collisions without nuclear contact have been used very successfully over the past 50 years to study nuclear structure, especially low lying collective excitations. Coulomb excitation, mainly at energies below the Coulomb barrier has been reviewed by Alder et al. [37–39]. The theory of relativistic electromagnetic excitation was given by Winther and Alder in [40]. This seminal paper started a whole new era of investigations. It was recognized for some time that the cross section for the excitation of the giant dipole resonance is huge. This is the reason why also new phenomena like the double giant dipole resonance excitation could be studied by electromagnetic excitation. The excitation of the giant dipole resonance is also an important loss process in the relativistic colliders, as the giant dipole resonance decays predominantly by neutron emission. The decay neutrons are also a useful tool to measure the collider luminosity.

In addition it was recognized in [41] that there is a sizeable cross section for photon-nucleus interactions beyond 1 GeV. Thus a field of studies similar to the one at HERA will be opened. However, as mentioned already above, in the heavy ion case the photon is restricted to be quasireal, and the study of

interactions of virtual photons with high Q^2 with hadrons is not possible. On the other hand, the photon-nucleus interaction (rather than the photon-proton interaction) can be studied with RHIC and LHC. This is described in [19,20]. Since the vector meson production cross section is very big — of the order of the geometric cross section — relativistic heavy ion colliders may justly be called "vector meson factories" [19]. Photon-gluon processes were discussed in [42] and later in [43,44]. The very interesting possibility to produce $t\bar{t}$ in this way was recently described in [45].

At the STAR (Solenoidal Tracker At RHIC) detector at RHIC a program to study photon-photon and photon-nucleus (especially diffractive "photon-Pomeron") interactions in very peripheral collisions exists [9,46–49]. First experimental results are just becoming available [50,51]. At RHIC the equivalent photon spectrum goes up to about 3 GeV. Therefore the available $\gamma\gamma$-invariant mass range is up to about the mass of the η_c. At the RHIC/INT workshop at the LBNL (Berkeley), the physics of very peripheral collisions was discussed by Klein [52] and Brodsky [53]. The experimental feasibility of making these measurements with STAR were described, expected backgrounds along with the techniques and triggering algorithms to reject these signals are discussed, see also [9,46–49].

When the "Large Hadron Collider" will be scheduled to begin taking data in 2006/2007, the study of these reactions can be extended to both higher luminosities but also to much higher invariant masses, hithero unexplored, see, e.g., [54,55,22].

To conclude this introduction we quote Bjorken [56]: *It is an important portion (of the FELIX program at LHC [24]) to tag on Weizsäcker Williams photons (via the non-observation of completely undissociated forward ions) in ion-ion running, creating a high luminosity $\gamma\gamma$ collider.* Although the FELIX detector will not be realized in this form at the LHC, these photon-photon and photon-ion collisions can and will be studied at other LHC detectors (ALICE and CMS).

2 From Impact-Parameter Dependent Equivalent Photon Spectra to $\gamma\gamma$-Luminosities

Electron-positron colliders have been and still are the basic tool to study $\gamma\gamma$ physics, see, e.g., the rich physics program at LEP [57,58]. The lowest order graph of two-photon (TP) processes is given in Fig. 3(a). The plane-wave description is very accurate for e^+ and e^-, which only interact electromagnetically. This is, for example, described in great detail in [59]. For lepton-hadron and lepton-ion collisions (e.g., for ep, or eA) and hadron-hadron, hadron-ion, and ion-ion collisions (like pp, pA, and AA) such kind of two-photon interactions occur as well. If both particles are nuclei with charge Z (symmetric AA collisions), the cross section of a TP process is enhanced by a factor of Z^4. For eA and pA collisions the enhancement is a factor Z^2. This has been called "*the power of coherence*" by Brodsky [53]. In these later cases there is also the interesting possibility of photon-ion processes, see Fig. 3(b), which we will call one-photon (OP) processes in the following.

Under rather general circumstances these processes can be described by the concept of equivalent photons. In this way a great simplification is achieved. The cross section factorizes into an equivalent photon spectrum $n(\omega)$ and the cross section for the photon-ion interaction process $\sigma_\gamma(\omega)$ in the case of one-photon processes:

$$\sigma_{OP} = \int \frac{d\omega}{\omega} n(\omega)\sigma_\gamma(\omega). \tag{6}$$

For the general case of two-photon collisions the cross section for the reaction $A_1A_2 \to A_1'A_2'X_f$ factorizes into the photon-photon luminosity $L_{\gamma\gamma}$ and the cross section of the photon-photon interaction process $\gamma\gamma \to X_f$ where A_1, A_2 are the initial particles, A_1', A_2' their final state after the photon emission, and X_f the final state produced in the photon-photon collision, see also Fig. 4 and Eq. (14) below:

$$\sigma_{TP} = \int \frac{d\omega_1}{\omega_1} n_1(\omega_1) \int \frac{d\omega_2}{\omega_2} n_2(\omega_2)\sigma_{\gamma\gamma\to X_f}(\sqrt{4\omega_1\omega_2}) \tag{7}$$

$$= \int \frac{dW}{W} \int dY \frac{dL_{\gamma\gamma}}{dWdY}\sigma_{\gamma\gamma\to X_f}(W) \tag{8}$$

$$= \int \frac{dW}{W} \frac{dL_{\gamma\gamma}}{dW}\sigma_{\gamma\gamma\to X_f}(W). \tag{9}$$

The cross sections for the corresponding subprocesses are given by σ_γ and $\sigma_{\gamma\gamma\to X_f}$; the equivalent photon spectra and the $\gamma\gamma$ luminosity are denoted by $n(\omega)$ and $dL_{\gamma\gamma}/dWdY$, respectively, where Y is the rapidity of the produced system X_f. The invariant mass of the $\gamma\gamma$ system is denoted by $W = \sqrt{4\omega_1\omega_2}$.

The $\gamma\gamma$ luminosity is obtained by a folding of the equivalent photon spectra, as will be explained below.

As compared to the point-like and non-strongly interacting electrons and positrons there are in the case of incoming hadrons or nuclei additional initial and final state interaction effects. They must be taken into account in the calculation of the equivalent photon spectra and $\gamma\gamma$ luminosities. We distinguish three conceptually different kinds:

(1) For extended objects one has an extended charge distribution, as well as, an excitation spectrum. This is taken care of by elastic and inelastic form factors, see Fig. 3(c).
(2) For strongly interacting particles (like in pp, pA, or AA systems) there are effects like absorption (nuclear interaction), which modify the $\gamma\gamma$ luminosities. They may be called "initial state interactions", see Fig. 3(d) and (e). In the case of heavy ions the "initial state interaction" consists of both the nuclear absorption and the Coulomb interaction. For the Coulomb interaction the Sommerfeld parameter $\eta \approx Z_1 Z_2 \alpha$ is larger than one and the semiclassical description can be used. The main initial state interaction is then the nuclear absorption for trajectories with $b < 2R$. This can be very conveniently taken into account by introducing the appropriate cutoff for the impact parameter dependent equivalent photon spectrum. It would be much more cumbersome to take these strong interaction effects into account in a purely quantal description.
(3) Particles produced in $\gamma\gamma$ interactions, which have strong interactions, can have final state interactions with the incident particles, see Figs. 3(f).

2.1 Equivalent Photon Numbers

Before looking in more detail at the equivalent photon approximation for the different cases of interest, let us discuss here first some of the main characteristics in a qualitative way. Here we make use of the plane wave approximation, neglecting the "initial state interaction" between the two ions. One should remember that therefore the statements made are only rather qualitative concerning the heavy ion cases, where the semiclassical straight line approximation is the relevant one, as the Sommerfeld parameter is always larger than one, see below and should be used instead.

For the elastic emission from a nucleus with spin 0, characterized by an elastic form factor $F_{el}(q^2)$ and using the plane wave approximation, the equivalent

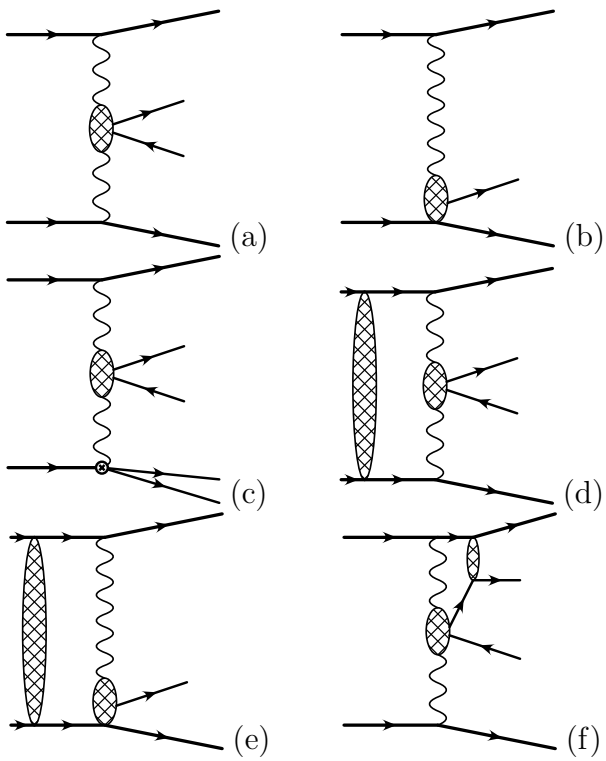

Fig. 3. In the collision of either leptons with hadrons or hadrons with hadrons photon-photon (a) and photon-hadron collisions (b) can be studied. The principal diagrams are shown schematically here. In the collisions of hadrons additional effects need to be taken into account: inelastic photon emission processes (c), "initial state interaction" (d) and (e), as well as final state interaction (f).

photon number of a nucleus with charge Z is given, see Eq. (24) below, by

$$n(\omega) = \frac{Z^2\alpha}{\pi^2}\int d^2q_\perp \frac{q_\perp^2}{\left[\left(\frac{\omega}{\gamma}\right)^2 + q_\perp^2\right]^2} F_{el}^2\left(\left[\frac{\omega}{\gamma}\right]^2 + q_\perp^2\right). \tag{10}$$

The elastic form factor F_{el} is characterized by the property, that it is ≈ 1 up to values of $Q^2 = -q^2$ of about $1/R^2$ and quickly falls of for larger values of Q^2. This leads to the two main characteristics already discussed in the introduction: for $\omega > \gamma/R$ the equivalent photon number quickly decreases due to the fall-off of the form factor, giving a maximum "usable" photon energy of $\omega_{max} \approx \gamma/R$.

In addition also the transverse momentum distribution of the photon is limited to rather small values. This is again due to the fall-off of the elastic form factor, restricting the transverse momenta essentially to $q_\perp \lesssim 1/R$. But in addition the integrand of the expression Eq. (10) peaks at values of $q_\perp \approx \omega/\gamma$. Most equivalent photons will therefore have even smaller transverse momenta. This will also apply to the TP case. Also here the produced system will be

characterized by rather small transverse momenta with $P_\perp \lesssim 1/R$.

Approximating rather crudely the form factor by $\Theta(1/R^2 - Q^2)$, where $Q^2 = -q^2$, the integration can be done analytically and the equivalent photon spectrum in the leading logarithmic approximation is given by

$$n(\omega) = \frac{2Z^2\alpha}{\pi} \ln\left(\frac{\gamma}{\omega R}\right). \tag{11}$$

There are more refined formulae for the equivalent photon approximation than Eq. (11).

For heavy ions the relevant equivalent photon number is the one obtained in the impact parameter approach given below, see Chap. 2.6. The approximate form of Eq. (11) can be obtained also in this case from Eqs. (44) and (46) below. This equation is useful for quick estimates and also to see in a simple way the general properties of the spectrum. We see that the spectrum falls off logarithmically with ω up to $\omega_{max} = \gamma/R$. Note also that the $1/\omega$ dependence, characteristic of the equivalent photon spectra, has been taken out in the definition of $n(\omega)$ in Eq. (9).

Equivalent photon spectra of point-like particles like the electron require a further discussion. The integral Eq. (10) is divergent, if the form factor is constant. The choice of the cutoff depends then on the specific process to be considered. This is thoroughly discussed in [59], and it is sufficient here to refer to this reference.

The photon-photon luminosity can be found (again neglecting possible initial state effects)from Eq. (9). One obtains, see also Eq. (39) and Eq. (49) below,

$$\frac{dL_{\gamma\gamma}}{dW dY} = \frac{2}{W} n\left(\frac{W}{2}e^{Y}\right) n\left(\frac{W}{2}e^{-Y}\right). \tag{12}$$

Due to the decrease of the equivalent photon number with ω, this luminosity has a maximum at rapidity $Y = 0$. It falls as a function of $|Y|$. The width Y_{max} of the distribution can be estimated to be

$$Y_{max} = \ln(2\omega_{\max}/W). \tag{13}$$

The width decreases with larger invariant mass W.

Let us first deal with the effects due to the finite size of the particles. This leads to two effects: we need to introduce a form factor for the elastic photon emission and in addition have to take the inelastic photon emission into account, where the particle makes a transition to an excited state. Both can be dealt within the general plane wave framework, we are showing here. We will in the following deal only with the derivation of the equivalent photon approximation in the two-photon case; the one-photon case then follows along the same line.

Let us look at the most general case, where two incoming particle A_1 and A_2 undergo a transition to A_1' and A_2' while emitting a photon each and where the collision of these photons then produces a final state X_f, see Fig. 4. We follow in our derivation here [59], but are more general in treating both the elastic and inelastic case and using a somewhat different notation, see also [60]. The cross section of this two-photon process can be written as

$$d\sigma_{A_1A_2\to A_1'A_2'X_f} = \frac{(2\pi)^4(4\pi\alpha)^4}{8E_1E_2}\int \delta^{(4)}(q_1+q_2-p_f')\,|T|^2 \\ d^4q_1d^4q_2dR_1(p_1-q_1)dR_2(p_2-q_2)dR_f(q_1+q_2), \tag{14}$$

where p_1,p_2 are the four-momenta of the initial particles, $E_1 = p_1^0$, $E_2 = p_2^0$ their energies; q_1,q_2 are the four-momenta of the exchanged photons and $dR_i(p_i')$ denotes the integration over the final state i (the summation and averaging over the final and initial spin states is assumed to be implicitly included):

$$dR_i(p_i') = \prod_{k\in i}\frac{d^3p_k}{(2\pi)^3 2E_k}\delta^{(4)}\left(p_i' - \sum_{k\in i} p_k\right). \tag{15}$$

The square of the matrix element $|T|^2$ is given by

$$|T|^2 = \frac{1}{(q_1^2)^2}\frac{1}{(q_2^2)^2}\Gamma_1^\mu\Gamma_1^{\mu'*}\Gamma_2^\nu\Gamma_2^{\nu'*}M_{\mu\mu'\nu\nu'}, \tag{16}$$

where $M_{\mu\mu'\nu\nu'}$ describes the production of the system X_f in the photon-photon interaction and Γ_i are the electromagnetic transition currents. Integrating over all possible final state with momentum $p_i' = p_i - q_i$ $(i = 1, 2)$, we can reexpress these electromagnetic currents in terms of the electromagnetic tensor $W_i^{\mu\mu'}$,

see, e.g., [61]

$$W_i^{\mu\mu'} = \frac{1}{2\pi 2m_i} \int dR_i(p-q)(2\pi)^4 \Gamma_i^{\mu} \Gamma_i^{\mu'}. \tag{17}$$

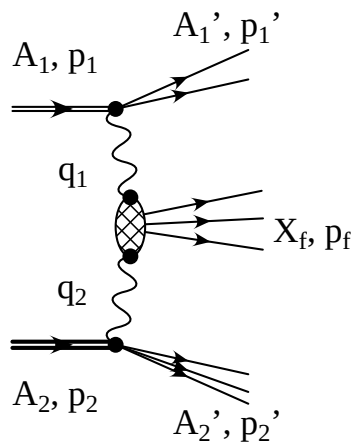

Fig. 4. The general form of a two-photon process is shown. The two incoming particles A_1 and A_2 either stay in their ground states or undergo a transition to exited states A_1 and A_2', while each emitting a photon. The two photon fuse to a final state X_f. Also shown are the momenta of all particles involved

From Lorentz invariance and current conservation considerations the general form of the tensor $W^{\mu\mu'}$ can be written as

$$\begin{aligned} W_i^{\mu\mu'} = & \left(-g^{\mu\mu'} + \frac{q_i^{\mu} q_i^{\mu'}}{q_i^2} \right) W_{i,1} \\ & + \left(p_i^{\mu} - \frac{p_i \cdot q_i}{q_i^2} q_i^{\mu} \right) \left(p_i^{\mu'} - \frac{p_i \cdot q_i}{q_i^2} q_i^{\mu'} \right) \frac{W_{i,2}}{M^2}, \end{aligned} \tag{18}$$

where $W_{i,1}$ and $W_{i,2}$ are two scalar functions of the two independent invariants q_i^2 and $\nu_i = -p_i \cdot q_i / m_i$, which characterize generally the electromagnetic structure of the electromagnetic currents. Please keep in mind that we are treating the photons as being emitted here, whereas in electron scattering, the photons are normally assumed to be absorbed by the particle. The cases differ only by the sign of q.

At high energies the main contribution to this cross sections comes from small values of q^2 and where the three-momentum of the photon is almost aligned to the beam axis. In this case only the transverse part (with respect to the momentum of the photon) of the tensor $W^{\mu\nu}$ is important. Assuming in addition that $M_{\mu\mu'\nu\nu'}$ in this case essentially only depends on the energies of the two photons ($\omega_i = q_{0,i}$) and not on the photon virtualities q_i^2, it can be related to the cross section $d\sigma_{\gamma\gamma}$ of the corresponding process for two real photons. For a more thorough discussion of the applicability of the EPA, we refer to [59].

Under these assumptions the cross section can be written as

$$d\sigma_{A_1A_2\to A_1'A_2'X_f} = \int \frac{d\omega_1}{\omega_1}\int \frac{d\omega_2}{\omega_2} n_1(\omega_1)n_2(\omega_2)d\sigma_{\gamma\gamma\to X_f}(\omega_1,\omega_2), \tag{19}$$

with the equivalent photon number given by

$$n_i(\omega_i) = \int d^3q\ \frac{\alpha}{\pi^2}\frac{\omega_i^2 m_i}{E_i\left(q_i^2\right)^2}\left[2W_{i,1} + \frac{q_{i\perp}^2 P_i^2}{\omega_i^2 m_i^2}W_{i,2}\right] \tag{20}$$

$$= \frac{\alpha}{\pi^2}\int d^2q_{i\perp}\int d\nu_i \frac{1}{\left(q_i^2\right)^2}\left[2\frac{\omega_i^2 m_i^2}{P_i^2}W_{i,1} + q_{i\perp}^2 W_{i,2}\right], \tag{21}$$

where $E_i \approx P_i$ are energy and momentum of the incoming particle. This equation corresponds to Eq. (D.4) of [59].

One important feature of the description of the electromagnetic structure (and therefore of the equivalent photon spectrum) in terms of W_1 and W_2 is the fact that they are Lorentz scalars and can therefore be calculated in any frame — e.g., in the rest frame of the projectile (nucleus).

2.3 Elastic Photon Emission

Let us first discuss the most relevant case: the elastic photon emission. In this case the two invariants are not independent of each other but are related via $2m\nu = -q^2$. Therefore the two structure function will be of the form

$$W_{1,2}(\nu, q^2) = \widehat{W}_{1,2}(q^2)\delta(\nu + q^2/2m_i) \tag{22}$$

and the integration over ν can be done trivially. In many cases — and especially in the heavy ion case — we have $Q^2 = -q^2 \ll m_i^2$; we can then neglect the recoil and use to a good approximation $\nu \approx 0$. We then get $q_z = \omega/\beta$, where β is the velocity of the particle and

$$-q^2 = \left(\frac{\omega}{\beta\gamma}\right)^2 + q_\perp^2 \tag{23}$$

For the case of a nucleus with a $J^P = 0^+$ ground state (an even-even nucleus) we have $\widehat{W}_1 = 0$ and $\widehat{W}_2 = Z^2\left|F_{el}(-q^2)\right|^2$, with the elastic form factor normalized to $F_{el}(0) = 1$. In this case the equivalent photon number is given

by

$$n(\omega) = \frac{Z^2\alpha}{\pi^2} \int d^2q_\perp \frac{q_\perp^2}{(q^2)^2} F_{el}^2(q^2). \tag{24}$$

It should be clear that in this equation coming from the plane wave approximation the important strong interaction effects (which correspond to a cutoff in impact parameter space, as will be explained below) are not taken into account. For a collection of some other relevant cases see, e.g., Table 8 of [59] (with the relation of C and D there to $\widehat{W}_1$ and $\widehat{W}_2$ given by $C = \frac{4m^2}{(-q^2)}\widehat{W}_1$, $D = \widehat{W}_2$). In many cases the dominant contribution comes from W_2 alone and W_1 can be neglected.

For nuclei various degrees of sophistication for the elastic form factor can be applied: Gaussian form factors or form factors corresponding to a homogeneously charged sphere have been used in the literature. A comparison of the different results can be found, e.g., in [16].

One can include also the effects of electromagnetic moments like $M1$ and $E2$, with their corresponding contributions to $\widehat{W}_1$ and $\widehat{W}_2$, see also Eqs. (31) and (31) below. E.g., the projectile ^{197}Au — which is used at RHIC — has a magnetic moment of $\mu = 0.14485$ n.m. and an electric quadrupole moment of $q = +0.6$ barn [62]. A classical version of an $E2$ equivalent photon spectrum is given in [63]. Perhaps at some level of accuracy of the RHIC experiments the inclusion of such effects will become necessary.

Quite general spectra of the equivalent photons in the plane wave approximation are given explicitly in [16] (with their definition of $n(\omega)$ including an extra $1/\omega$):

$$n(\omega) = \frac{2Z^2\alpha}{\pi} \int\limits_{\omega/\gamma}^{\infty} d\kappa \frac{\kappa^2 - \left(\frac{\omega}{\gamma}\right)^2}{\kappa^3} F_{el}^2(\kappa^2), \tag{25}$$

for any elastic form factor F_{el}. The elastic form factor for extended charge distributions is in general characterized by a radius R. Defining a maximum photon energy $\omega_0 = \gamma/R$, the equivalent photon number can then be cast into the form

$$n(\omega) = \frac{2Z^2\alpha}{\pi} \widehat{f}(\omega/\omega_0), \tag{26}$$

where $\widehat{f}$ is a universal function, independent of γ and given by

$$\widehat{f}(x) = \int_x^\infty dz \frac{z^2 - x^2}{z^3} F_{el}^2 \left(\frac{z^2}{R^2} \right). \tag{27}$$

Three different cases are given in [16] point particle, homogeneous charged sphere and a Gaussian form factor. The exact result for the equivalent photon spectrum of the proton can be found in [64], where the usual dipole parameterization of the form factors is used.

2.4 Inelastic Form Factors

The structure of the electromagnetic current in Eq. (18) is equally valid for inelastic photon emission processes. In this case $W_1(\nu, q^2)$ and $W_2(\nu, q^2)$ are functions of both invariants ν and q^2. At low excitation energies, discrete states will dominate — resonances of either the nucleus or the proton. These resonances will be at well defined discrete energies (neglecting their finite width), and — as we can again neglect recoil effects in most cases — ν has to be equal to Δ, where Δ is the energy of the excited state in its rest frame. This can be seen by evaluating the relation $(p-q)^2 = (m+\Delta)^2$ and neglecting terms quadratic in q and Δ. Therefore, similar to the elastic case, W_1 and W_2 will be of the form

$$W_{1,2}(\nu, q^2) = \widehat{W}_{1,2}(q^2)\delta(\nu - \Delta), \tag{28}$$

and the integration over $d\nu$ in Eq. (21) can be done trivially. The effect of the finite excitation energies on q^2 can be taken into account [60], with q^2 in this case given by

$$-q^2 = \frac{\omega^2}{\gamma^2} + 2\frac{\omega\Delta}{\gamma} + \frac{\Delta^2}{\gamma^2} + q_\perp^2. \tag{29}$$

One clearly sees that as long as $\omega > \gamma\Delta$ the modification of q^2 is small and can be neglected in these cases.

In the case of nuclei it is more convenient to express $\widehat{W}_1$ and $\widehat{W}_2$ in terms of the more familiar (to nuclear physicists) Coulomb, transverse electric or transverse magnetic matrix elements [65–67,60]:

$$\widehat{W}_1 = 2\pi \left[|T^{\mathrm{e}}|^2 + |T^{\mathrm{m}}|^2 \right] \tag{30}$$

$$\widehat{W}_2 = 2\pi \frac{q^4}{(\Delta^2 - q^2)^2} \left[2|M^{\mathrm{C}}|^2 - \frac{\Delta^2 - q^2}{q^2} \left(|T^{\mathrm{e}}|^2 + |T^{\mathrm{m}}|^2 \right) \right]. \tag{31}$$

Inelastic photon processes on nuclei are dominated by the giant dipole resonance (GDR). For them the Goldhaber-Teller model gives [60]

$$\widehat{W}_1 = \frac{NZ}{A} \frac{\Delta}{2m_N} \left| F_{el}(\Delta^2 - q^2) \right|^2 \tag{32}$$

$$\widehat{W}_2 = \frac{NZ}{A} \frac{-q^2}{2m_N \Delta} \left| F_{el}(\Delta^2 - q^2) \right|^2, \tag{33}$$

where F_{el} is the elastic form factor of the nucleus, m_N the nucleon mass and the excitation energy Δ is given experimentally by

$$\Delta = E_{GDR} = \frac{80\mathrm{MeV}}{A^{1/3}}. \tag{34}$$

For protons the lowest excited state is the Δ-resonance. For this transition the contribution to the photon spectrum was estimated in [15], using the parameters given in [68]. A contribution of the order of 10% was found. This is in contrast to the similar situation in heavy ion collisions, where the contribution of the most important excited state, the GDR, is in general less than 1% [60].

For higher excitation energies and momentum transfers on nuclei the quasielastic emission of nucleons is dominating and the quasifree approximation can be used. For an estimate the Fermi gas model can be used. One obtains a simple expression in terms of the elastic nucleon form factors [69,70]:

$$W_i^{qe} = C(t) \left[Z W_i^p + (A - Z) W_i^n \right], \tag{35}$$

with

$$C(t) = \begin{cases} 1 & Q_{rec} > 2P_F \\ \frac{3Q_{rec}}{4P_F} \left[1 - \frac{1}{12} \left(\frac{Q_{rec}^2}{P_F} \right)^2 \right] & \text{otherwise,} \end{cases} \tag{36}$$

with $Q_{rec}^2 = (-q^2)^2/(2m_p)^2 + (-q^2)$ and the Fermi momentum $P_F = 0.25$ GeV.

Finally at very large momentum transfer ($|-q^2| \gg 1\mathrm{GeV}^2$) the parton model applies and W_1 and W_2 can be expressed in terms of the quark structure functions $f_i(x)$ [71,72]:

$$W_1 = \frac{1}{2M} \sum_i e_i^2 f_i(x) \tag{37}$$

$$W_2 = \frac{1}{\nu} \sum_i e_i^2 x f_i(x), \tag{38}$$

that is, W_1 and W_2 are related by $2MW_1 = \nu W_2/x$ and the Bjorken variable is $x = -q^2/(2m\nu)$. Of course in this case the integration over $d\nu$ can be replaced by one over dx. In the case of the proton, the equivalent photon spectra were calculated in [71,72]. Whereas the integration over q^2 in the elastic case is limited due to the form factor to small values of q^2, here the integration goes up to the kinematical limit ($-q^2 < 4E^2$).

2.5 Integrated Photon-Photon Luminosity

Let us now calculate the luminosity function $dL_{\gamma\gamma}/dW$ as defined in Eq. (9). Neglecting possible "initial state effects" between the collision partners, we can fold the equivalent photon spectra $n_1(\omega_1)$ and $n_2(\omega_2)$ to obtain [32]

$$\tau \frac{dL}{d\tau} = \int_\tau^1 \frac{dx}{x} f(x) f\left(\frac{\tau}{x}\right), \tag{39}$$

where $\tau = W^2/s = 4\omega_1\omega_2/s$ is the square of the fraction of the total energy carried away by the photon-photon system with $s = (p_1 + p_2)^2$. The photon distribution function f here is related to the equivalent photon number via

$$f(x) = \frac{E}{\omega}\, n(xE) = \frac{n(xE)}{x} \tag{40}$$

and E is the total energy of the initial particle in a given reference frame. $x = \omega/E$ is as before the ratio of the photon energy ω to the energy of the incoming particle E.

Explicit calculations of $\gamma\gamma$ luminosity functions exist for the pp case. The strong interaction between the protons are not taken into account. Several approximate results are given in [72]. The simplest one (in leading order of $\ln(\tau)$) is given by

$$\tau \frac{dL}{d\tau} = \left(\frac{\alpha}{\pi}\right)^2 \frac{2}{3} \ln^3\left(\frac{1}{\tau}\right). \tag{41}$$

A more detailed result is given by Drees et al. [73] based on the equivalent photon spectra of the proton given in [74].

Such a formula for the $\gamma\gamma$-luminosity (Eq. (39)), in which the initial state interactions are neglected, can be applied to $\gamma\gamma$ interactions in ep and eA collisions. For eA collisions this was done by Levtchenko [75]. Eq. (25) was used for the equivalent photon spectrum of the nucleus. In ep and eAcollisions initial state interactions are weak and can be safely neglected.

In the case of protons calculations have been made with either one or both protons breaking up [71,72]. This leads to $\gamma\gamma$ luminosities which are larger than the ones in the elastic-elastic case. Since the charges of the quarks $(2/3, -1/3)$ are comparable to the proton charge, this is not unexpected. In the case of a heavy nucleus on the other hand the charges of the constituents (protons) are much smaller compared to the total charge Z of the ion; therefore incoherent effects, although present, are generally less important. Possible strong interaction effects in the initial state are not taken into account in these calculations.

The interesting possibility to study photon-photon events in pp collisions at the LHC by tagging the two final protons was studied in [76]. Only protons emitting a photon with a substantial part of their energy (corresponding to $x > 0.1$) can be tagged in this way, as their path after the interaction deviates sufficiently from the non-interacting ones. Photon-Photon luminosities under these conditions (and also including transverse momentum cuts, which are less important) were calculated.

2.6 Semiclassical Impact Parameter Description

For heavy ions (as opposed to, e.g., pp collisions) the semiclassical description works very well, as the Sommerfeld parameter $\eta = \frac{Z_1 Z_2 e^2}{\hbar\beta}$ is much larger than one, see, e.g., the discussion in Chap. 2 of [15]. Therefore an impact parameter dependent equivalent photon number $N(\omega, b)$ can be defined. It is most important to note that in this semiclassical impact parameter description it is very easy to take strong absorption effects into account. This is done by introducing a cutoff for those impact parameters where the ions interact strongly with each other. The calculation of the impact parameter dependent equivalent photon spectra is explained in [7] for the case of $E1$ (electric dipole) excitations. The generalization of the equivalent photon spectrum to all electromagnetic multipoles was given by [40]. For the $E1$ case

$$N_{E1}(\omega, b) = \frac{Z^2\alpha}{\pi^2}\left(\frac{\omega}{\gamma\beta}\right)^2\left[K_1^2(u) + \frac{1}{\gamma^2}K_0^2(u)\right], \tag{42}$$

with β and γ the velocity and Lorentz factor of the ion and where $u = \omega b/(\gamma\beta)$. Integrating from some R_{min} to infinity gives

$$n_{E1}(\omega) = \frac{2}{\pi} Z^2 \alpha \left[\xi K_0(\xi) K_1(\xi) - \frac{\xi^2}{2} \left(K_1^2(\xi) - K_0^2(\xi) \right) \right], \tag{43}$$

where $\xi = \omega R_{min}/\gamma\beta$. Using the expression for K_0 and K_1 for $\xi \to 0$, it can easily be seen, that this expression agrees in logarithmic approximation with Eq. (11). Impact parameter dependent equivalent photon spectra $N(\omega, b)$ for extended charge distributions are calculated in [77]. They are

$$N(\omega, b) = \frac{Z^2 \alpha}{\pi^2} \frac{1}{\beta^2 b^2} \left| \int_0^\infty dv \; v^2 J_1(v) \frac{F_{el}\left(-\frac{u^2+v^2}{b^2}\right)}{u^2 + v^2} \right|^2, \tag{44}$$

where $u = \omega b/\gamma\beta$ as above. In the case of a monopole or dipole form factor analytical results can be found [78,79].

2.7 Effects of Strongly Interacting Particles

Let us now turn to the effects of strong interactions between the colliding particles ("initial state interactions"). For the case of nucleus-nucleus (AA) collisions we can use the semiclassical method: to a very good approximation the nuclei move on classical straight line trajectories with an impact parameter b. Collisions with $b < R_{min} = R_1 + R_2$ are dominated by strong interactions and electromagnetic effects (even though they still occur) are generally completely swamped by those violent processes. As an example for the presence of these electromagnetic effects in central collisions we mention Ref. [80]. In this paper e^+e^- production due to the electric fields of the ions is calculated. Their effect was found to be much smaller than e^+e^--pair production due to hadronic processes and from meson decay [81]. Usually, the experimental conditions imposed on the study of electromagnetic processes ($\gamma\gamma$, γh and γA) exclude these collisions, as they cannot be extracted from hadronic events. Of course one has to be careful to exclude them in the same way in the theoretical study of these processes as well. One generally imposes a (sharp) cutoff on the impact parameter

$$b > R_{min} = R_1 + R_2. \tag{45}$$

In the one-photon case one then gets the equivalent photon number as

$$n(\omega) = \int_{R_{min}}^{\infty} 2\pi b db N(\omega, b). \tag{46}$$

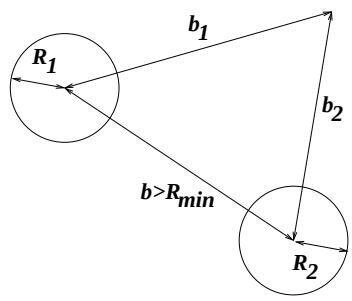

Fig. 5. In the semiclassical picture, which is valid in the case of heavy ion collisions, initial state interactions between the two ions take place if the impact parameter between the two ions is smaller than $R_{min} = R_1 + R_2$. Final state interaction can occur if the individual b_i are smaller than R_i.

Let us look first at the one-photon case ("γA collisions") between two ions. It is a good assumption that the total nuclear charge is contained inside the sphere with radius R_i. As it is well known from electrostatics, the electric field outside of a spherical symmetric charge distribution is the same as if the total charge is concentrated in the center. The two ions cannot come closer than $R_{min} = R_1 + R_2$. Impact parameter dependent equivalent photon spectra for extended charge distributions can in principle be calculated. But from the argument given above it is clear that the form of the charge distribution does not enter in this case in Eq. (46). It only matters that the nuclear charge Z is entirely contained inside the nuclear radius R_i.

The corresponding electromagnetic process can be written as

$$\sigma_{OP} = \int_{R_{min}}^{\infty} 2\pi b db \int \frac{d\omega}{\omega} N(\omega, b) \sigma_\gamma(\omega) \tag{47}$$

$$= \int_{R_{min}}^{\infty} 2\pi b db P_{OP}(b), \tag{48}$$

see Eq. (6), allowing to define the impact parameter dependent probability for the one-photon process in this case. In numerous studies of nuclear excitations of fast (relativistic) heavy ions this has been proven to be a good approximation.

The sharp cutoff assumption may be relaxed using a smooth absorption profile $T(b)$, see, e.g., Chap. 2 of [15]. The importance of such uncertainties depends

on each case: for dipole excitations the dependence on R_{min} is only logarithmic, for higher multipolarities it depends on an inverse power of the cutoff R_{min}. So in the former case the uncertainties in the choice of a cutoff will be small. For RHIC the effect of the surface thickness was calculated and found to contribute to about 5–10% [49]. An interesting question is the choice of a cutoff in the case of deformed nuclei. Depending on the orientation of the nuclei, the minimum impact parameter varies. It would be interesting to study this effect in the future. For a related problem we refer to [82].

Let us mention the attempt by Benesh, Haynes and Friar [83] to include the effects of the R_{min}-cutoff by using plane waves, a nuclear form factor, and some cutoff q_{max} (corresponding loosely to a minimum impact parameter R_{min}). From the above it is clear that this cannot work quantitatively, as is explained in detail in a comment by Baur and Bertulani [84], see also [85]. The equivalent photon spectrum used in [83] corresponds to the "point-form" spectrum in Fig. 2.3 of [16]. In addition the results of [83] were compared to experimental data for giant resonance excitations in [86].

For the $\gamma\gamma$ luminosity in the two-photon (TP) case for AA collisions, modifications due to the strong interaction are important especially for the high energy end of the luminosity function. Again we apply the condition that the minimum impact parameter between the two ions must be larger than R_{min}. The photon-photon luminosity can then be calculated as [30,32]

$$\frac{dL_{\gamma\gamma}}{dW\,dY} = \frac{2}{W}\int d^2b_1 \int d^2b_2 \times N_1(\frac{W}{2}e^Y, b_1)N_2(\frac{W}{2}e^-Y, b_2)\Theta(|\vec{b}_1 + \vec{b}_2| - R_{min}). \tag{49}$$

Here, especially for non-strongly interacting final states, one does not necessarily have a condition for the individual b_i to be larger then R_i. Therefore form factor effects might become important in contrast to the γA collisions considered above.

This formula has also been derived ab initio within the semiclassical approximation in [87,88]. Effects due to the photon polarization are also included. They are neglected here for simplicity, as they were found to be small. A similar approach for the derivation of the impact parameter dependent luminosity $L_{\gamma\gamma}$ was done in [89]. There an expression not in terms of the individual b_i, but a direct impact parameter dependent luminosity function $L_{\gamma\gamma}(b)$ or $n(\omega_1, \omega_2, b)$ was derived. (Of course this expression can also be transformed into a formula dependent on the individual b_i, as explained in [16]).

For a calculation of the $\gamma\gamma$ luminosities it is easiest to calculate first the $\gamma\gamma$ luminosities without the restriction $b < R_{min} = R_1 + R_2$, which can be done

analytically, e.g., for point particles with the restriction $b_i > R_i$. The correct result will then be obtained by subtracting those cases, where $b < R_{min}$. One obtains [32]

$$\frac{dL_{\gamma\gamma}}{dW dY} = \frac{2}{W} n\left(\frac{W}{2}e^{Y}\right) n\left(\frac{W}{2}e^{-Y}\right) - \frac{d\Delta L_{\gamma\gamma}}{dW dY}, \tag{50}$$

with

$$\frac{d\Delta L_{\gamma\gamma}}{dW dY} = \frac{8\pi}{W} \int\limits_{R_1}^{\infty} b_1 \; db_1 \int\limits_{\max(b_1 - R_{min}, R_2)}^{b_1 + R_{min}} b_2 \; db_2 \times N\left(\frac{W}{2}e^{Y}, b_1\right) N\left(\frac{W}{2}e^{-Y}, b_2\right) \phi_{\text{crit}}. \tag{51}$$

The integral over ϕ goes only from 0 to ϕ_{crit} and from $2\pi - \phi_{\text{crit}}$ to 2π. Only in these cases do we have contributions from $b < R_{min}$. ϕ_{crit} is given by

$$\phi_{\text{crit}} = \arccos\left(\frac{b_1^2 + b_2^2 - R_{min}^2}{2 b_1 b_2}\right). \tag{52}$$

For $b_1 \to \infty$ we also have $b_2 \to b_1$ and $\phi_{\text{crit}} \to 0$. The integral converges rapidly. It was also noted in [32] that for symmetric collisions the $\gamma\gamma$ luminosity can be written in the form

$$\tau \frac{dL_{\gamma\gamma}}{d\tau} = L_0 \xi(z), \tag{53}$$

with

$$L_0 = \frac{16 Z^4 \alpha^2}{3\pi^2} \tag{54}$$

and a universal function $\xi(z)$ of $z = 2MR\sqrt{\tau} = mR/\gamma$. A parameterization of this universal function is given there as well. The case $z \ll 1$ was first discussed in [27].

The last modification concerns possible final state interactions of the produced particles with the colliding particles. If the produced particles are hadrons, they can interact with the ions, if they are produced "within" one of the ions $b_1 < R_1$ or $b_2 < R_2$. Such processes are excluded in the approach given above, as integration over b_1 and b_2 are starting from R_1 and R_2, respectively. Since the electric field strength inside the nucleus decreases with decreasing radius such effects are expected to be small. They will be of importance only at

the very high end of the $\gamma\gamma$ spectrum. A calculation taking into account the final state interaction has to our knowledge not been performed. But one can obtain an estimate (or an upper bound) of the size of this effect by comparing $\gamma\gamma$ luminosities with either an integration over all b_i or restricted to $b_i > R_i$ respectively. Of course for this one needs to use impact parameter dependent equivalent photon spectra with an elastic form factor.

2.8 Effective $\gamma\gamma$-Luminosities and Perspectives for RHIC and LHC

The effective $\gamma\gamma$ luminosity $L_{\rm eff}$ in ion-ion collisions is defined in terms of the the beam luminosity L_{AA} as

$$\frac{dL_{\rm eff}}{dM} = L_{AA}\frac{dL_{\gamma\gamma}}{dM}, \tag{55}$$

where the $\gamma\gamma$ luminosity $L_{\gamma\gamma}$ is given by Eq. (49). Luminosities of the heavy ion beams are several orders lower compared to those of light ions and protons. One reason is the large cross sections of electromagnetic processes of heavy ions, which either disintegrate the ions or change their charge state due to electron capture. In [90] the influence of different beam-beam interaction processes on the beam lifetime is considered for the LHC. The main processes, which contribute to the beam-beam interactions, are hadronic nuclear interactions, electromagnetic dissociation, where an ion is excited and subsequently decays, and bound free electron-position pair production, see below. Thus, the maximum ion luminosity is derived from the cross sections of the beam-beam interaction. The luminosities for different ion species at the RHIC and the LHC are given in [91] and [92], respectively. In Table 1 we quote the average

	Projectile	Z	A	$\sqrt{s}$, A GeV	Luminosity, cm^{-2}s^{-1}
L	p	1	1	14000	$1.4 \cdot 10^{31}$
H	Ar	18	40	7000	$5.2 \cdot 10^{29}$
C	Pb	82	208	5500	$4.2 \cdot 10^{26}$
R	p	1	1	500	$1.4 \cdot 10^{31}$
H	Cu	29	63	230	$9.5 \cdot 10^{27}$
I	Au	79	197	200	$2.0 \cdot 10^{26}$
C					

Table 1
Average luminosities at LHC and RHIC for pp, medium and heavy ion beams.

luminosities at RHIC and LHC for pp, medium and heavy ion collisions. The

specific experiments may also apply their requirement to lower the luminosities to satisfy the detector load [93].

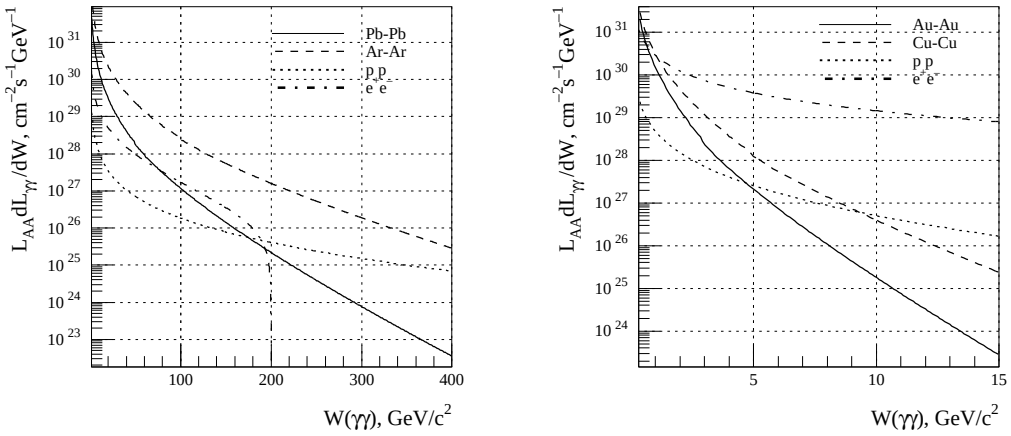

Fig. 6. Effective $\gamma\gamma$ luminosity at LHC (left) and RHIC (right) for different ion species and protons as well as at the e^+e^- collider LEP-II. The L_{AA} in the last two cases of course corresponds to the pp or ee beam luminosity.

Two-photon luminosities for various ion species and protons as a function of $\gamma\gamma$ mass are shown in Fig.6 (left) for LHC and (right) for RHIC. The $\gamma\gamma$ luminosities are calculated by the Monte Carlo program TPHIC [54]. The luminosities at the ion colliders are compared with the $\gamma\gamma$ luminosity at LEP-II with a c.m. energy of 200-GeV and an e^+e^- luminosity of $5 \cdot 10^{31}$ cm^{-2}s^{-1} [94].

Although the heaviest ions generate the highest $\gamma\gamma$ luminosities due to their large charge, the beam luminosities are lower for these ions. As a result, the medium-weight ions (Argon at LHC, Copper at RHIC) are the most prominent source of two-photon processes. RHIC can compete with LEP in two-photon studies at low $\gamma\gamma$ masses while LHC will be the best machine to study two-photon physics at all ranges of $\gamma\gamma$ masses.

3 $\gamma\gamma$ Physics at Hadron Colliders, General Considerations

We will now give a general discussion of possible photon-photon physics at relativistic heavy ion colliders. Two-photon interactions allow to test the main properties of the standard model in both the electroweak sector and in QCD, as well as, physics beyond the Standard Model. In contrast to hadronic processes, many of the processes here can be calculated in principle to some degree of accuracy. Below we review QCD interactions and also physics related to electroweak interactions, which are of interest to be studied in two-photon interactions in heavy ion collisions. This covers the range starting from exclusive meson production, meson pair production up to the total hadronic cross section. In the next chapter we will then be concerned with the potential for the discovery of new physics, which seems to be possible in principle due to the high two-photon invariant masses of up to about 100 GeV, which are available at the LHC. An interesting topic in itself is the electron-positron pair production. The fields are strong enough to produce multiple pairs in a single collision. A discussion of this subject will be given in Chap. 7 below.

Up to now photon-photon scattering has been mainly studied at e^+e^- colliders. Many reviews [59,95,96] as well as conference reports [97–100,57,58] on this subject exist. Whereas in the past the range of invariant masses has been the region of mesons, ranging from π^0 ($m_{\pi^0} = 135$ MeV) up to about η_c ($m_{\eta_c} = 2980$ MeV), the higher invariant masses at LEP2 have allowed to study an invariant mass range up to about 185 GeV [101], where one interesting subject has been the study of the total $\gamma\gamma \to$ hadron cross-section.

We are concerned here mainly with the invariant mass region relevant for the LHC; see the $\gamma\gamma$-luminosity in Fig. 6. At RHIC $\gamma\gamma$ physics can be done in the $\gamma\gamma$ invariant mass region up to several GeV. This topic has also been studied experimentally now by the "Peripheral Collision Group" at STAR and this will be discussed below in Chap. 8. Apart from the production of e^+e^- (and $\mu^+\mu^-$) pairs, the photons can always be considered as quasireal. The cross section for virtual photons deviates from the one for real photons only for Q^2, which are much larger then the coherence limit $Q^2 \lesssim 1/R^2$, see also the discussion in [59]. Therefore photon-photon processes are restricted to *quasireal* photons. Tagging of the elastic scattered beams is very difficult in the heavy ion case, but for the *pp* case at the LHC such a possibility has been investigated in [76]. The standard detector techniques used for measuring very forward proton scattering will allow a reliable separation of interesting $\gamma\gamma$ interactions

Real photons have a complicated nature. In a first approximation the photon is a point-like particle, although in field theory it may fluctuate also into a fermion pair [102]. Fluctuations into a quark-antiquark pair $\gamma \to q\bar{q}$ can interact strongly and give a large contribution to the two-photon hadronic cross section, while fluctuations into a lepton pair $\gamma \to l\bar{l}$ interact electromagnetically only and do not influence the total $\gamma\gamma$ cross section very much (see also the rates predicted for the different contributions below for the LHC). Lepton fluctuations can be calculated perturbatively, which is not true for the quark pairs, as low-virtuality fluctuations need to be described by nonperturbative QCD. Therefore, the spectrum of the photon fluctuation can be separated into low-virtuality and high-virtuality parts, according to [102]. To describe the first part, a phenomenological model of vector-meson dominance (VMD) is used, according to which the photon fluctuates into a sum of vector meson states. Quark pair with high virtuality are described by the perturbative theory. As a whole, the photon wave function can be written then as follows

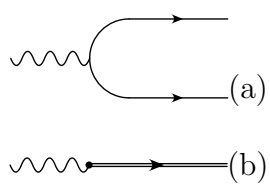

Fig. 7. The photon can fluctuate into other states, among them into a pair of fermions (leptons, quarks, (a)), but also into vector mesons (b). The total cross section in photon-photon collisions is dominated by the fluctuations into two quarks and their strong interaction.

$$\begin{aligned} \mid \gamma\rangle = c_0 \mid \gamma_0\rangle + \textstyle\sum_{V=\rho^0,\omega,\phi,J/\psi,\Upsilon} c_V \mid V\rangle + \sum_{q=u,d,s,c,b} c_q \mid q\bar{q}\rangle + \\ \textstyle\sum_{l=e,\mu,\tau} c_l \mid l^+l^-\rangle, \end{aligned} \tag{56}$$

where $\mid \gamma_0\rangle$, $\mid V\rangle$, $\mid q\bar{q}\rangle$ and $\mid l^+l^-\rangle$ are wave functions of the point-like photon, a vector meson, a quark- and a lepton pair, respectively. The coefficients c_i in general depend on the scale μ, which probes the photon. The coefficients for the contribution to a lepton pair are well known to be equal to

$$c_l \approx \frac{2}{3}\,\frac{\alpha_{\rm em}}{2\pi}\,\ln(\mu^2/m_l^2).$$

To separate the low- and high-virtuality quark fluctuations one introduces a parameter p_0. For high-virtuality fluctuations one sets

$$c_q \approx (\alpha_{\rm em}/2\pi)2Q_q^2 \ln(\mu^2/p_0^2).$$

The $q\bar{q}$ fluctuations with virtuality below p_0 are described by the vector meson dominance part, which does not depend on the scale μ. As a rule of thumb

the scale μ is taken equal to the transverse momentum of the parton process. The value of p_0, which provides the best description of the total cross section, is found to be $p_0 = 0.5$ GeV [102]. The c_V are defined as

$$c_V^2 = 4\pi\alpha_{\rm em}/f_V^2,$$

where the decay constants $f_V^2/4\pi$ are determined from experimental data on $V \to l^+l^-$; they are $f_V^2/4\pi = 2.20$ for ρ^0, 23.6 for ω, 18.4 for ϕ, 11.5 for J/ψ. Finally the c_0 is then defined from unitarity, and is usually close to one.

According to the photon wave function representation of Eq. (56), the following partonic processes can take place in two-photon interactions, see also Fig. 8:

- Purely electromagnetic processes of order $O(\alpha_{\rm em}^2)$ involving quarks q and leptons l, i.e., $\gamma\gamma \to q\bar{q}$, $\gamma l \to \gamma l$, $\gamma\gamma \to l\bar{l}$, $ll' \to ll'$, as well as, the production of W^+W^- pairs and of pairs of particles beyond the Standard Model.
- Processes with one electromagnetic and one strong vertices of order $O(\alpha_{\rm em}\alpha_{\rm s})$ such as $\gamma q \to gq$ and $\gamma g \to q\bar{q}$.
- Strong processes involving quarks and gluons of order $O(\alpha_{\rm s}^2)$ $qq' \to qq'$, $q\bar{q} \to q'\bar{q}'$, $q\bar{q} \to gg$, $qg \to qg$, $gg \to q\bar{q}$, $gg \to gg$.
- Nonperturbative QCD processes (elastic, diffractive scattering, normally at low transverse momentum).

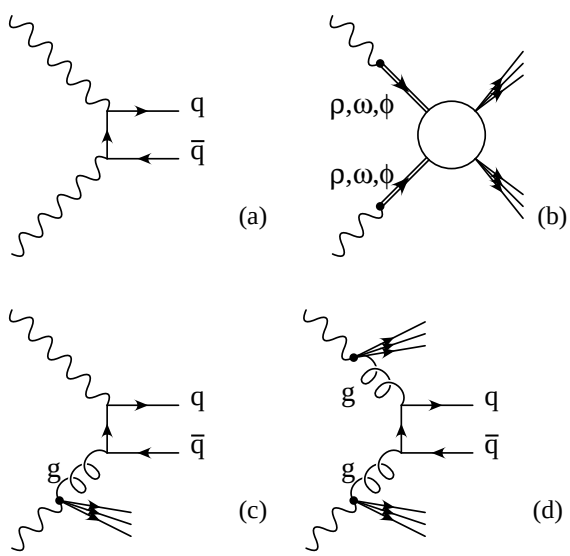

Fig. 8. *Diagrams showing the contribution to the $\gamma\gamma \to$hadron reaction: direct mechanism (a), vector meson dominance (b), single (c) and double (d) resolved photons.*

To describe those two-photon processes where quarks and gluons interact, one uses the structure function of the photon, which has been measured experimentally (see, e.g. [103,104]). The structure functions of the vector mesons are less well known, therefore the approximation $|\rho^0\rangle \approx |\pi^0\rangle \approx (|\pi^+\rangle + |\pi^-\rangle)/2$ is

often used, where the structure functions of pions are known [105]. Below we give the cross section formulae of the elementary processes within the leading order of the perturbative theory and describe some nonperturbative models, which involve photons.

3.2 Total $\gamma\gamma$ Cross Section

The main contributions to the total $\gamma\gamma$ collision comes from the strong interactions. The total cross section $\gamma\gamma \to$ hadrons can be parameterized in the form predicted by Regge theory

$$\sigma_{\rm tot}^{\gamma\gamma} \approx A\,(s/s_0)^{\epsilon} + B\,(s/s_0)^{-\eta}\,, \tag{57}$$

where s is the square of the invariant $\gamma\gamma$ mass, $s_0 = 1GeV^2$, and the exponents ϵ and η are universal parameters, that is, they are identical to those in γp, pp, but also πp total cross sections, corresponding to Pomeron and Reggeon exchange, respectively. The universal values for these exponents from a combined fit of all cross section are $\epsilon = 0.093(2)$ and $\eta = 0.358(15)$ [106].

This total cross section is an important input in the study of high energy e^+e^- collisions, see, e.g., the review of Peskin [107]. It is also interesting to understand what part comes from point-like processes and what part from soft processes involving the hadronic constituents of the photon. Eventually theory should explain, as well as, be constrained by the data of both $\sigma(\gamma\gamma)$ and $\sigma(\gamma p)$. As also done in [101] there are in general two fits to the total cross section data: one with PHOJET and the other one with the PYTHIA event generators. They differ substantially, and this is due to the fact that about 40% of the cross-section is unobserved at LEP and that theoretical models differ considerably in the size of the contribution from these very soft events.

The best fitted values *before LEP2* were as follows [102]:

$$A \approx 211\text{nb}, \quad B \approx 297\text{nb}, \quad \epsilon \approx 0.0808, \quad \eta \approx 0.4525. \tag{58}$$

The L3 collaboration recently made a measurement of the total hadron cross-section for photon-photon collisions in the interval $5GeV < W_{\gamma\gamma} < 185GeV$ [108,101]. Fitting the data up to 65 GeV, it was found that the $\gamma\gamma \to$hadrons cross-section is consistent with the universal Regge behavior of total hadronic cross-sections. Values of

$$A = 173 \pm 7\text{nb}, \quad B = 519 \pm 125\text{nb}, \quad \epsilon = 0.0790, \quad \eta = 0.4678 \tag{59}$$

were given in [108] (where the values of ϵ and η had been held fixed). Their cross section were found to be in agreement with the universal values of η and ϵ.

Using the larger invariant mass range up to 185 GeV in [101] a deviation from the universal value for ϵ was found. Fitting the data with $\eta = 0.358$ fixed gave values of

$$A = 59 \pm 10\text{nb}, \quad B = 1020 \pm 146\text{nb}, \quad \epsilon = 0.225 \pm 0.021, \tag{60}$$

that is a value for ϵ more than twice as large as the universal one. This large exponent was also found to be independent of the Monte Carlo model used to correct the data.

3.3 Charged Fermion Pair Production

For the invariant mass of the $\gamma\gamma$ system above the threshold $\sqrt{s} > 2m_f$ a fermion (lepton or quark) pair can be produced in two-photon collision. In lowest order of QED this process is shown in Fig.9. The differential cross

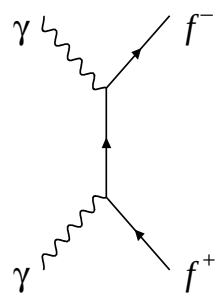

Fig. 9. Process $\gamma\gamma \to f^+f^-$ in the lowest order QED.

section of the process $\gamma\gamma \to f^+f^-$ in the c.m. system is given by the equation [109,110]

$$\frac{d\sigma}{d\cos\theta}(\gamma\gamma \to f^+f^-) = \frac{e^4\beta Q_f^4 N_c}{8\pi s}\frac{1 + 2\beta^2(1-\beta^2)(1-\cos^2\theta) - \beta^4\cos^4\theta}{(1-\beta^2\cos^2\theta)^2}, \tag{61}$$

where Q_f is a fermion charge in units of electron charge, N_c in a number of colors, $\beta = \sqrt{1 - 4m_f^2/s}$ is the velocity of the fermion in the $\gamma\gamma$ rest frame. The integral cross section of this process is

$$\sigma(\gamma\gamma \to f^+f^-) = \frac{4\pi\alpha^2 Q_f^4 N_c}{s}\beta\left[\frac{3-\beta^4}{2\beta}\ln\frac{1+\beta}{1-\beta} - 2 + \beta^2\right]. \tag{62}$$

The dependence of the integral cross section on the ratio of the fermion mass to the beam energy in the c.m. system, $2m_f/\sqrt{s}$ is shown in Fig.10.

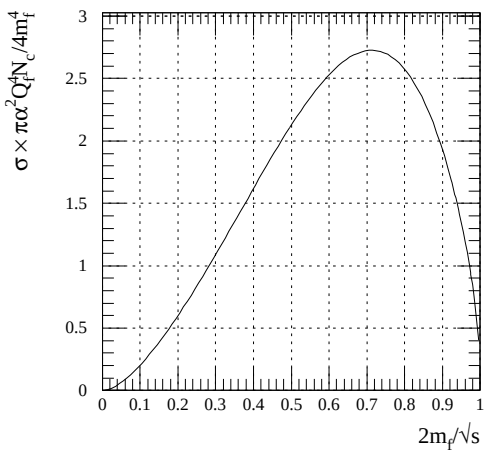

Fig. 10. Dependence of the process $\gamma\gamma \to f^+f^-$ cross section on $2m_f/\sqrt{s}$.

The production of fermion pairs in two-photon collisions can be used to study the coupling of s-, c- and b-quarks to photons and to study the fragmentation of these quarks into K, D and B mesons, because these processes are clean from hadronic background. To normalize the two-photon luminosity the process $\gamma\gamma \to \mu^+\mu^-$ can be used as it is easy to observe and simple to calculate [35,111,112]. In Table 2 production cross section of $\mu^+\mu^-$, $s\bar{s}$, $c\bar{c}$ and $b\bar{b}$ are shown in different invariant mass intervals in collisions of various species of ions at the RHIC and LHC. Figure 15 shows cross section and event rates for the LHC.

f^+f^-	Mass range, GeV	$\sigma(AA \to AA + f^+f^-)$ μb		
		AuAu	CaCa	PbPb
$\mu^+\mu^-$	$1 < W < 10$	280	730	$1.1 \cdot 10^5$
$s\bar{s}$	$1 < W < 10$	7.6	20	$3.1 \cdot 10^3$
$c\bar{c}$	$3.7 < W < 10$	$1.5 \cdot 10^{-2}$	6.2	790
$b\bar{b}$	$10.6 < W < 20$	—	$1.3 \cdot 10^{-2}$	1.2

Table 2
Production cross sections of fermion pairs in two-photon interactions in AuAu collisions at $\sqrt{s_{AA}} = 100$ GeV per nucleon at the RHIC, as well as in CaCa and PbPb collisions at $\sqrt{s_{AA}} = 7.2$ TeV per nucleon $\sqrt{s_{AA}} = 5.5$ TeV per nucleon at the LHC.

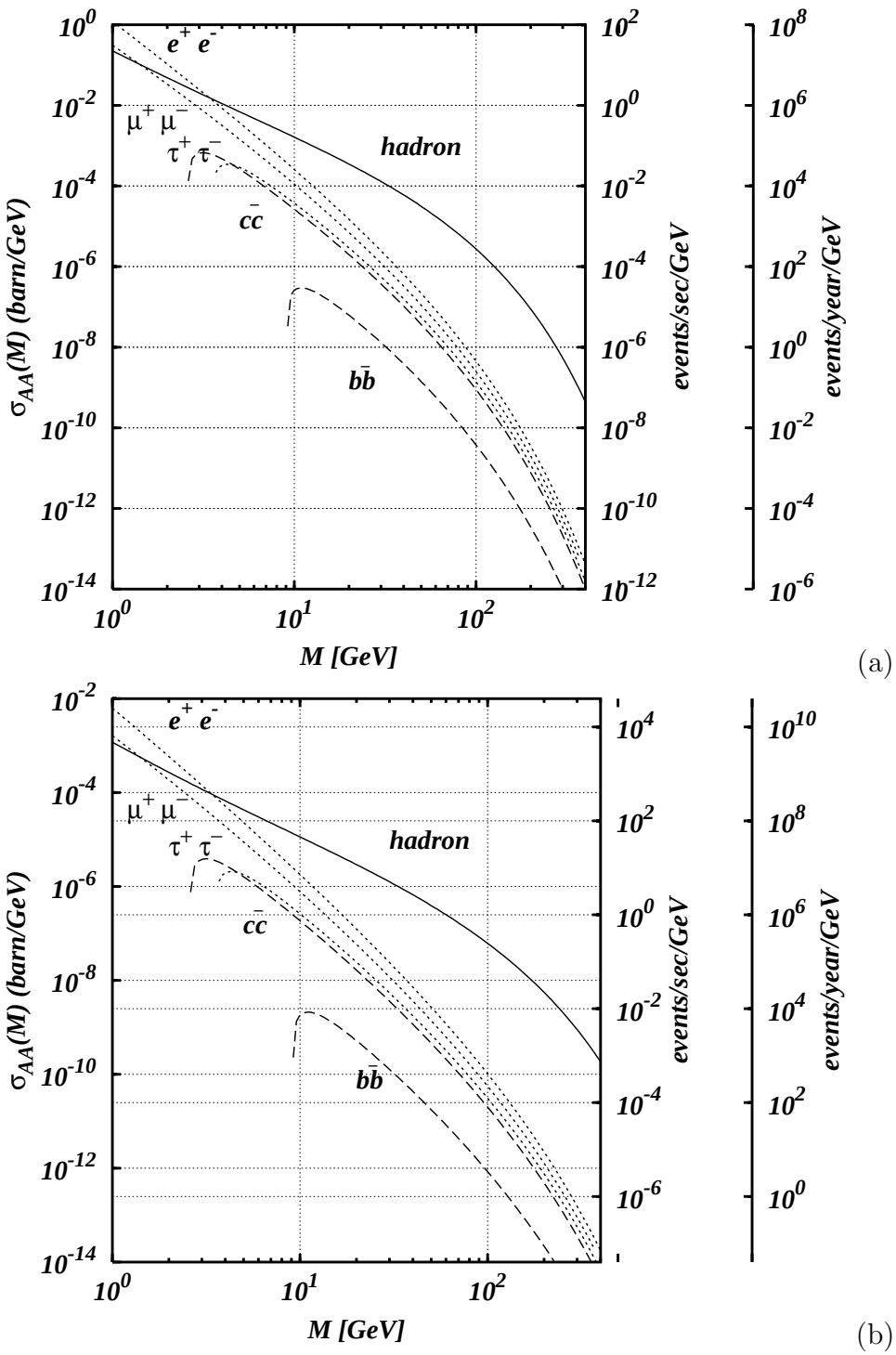

Fig. 11. Cross section per GeV for different charged fermion pair production at the LHC for PbPb (a) and CaCa (b) collisions, using the lowest order QED cross section. Also shown is the total rate for $\gamma\gamma \to$hadrons, see Eq. (57). Also shown are event rates per s and per (10^6) year.

3.4 W^+W^--Pair Production

If the energy of the two-photon collision is higher than twice the mass of $W^\pm$, the process $\gamma\gamma \to W^+W^-$ is possible. This process involves the gauge

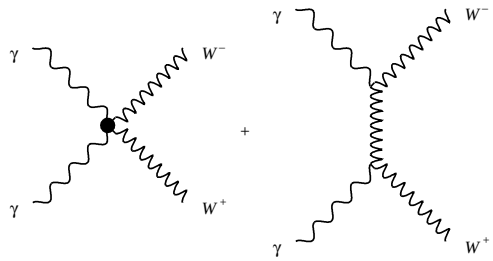

Fig. 12. Process $\gamma\gamma \to W^+W^-$ in the lowest order.

couplings of these gauge bosons . The lowest order graphs are shown in Fig. 12. The differential cross section of this process is given by

$$\frac{d\sigma}{d\cos\theta}(\gamma\gamma \to W^+W^-) = \frac{\pi\alpha^2\beta}{s}\frac{19 - 6\beta^2(1-\beta^2) + 2(8-3\beta^2)\beta^2\cos^2\theta + 3\beta^4\cos^4\theta}{(1-\beta^2\cos^2\theta)^2}, \tag{63}$$

with the same notations as those in Eq. (61). The integral cross section is [113]

$$\sigma(\gamma\gamma \to W^+W^-) = \frac{\pi\alpha^2}{s}\beta\left[-3\frac{1-\beta^4}{\beta}\ln\frac{1+\beta}{1-\beta} + 2\frac{22-9\beta^2+3\beta^4}{1-\beta^2}\right]. \tag{64}$$

The magnetic moment, as well as, the quadrupole moment of the W are fixed in the standard model, for the more general case of a magnetic moment different from the one given by the standard model see also [114].

Fig. 13 shows the dependence of the integral cross section on the ratio of a $W^\pm$ mass to the beam energy in the c.m. system, $2m_W/\sqrt{s}$. For example, the cross

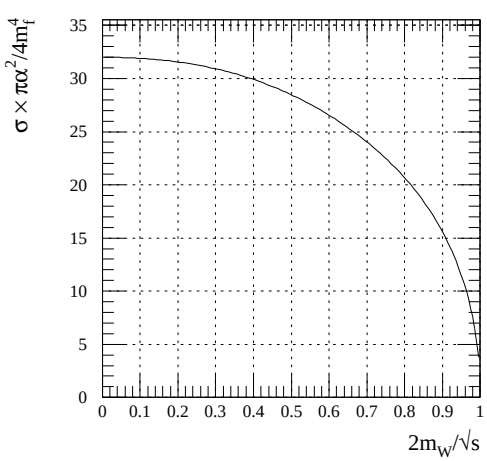

Fig. 13. The process $\gamma\gamma \to W^+W^-$ cross section as function of $2m_W/\sqrt{s}$.

section estimates of the W^+W^- production in CaCa and PbPb collisions at the LHC energies are $\sigma(AA \to AA + W^+W^-) = 29$ pb and 190 pb, respectively.

3.5 Vector Meson Pair Production

Among the nonperturbative processes in photon-photon interactions there is the exclusive vector-meson pair production. There are various mechanisms to produce hadrons in such collisions, recall the discussion about the nature of the photon above. According to this idea, vector meson pair production is explained to happen in the following way: both photons fluctuate first into a vector meson (ρ, ω, ϕ, J/ψ and so on, the VMD component). These vector mesons then scatter elastically to produce the (real) vector meson pair in the final state. The study of these processes allows a test of the Pomeron-exchange factorization relation, see [115,116]. If the exchange of a single Pomeron dominates in these processes, the factorization relation among pp, $p\gamma$ and $\gamma\gamma$ collisions predicts

$$[\sigma_{\rm tot}(\gamma p)]^2 = \sigma_{\rm tot}(pp) \times \sigma_{\rm tot}(\gamma\gamma). \tag{65}$$

As for the available experimental data there exist measurements of the production cross section of vector meson pairs $\rho^0\phi$ in $\gamma\gamma$-interactions by the ARGUS [117] and $\rho\rho$ by the L3 [118,119] collaboration. These data were compared with the cross section estimate of the reaction $\gamma\gamma \to VV'$ ($V, V' = \rho^0, \phi$) based on the Pomeron factorization model and all possible combinations of the existing sets of data on the reactions $\gamma p \to Vp$ and $pp \to pp$ [120,121]. A strong discrepancy between the existing experimental data (by order of magnitude) and the factorization model prediction was found. These estimates are in good agreement with independent calculations in [102]. Thus we come here to the puzzling situation: why does one of the most well-grounded phenomenological models predict cross sections, which are larger by order of magnitude in the reaction $\gamma\gamma \to VV'$ compared to those measured in the experiments? One explanation proposed in [121] is that we face here a new "*defiant phenomenon in the formation mechanism of the Pomeron exchange for quasi-two-body reactions*".

The production of vector meson pairs can well be studied at RHIC with high statistics in the region of up to several GeV [9]. In connection with the above mentioned puzzle the results from the STAR would be quite desirable and interesting. For the possibilities at LHC, we refer the reader to [24] and [22], where also experimental details and simulations are given.

3.6 Resonance Production

One may say that photon-photon collisions provide an independent view on meson and baryon spectroscopy. They provide powerful information on both

the flavor and spin/angular momentum internal structure of the mesons. Much has already been done at e^+e^- colliders. Light quark spectroscopy is very well possible at RHIC, benefitting from the high $\gamma\gamma$-luminosities. Detailed feasibility studies exist [9,46–48]. In these studies, $\gamma\gamma$ signals and backgrounds from grazing nuclear and beam gas collisions were simulated with both the FRITIOF and VENUS Monte Carlo codes. The possibilities to produce these mesons at the LHC have been discussed in detail in the FELIX LoI [24]. Rates are given and possible triggers are discussed. The general conclusion is that all these processes are very promising tools for meson spectroscopy.

In two-photon collisions with real photons general symmetry requirements restrict the possible final states, as is well known from the Landau-Yang theorem [122]. Especially it is impossible to produce spin 1 final states. Only resonance states with positive C-parity can be produced, such as $J^{PC} = 0^{-+}$, 0^{++}, 2^{++}, $\cdots$. Two photon collisions therefore give access to most of the $C = +1$ mesons. In e^+e^- annihilation on the other hand only states with $J^{PC} = 1^{--}$, that is, with odd C-parity can be produced directly.

In principle $C = -1$ vector mesons can be produced by the fusion of three (or, even less important, five, seven, ...) equivalent photons. This cross section scales with Z^6. But it is smaller than the contribution coming from γ-A collisions, as discussed in Chap. 5, even for nuclei with large Z (see also [15] and the corresponding discussion for the positronium in Sec. 7.7).

The production cross section of the resonance is given by

$$\sigma_{\gamma\gamma\to R} = 8\pi(2J+1)\frac{\Gamma_{\gamma\gamma}\Gamma_{\rm tot}}{(W^2-M_R^2)^2+M_R^2\Gamma_{\rm tot}^2}, \tag{66}$$

where W is the $\gamma\gamma$ invariant mass , M_R is the mass of the resonance R, $\Gamma_{\gamma\gamma}$ and $\Gamma_{\rm tot}$ its two-photon and total width. For sufficiently narrow state ($\Gamma_{\rm tot} \ll M_R$) the expression (66) can be approximated by

$$\lim_{\Gamma_{\rm tot}/M_R\to 0} \sigma_{\gamma\gamma\to R} = 4\pi^2(2J+1)\frac{\Gamma_{\gamma\gamma}}{M_R^2}\,\delta(W-M_R). \tag{67}$$

This makes it easy to calculate the production cross-section $\sigma_{AA\to AA+R}$ of a particle in terms of its basic properties.

In this case the production cross section of a resonance in heavy ion collisions factorizes, according to equation (9), to

$$\sigma(AA\to AA+R) = 4\pi^2(2J+1)\frac{\Gamma_{\gamma\gamma}}{M_R^2}\,\frac{dL_{\gamma\gamma}}{dW}\bigg|_{W=M_R}, \tag{68}$$

i.e., it is given only by its two-photon width and the value of the $\gamma\gamma$-luminosity function at its resonance mass.

In Fig. 14 the function $4\pi^2 dL_{\gamma\gamma}/dW/W^2$, which is universal for a produced resonances, is plotted for various systems. It can be directly used to calculate the cross-section for the production of a resonance R with Eq. (68).

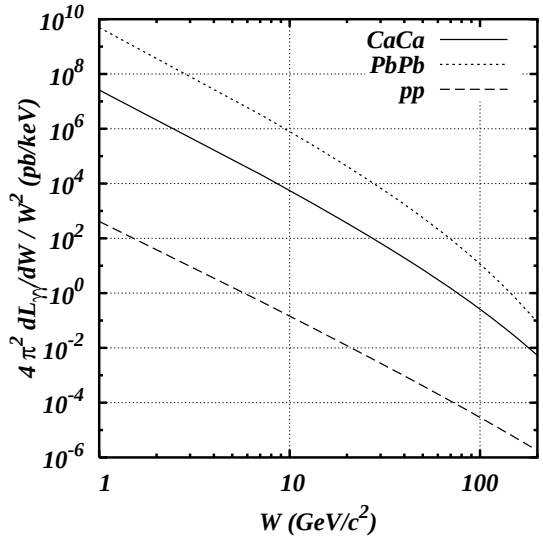

Fig. 14. *The universal function* $4\pi^2 dL_{\gamma\gamma}/dW/W^2$ *is plotted for different ion species at LHC. We use* $R = 1.2 \times A^{1/3}$ *fm and* $\gamma = 2950$, 3750 *and* 7000 *for PbPb, CaCa and pp collisions, respectively.*

3.6.1 Quarkonia

Among the interesting processes for resonance production is the study of the quarkonium states $c\bar{c}$ and $b\bar{b}$ such as $\eta_{c(b)}$ $(^1S_0)$, $\chi_{c(b)0}$ $(^3P_0)$, $\chi_{c(b)2}$ $(^3P_2)$ with the aim of measuring their two-photon widths, and therefore to test quarkonium models, as well as, studying their decay modes. Production of light $q\bar{q}$ states, like π^0, η and η', whose widths are well-known, can be used for calibration.

In the nonrelativistic quarkonium model of [123], which takes into account first-order QCD terms, analytical expressions for gluon, lepton and photon widths of various quarkonium states are obtained.

In Table 3 these expressions for states with even total angular momentum are given, as well as, those for the vector state $^3S_1$ for normalization. In these expressions Q denotes the electric charge of a quark, constituting the quarkonium, M is the quarkonium mass, and m_q the quark mass. For the quark masses we use $m_c = 1.5$ GeV, $m_b = 4.8$ GeV. The strong coupling constant α_s is derived from the relation between the total and partial widths of the decay of the known states. Comparison with experimental data gives [123]

Process	Width	Correction $O(\alpha_s)$
${}^1S_0 \to \gamma\gamma$	$12\pi Q^4 \alpha_{em}^2 \lvert\Psi(0)\rvert^2/m_q^2$	$1 - 3.4\alpha_s/\pi$
${}^1S_0 \to gg$	$8\pi\alpha_s^2 \lvert\Psi(0)\rvert^2/3m_q^2$	$1 + 4.8\alpha_s/\pi \quad (\eta_c)$
		$1 + 4.4\alpha_s/\pi \quad (\eta_b)$
${}^3S_1 \to e^+e^-$	$16\pi Q^2 \alpha_{em}^2 \lvert\Psi(0)\rvert^2/M^2$	$1 - 16\alpha_s/3\pi$
${}^3S_1 \to ggg$	$40(\pi^2 - 9)\alpha_s^3 \lvert\Psi(0)\rvert^2/81m_q^2$	$1 - 3.7\alpha_s/\pi \quad (J/\psi)$
		$1 - 4.9\alpha_s/\pi \quad (\Upsilon)$
${}^3P_0 \to \gamma\gamma$	$27Q^4 \alpha_{em}^2 \lvert R'_{nP}(0)\rvert^2/m_q^4$	$1 + 0.2\alpha_s/\pi$
${}^3P_0 \to gg$	$6\alpha_s^2 \lvert R'_{nP}(0)\rvert^2/m_Q^4$	$1 + 9.5\alpha_s/\pi \quad (\chi_{c0})$
		$1 + 10.0\alpha_s/\pi \quad (\chi_{b0})$
${}^3P_2 \to \gamma\gamma$	$36Q^4 \alpha_{em}^2 \lvert R'_{nP}(0)\rvert^2/5m_q^4$	$1 - 16\alpha_s/3\pi$
${}^3P_2 \to gg$	$8\alpha_s^2 \lvert R'_{nP}(0)\rvert^2/5m_q^4$	$1 - 2.2\alpha_s/\pi \quad (\chi_{c2})$
		$1 - 0.1\alpha_s/\pi \quad (\chi_{b2})$

Table 3
Quarkonia decay widths in the nonrelativistic model. Adapted from [123].

$\alpha_s(m_c) = 0.19$, $\alpha_s(m_b) = 0.17$. The unknowns are the value of the wave functions at the origin $\Psi(0)$ and $R'_{nP}(0)$.

Assuming that the wave function $\Psi(0)$ is the same for all $1S$ states, and equal to those in Table 3, the width ratio of $J/\psi(\Upsilon)$ (1^3S_1) to η_c (η_b) (1^1S_0) can be calculated:

$$\frac{\Gamma(1^3S_1 \to e^+e^-)}{\Gamma(1^1S_0 \to \gamma\gamma)} = \frac{1}{3Q^2}\left(\frac{2m_q}{M}\right)^2\left(1 - 1.9\frac{\alpha_s}{\pi}\right). \tag{69}$$

This ratio for J/ψ and η_c is equal to 0.74, in perfect agreement with the experimental result 0.71 ± 0.14 [106]. Therefore, one can predict two-photon width of the η_b from the lepton width of the $\Upsilon(1S)$. The ratio of the total and two-photon width of the η_b is obtained analogously, assuming that the two-gluon decay dominates:

$$\frac{\Gamma(\eta_b \to gg)}{\Gamma(\eta_b \to \gamma\gamma)} = \frac{2\alpha_s^2}{9\alpha_{em}^2 Q^2}\left(1 + 7.8\frac{\alpha_s}{\pi}\right). \tag{70}$$

Using the experimental lepton decay width $\Gamma(\Upsilon(1S) \to e^+e^-) = 1.32$ keV [106], one obtains from Eqs. (69) and (70) the total and the two-photon widths

of the η_b:

$$\Gamma_{\rm tot}(\eta_b) = 6 \text{ MeV}, \qquad \Gamma_{\gamma\gamma}(\eta_b) = 0.43 \text{ keV}. \tag{71}$$

P-states of bottomonium are not yet studied, therefore predictions of their total and partial widths cannot be obtained from a comparison of experimental data. In [124] lattice calculations give a value for the wave function of the $1P$-state of bottomonium at the origin $|R'_{1P}(0)|^2 = 0.75$ GeV^5. These calculations allows to define total and two-photon widths of the χ_{b0} and the χ_{b2} from the analytical expression of Table 3:

$$\Gamma_{\rm tot}(\chi_{b0}) = 0.24 \text{ MeV}, \qquad \Gamma_{\gamma\gamma}(\chi_{b0}) = 25 \text{ eV}, \tag{72}$$

$$\Gamma_{\rm tot}(\chi_{b2}) = 65 \text{ keV}, \qquad \Gamma_{\gamma\gamma}(\chi_{b2}) = 6.7 \text{ eV}. \tag{73}$$

For charmonium production, the two-photon width $\Gamma_{\gamma\gamma}$ of the η_c (2960 MeV, $J^{PC} = 0^{-+}$) is known from experiment [106]. But the two-photon widths of the P-wave charmonium states have been measured only with modest accuracy. Two photon widths of P-wave charmonium states can be estimated following the PQCD approach of [124]. Similar predictions of the bottomonium two-photon widths can be found in [123]. For RHIC the study of η_c is a real challenge [46]; the luminosities are falling strongly with increasing $\gamma\gamma$ mass and the branching ratios to experimentally interesting channels are small.

In Table 4 (adapted from Table 2.6 of [24]) properties of some $q\bar{q}$ states are given, and their production cross sections are predicted, where possible. Similarly an overview of different rates is also given in Fig. 11 for both PbPb and CaCa collisions at the LHC. The results for AuAu collisions at RHIC and PbPb collisions at LHC are done on the basis of [31] and from calculations of the program Tphic [54]. Mass values and known widths are taken from [106], bottomonium widths are used from Eqs. (71) to (73). Also given is the number of events in a 10^6s run. Ion luminosities of 2×10^{26}cm^{-2}s^{-1} for AuAu collisions at RHIC and 4×10^{30}cm^{-2}s^{-1} for CaCa and 10^{26}cm^{-2}s^{-1} for PbPb collisions at LHC are used. Millions of C-even charmonium states will be produced in coherent two-photon processes during a standard 10^6s heavy ion run at the LHC. The detection efficiency of the charmonium events has been estimated to be about 5% for the forward-backward FELIX geometry [24], i.e., one can expect the detection of about 5×10^3 charmonium events in PbPb and about 10^6 events in CaCa collisions. This is two to three orders of magnitude higher than what is expected during the five years of LEP200 operation. Experiments with a well-equipped central detector like CMS on the other hand should have a much better efficiency. Further details — also on experimental cuts, backgrounds and the possibilities for the study of C-even bottomonium states — are given in [24].

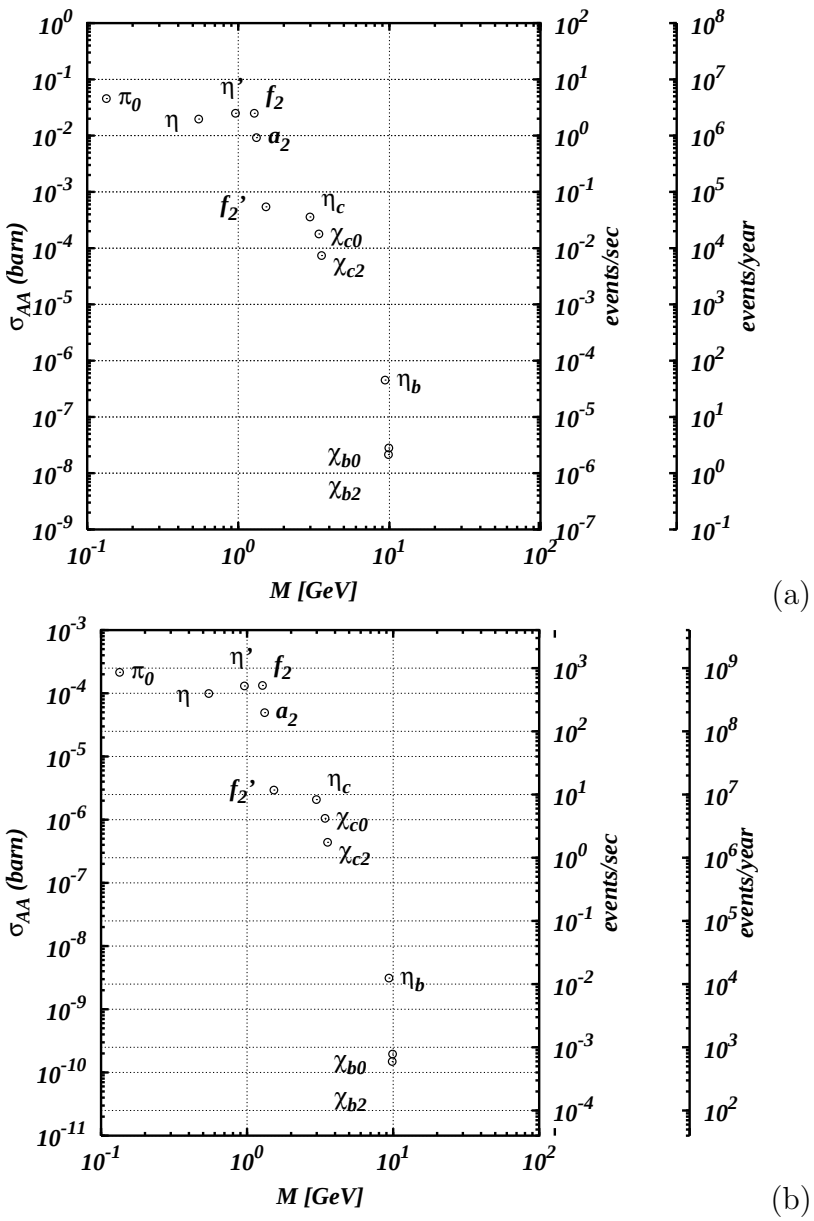

Fig. 15. Cross section for the production of different resonances at the LHC for PbPb (a) and CaCa (b) collisions, using the parameters of Table 4. Also shown are the event rates per s and per (10^6s) year.

3.7 Exotic Mesons

The two-photon width of a resonance is a probe of the charge of its constituents, so the magnitude of the two-photon coupling can serve to distinguish quark dominated resonances from glue-dominated resonances ("glueballs"). The absence of meson production via $\gamma\gamma$ fusion would therefore be one signal of great interest for glueball search. In $\gamma\gamma$ collisions a glueball can only be produced via the annihilation of a $q\bar{q}$ pair into a pair of gluons, whereas a

normal $q\bar{q}$-meson can be produced directly. Therefore we expect the ratio for the production of a glueball G compared to a normal $q\bar{q}$ meson M to be

$$\frac{\sigma(\gamma\gamma \to G)}{\sigma(\gamma\gamma \to M)} = \frac{\Gamma(G \to \gamma\gamma)}{\Gamma(M \to \gamma\gamma)} \sim \alpha_s^2, \tag{74}$$

where α_s is the strong interaction coupling constant. On the other hand glueballs are most easily produced in a glue-rich environment, for example, in radiative J/Ψ decays, $J/\Psi \to \gamma gg$. In this process we expect the ratio of the cross section to be

$$\frac{\Gamma(J/\Psi \to \gamma G)}{\Gamma(J/\Psi \to \gamma M)} \sim \frac{1}{\alpha_s^2}. \tag{75}$$

A useful quantity to describe the gluonic character of a mesonic state X is therefore the so called "stickiness" [125], defined as

$$S_X = \frac{\Gamma(J/\Psi \to \gamma X)}{\Gamma(X \to \gamma\gamma)}. \tag{76}$$

One expects the stickiness of all mesons to be comparable, while for glueballs it should be enhanced by a factor of about $1/\alpha_s^4 \sim 20$. In the recent work of [126] results for the search for $f_J(2220)$ production in two-photon interactions were presented. A very small upper limit for the product of $\Gamma_{\gamma\gamma} B_{K_s K_s}$ was given, where $B_{K_s K_s}$ denotes the branching ratio of its decay into $K_s K_s$. From this it was concluded that this is a strong evidence that the $f_J(2220)$ is a glueball.

Two-photon processes can also be used as a tool to observe mesons beyond the quark model. The $a_0(980)$ and $f_0(980)$ could be four-quark states $q\bar{q}q\bar{q}$ (or "quarktets") [127]. The ARGUS collaboration observed a $I^G(J^{PC}) = 2^+(2^{++})$ peak in the reaction $\gamma\gamma \to \rho\rho$ near threshold [128]. This state was called by PDG $X(1600)$ and also interpreted as a four-quark state.

For a rather general discussion of glueballs but also other (even more) exotic mesons like "quarktets", "hybrids" (or "centauros", made of a quark, an antiquark and a gluon) we refer to [129]. The QCD studies in $\gamma\gamma$ collisions at the CLEO detector were summarized recently by Savinov in [130]. Also the anti-search for glueballs is described.

J^{PC}	particle	M, MeV	$\Gamma_{\gamma\gamma}$, keV	$\Gamma_{\rm tot}$, MeV	$\sigma(AA \to AA + R)$			Production rate per 10^6-sec run		
					AuAu, $\gamma = 100$	PbPb, $\gamma = 3000$	CaCa, $\gamma = 3700$	AuAu, $\gamma = 100$	PbPb, $\gamma = 3000$	CaCa, $\gamma = 3700$
0^{-+}	π^0	135	$8 \cdot 10^{-3}$	$8 \cdot 10^{-6}$	5.0 mb	46 mb	210 μb	$1.0 \cdot 10^6$	$4.6 \cdot 10^6$	$8.4 \cdot 10^8$
0^{-+}	η	547	0.46	$1.2 \cdot 10^{-3}$	0.85 mb	20 mb	100 μb	$1.7 \cdot 10^5$	$2 \cdot 10^6$	$4.0 \cdot 10^8$
0^{-+}	η'	958	4.2	0.2	0.59 mb	25 mb	130 μb	$1.2 \cdot 10^5$	$2.5 \cdot 10^6$	$5.2 \cdot 10^8$
2^{++}	$f_2(1270)$	1275	2.4	185	0.41 mb	25 mb	133 μb	$8.2 \cdot 10^4$	$2.5 \cdot 10^6$	$5.2 \cdot 10^8$
2^{++}	$a_2(1320)$	1318	1.0	107	0.14 mb	7.7 mb	49 μb	$2.8 \cdot 10^4$	$7.7 \cdot 10^5$	$2.0 \cdot 10^8$
2^{++}	$f_2'(1525)$	1525	0.1	112	6.6 μb	0.45 mb	2.9 μb	$1.3 \cdot 10^3$	$4.5 \cdot 10^4$	$1.2 \cdot 10^7$
0^{-+}	η_c	2979	7.4	13.2	1.8 μb	0.54 mb	3.7 μb	360	$5.4 \cdot 10^4$	$1.6 \cdot 10^7$
0^{++}	χ_{c0}	3415	4.0	14.9	0.38 μb	0.17 mb	1.2 μb	76	$1.7 \cdot 10^4$	$4.8 \cdot 10^6$
2^{++}	χ_{c2}	3556	0.46	2.0	0.17 μb	85 μb	0.59 μb	34	$8.5 \cdot 10^4$	$2.4 \cdot 10^6$
0^{-+}	η_b	9366	0.43	6		0.32 μb	2.8 nb		32	$1.1 \cdot 10^3$
0^{++}	χ_{b0}	9860	$2.5 \cdot 10^{-2}$	0.24		15 nb	0.15 nb		1.5	600
2^{++}	χ_{b2}	9913	$6.7 \cdot 10^{-3}$	$6.5 \cdot 10^{-2}$		20 nb	0.18 nb		2.0	720

Table 4. Prediction of production cross section and rates for a 10^6 sec-run of some mesons at RHIC and LHC. Masses and widths for mesons except bottomonia are taken from [106], bottomonium widths are given from equations (71), (72) and (73). The beam luminosities used are $2 \cdot 10^{26}\mathrm{cm}^{-2}\mathrm{s}^{-1}$ for AuAu at RHIC, $10^{26}\mathrm{cm}^{-2}\mathrm{s}^{-1}$ for PbPb and $4 \times 10^{30}\mathrm{cm}^{-2}\mathrm{s}^{-1}$ for CaCa at LHC

4 Two-Photon Collisions as a Tool for the Search of New Physics

The large photon-photon luminosity and the high invariant mass range make two-photon collisions at heavy ion colliders also of interest for the search for new particles and new physics. This includes the possible production of the Higgs-boson in the $\gamma\gamma$-production channel (unfortunately, this possibility is only marginal, see below) or new physics beyond the standard model, like supersymmetry or compositeness. Many studies for different extensions of the standard model have been performed. In the following the conclusions of some of these studies will be summarized, further discussions can also be found in [16].

Before doing this we mention the plans to build a future e^+e^- linear collider. Such a linear colliders will be used for e^+e^-, $e\gamma$ and $\gamma\gamma$-collisions (PLC, "photon linear collider"). The photons will be obtained by the scattering of laser photons (of eV energy) on high energy electrons (up to the TeV region), see [131]. These photons in the TeV energy range will be roughly monochromatic and polarized. The physics program at such future machines was discussed , e.g., in [132,133]; it includes Higgs boson and gauge boson physics and the discovery of new particles. A recent review can be found in Parts 3 and 6 of [134]. The physics topics reach from Higgs boson physics to supersymmetry and extra dimensions. Such a collider will provide a rather clean environment for physics in a new energy region. This is of interest for the (far) future, whereas the LHC and its detectors are built at present.

In [71,72] $\gamma\gamma$-processes at pp colliders (LHC) are studied. It is observed there that non-strongly interacting supersymmetric particles (sleptons, charginos, neutralinos, and charged Higgs bosons) are difficult to detect in hadronic collisions at the LHC. The Drell-Yan and gg-fusion mechanisms yield low production rates for such particles. Therefore the possibility of producing such particles in $\gamma\gamma$ interactions at hadron colliders is examined. Since photons can be emitted from protons which do not break up in the radiation process, clean events can be generated which should compensate for the small production number. In [71] it was pointed out that at the high luminosity of $L = 10^{34}\mathrm{cm}^{-2}\mathrm{s}^{-1}$ at the LHC(pp), one expects about 16 minimum bias events per bunch crossing. Even the elastic $\gamma\gamma$ events will therefore not be free of hadronic debris. Clean elastic events will be detectable at luminosities below $10^{33}\mathrm{cm}^{-2}\mathrm{s}^{-1}$. This danger of "overlapping events" has also to be checked for the heavy ion runs, but it will be much reduced due to the lower luminosities.

Similar considerations for new physics were also made in connection with the proposed eA collider at DESY (Hamburg). Again, the coherent field of a nucleus gives rise to a Z^2 factor in the cross-section for photon-photon processes in eA collisions [135,136].

Two-photon collisions allow to study the production of particles beyond the Standard Model. Here we consider the processes of chargino, slepton and charged Higgs pair production in the frame of the minimal supersymmetric standard model (MSSM) [137].

Charginos are coupled to photons as standard fermions of spin 1/2, and therefore the cross section of the process $\gamma\gamma \to \tilde{\chi}_1^+\tilde{\chi}_1^-$ is described by Eqs. (61) and (62) with $Q_f = 1$ and $N_c = 1$. Following [138] we assume R-parity conservation, i.e. continuity of supersymmetric lines. We take the chargino $\tilde{\chi}_1^\pm$ as the lightest observable supersymmetric particle and the neutralino $\tilde{\chi}_1^0$ as the lightest supersymmetric particle. Thus, it is not observable. Sleptons, squarks and gluinos are assumed to be much heavier than the $\tilde{\chi}_1^\pm$. All parameters of the supersymmetry breaking can be taken as real, i.e., CP-parity violation does not take place in the chargino processes. All these assumptions result in the fact that the $\tilde{\chi}_1^\pm$ decays to neutralino $\tilde{\chi}_1^0$ and a weak duplet of fermions via a virtual $W^\pm$, or via a sfermion $\tilde{f}^\pm$ or Higgs $H^\pm$: $\tilde{\chi}_1^+ \to (\tilde{\chi}_1^0 W^{+*}, \tilde{f}_i^* \bar{f}_j, \tilde{\chi}_1^0 H^{+*}) \to \tilde{\chi}_1^0 f_i \bar{f}_j$.

Experimental search for supersymmetric particles impose limits on their masses [106]. The lightest neutralino $\tilde{\chi}_1^0$ was not found at the mass $m < 32.5$ GeV. The chargino $\tilde{\chi}_1^\pm$ mass is bound by $m > 67.7$ GeV. This restricts the possibility to search for the processes of the chargino pair production in two-photon interactions at heavy ion colliders, since the invariant mass of the two-photon system must be above 130 GeV, while the spectrum of the $\gamma\gamma$-system at LHC is limited essentially to $W_{\gamma\gamma} \approx 200$ GeV (see Eq. (3)).

Cross sections of the chargino pair production vs. their mass in two-photon interactions in *Pb-Pb* and *Ca-Ca* collisions at LHC are shown in Fig. 16. The results are obtained with the program Tphic [54].

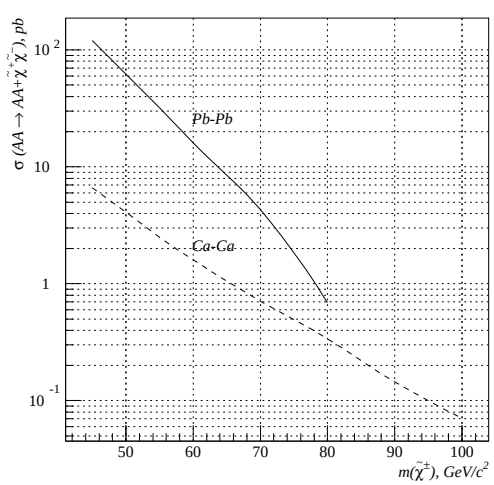

Fig. 16. Production cross section of $\tilde{\chi}_1^+\tilde{\chi}_1^-$ in *Pb-Pb* and *Ca-Ca* collisions at $\sqrt{s_{AA}} = 5.5$ and 7.2 TeV per nucleon respectively.

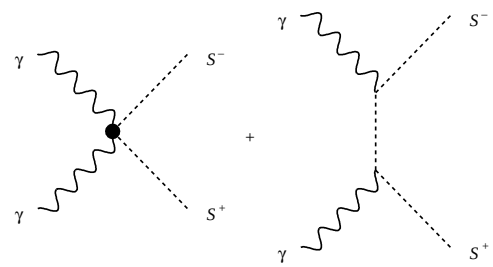

Fig. 17. Process $\gamma\gamma \to S^+S^-$ in the leading order, $S^\pm$ is either a slepton $\tilde{l}^\pm$, or charged Higgs $H^\pm$.

When the mass of sleptons $\tilde{l}^\pm$ and charged Higgs $H^\pm$ are not too high, their pairs can also be produced in the two-photon interactions. Sleptons and Higgs are scalar particles and the differential cross sections of the processes $\gamma\gamma \to \tilde{l}^+\tilde{l}^-$ and $\gamma\gamma \to H^+H^-$:

$$\frac{d\sigma(\gamma\gamma \to S^+S^-)}{d\cos(\theta)} = \frac{\pi\alpha^2}{s}\beta\left[1 - \frac{2\,(1-\beta^2)}{1-\beta^2\cos^2(\theta)} - \frac{2\,(1-\beta^2)^2}{(1-\beta^2\cos^2(\theta))^2}\right], \quad (77)$$

as well as, the total cross section

$$\sigma(\gamma\gamma \to S^+S^-) = \frac{4\pi\alpha^2}{s}\beta\left[2 - \beta^2 - \frac{1-\beta^4}{2\beta}\ln\frac{1+\beta}{1-\beta}\right]. \quad (78)$$

are well known, see [139,72]. Fig. 18 shows how the integral cross section depends on the ratio of a $S^\pm$ mass to the beam energy in c.m. system, $2m_S/\sqrt{s}$. Comparing this plot with the cross section behavior of fermions (Fig. 10 for

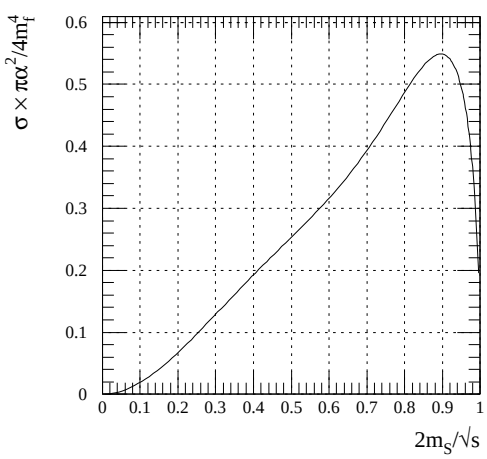

Fig. 18. The $\gamma\gamma \to S^+S^-$ cross section as a function of $2m_S/\sqrt{s}$.

$N_c = 1$, $Q_f = 1$) shows that the yield of supersymmetric scalars is lower than that of charginos.

The search for sleptons and charged Higgs imposes a lower limit on their mass $m(H^{\pm}) > 69.0$ GeV, $m(\tilde{l}^{\pm}) > 67.1$ GeV [106].

Recent (unpublished) studies done for FELIX and ALICE show that the chargino pair production can be detectable, if the lightest chargino would have a mass below 60 GeV. Unfortunately the chargino mass limits set recently by LEP experiments already exclude the existence of charginos below 67.7 GeV with 95% confidence level [106]. Therefore the observation of MSSM-particles in $\gamma\gamma$-interactions in heavy ion collisions seems to be hard to achieve. CMS on the other hand should be more suited for these observations.

4.2 Higgs Search

One of the most important tasks in present high energy physics is the discovery and the study of the properties of the Higgs boson. In this respect, the $\gamma\gamma$ production of the Higgs boson is of special interest.

There are a number of calculations of the $\gamma\gamma$ production of a medium heavy standard model Higgs [73,140,31,141,142]. For masses $m_H < 2m_{W^{\pm}}$ the Higgs boson decays dominantly into $b\bar{b}$. In [141] a comparison of $gg \to H$ and $\gamma\gamma \to H$ emphasized the favorable signal to background ratio for the latter process. Unfortunately, at the LHC a heavy ion year consists only of the order of 10^6 s instead of the assumed 10^7 s. Chances of finding the standard model Higgs in this case are marginal [22].

The search for anomalous Higgs couplings in peripheral heavy ion collisions at the LHC was studied by Lietti et al. [143]. They consider corrections to the standard model from new physics associated with a high energy scale Λ. It is concluded that "*limits for anomalous Higgs couplings which can be obtained in peripheral heavy ion collisions at the LHC via electromagnetic processes are one order of magnitude tighter than the limits that can be obtained in the upgraded Tevatron and comparable to limits coming from the pp mode of the LHC.* For further details we refer to this paper.

An alternative scenario with a light Higgs boson was, e.g., given in [144] in the framework of the "general two Higgs doublet model". Such a model allows for a very light particle in the few GeV region. With a mass of 10 GeV, the $\gamma\gamma$-width is about 0.1 keV. The authors of [144] proposed to look for such a light neutral Higgs boson at the proposed low energy $\gamma\gamma$-collider. We want to point out that the LHC CaCa heavy ion mode would also be very suitable for such a search. A systematic parameter study of the production of Higgs bosons in the minimal supersymmetric extension of the standard model (MSSM) was done in [145]. For certain values of the free parameters in enhancement of the cross section of up to a factor 10 was found.

In [76] it was shown how to tag two-photon production in pp collisions at the LHC, see Fig. 4 there. It was concluded that "*the significant luminosity of the tagged two-photon collisions opens an exciting possibility of studying the exclusive production of the Higgs boson as well as search for new phenomena.*"

Last year all 4 LEP experiments have reported on their Higgs search in the data collected during the LEP-II run. All of them set their new lower limits on the Higgs mass which are $M_H > 107.0$ GeV (L3), 109.7 GeV (OPAL), 110.6 GeV (ALEPH), 114.3 GeV (DELPHI) at 95% CL [146–149]. However, the likelihood analysis shows a preferences for a Higgs boson with a mass of 115.6 GeV.

In the Standard Model the arguments of self-consistency of the theory can be used to obtain upper and lower limits on the Higgs mass. The upper limit is obtained from arguments of perturbative continuation to the GUT scale up to $\Lambda_{GUT} = 10^{16}$ GeV [150], i.e., from the requirement that the electroweak interaction would be still "weak" up to this energy scale. The high-energy behavior of the weak interaction was discussed also in a more general framework [151,152]. A lower limit for the Higgs mass is obtained from quantum corrections involving top-loops to the Higgs interaction potential [153–157]. Thus it appears that the requirement of self-consistency of the SM up to 10^{16} GeV leads to the theoretical limits for the Higgs mass of 130 GeV $< M_{H^o} <$ 190 GeV (to be compared with the lower mass limits of $M_H > 107.0 - 114.3$ GeV at LEP, see above). This range is just the mass range acceptable for the Higgs production in two-photon processes of CaCa collisions at the LHC.

4.3 Search for Extra Dimensions

Graviton production in very peripheral heavy-ion collisions was recently studied theoretically in [158]. Such a possibility has recently become of interest due to a new class of theoretical models, for further explanations see, e.g., Chap. 6 of [107]. In these models quantum gravity and string physics may become accessible to experiment; they may even appear directly in the realm of LHC and the linear colliders. Graviton production in $\gamma\gamma$ collisions can be calculated in such models. It depends on a fundamental gravity scale M which is related to the scale R at which the Newtonian inverse-square law is expected to fail (see, e.g., Eq. (25) of [107]). Cross sections for graviton production in heavy ion collisions were found to be substantially greater than for graviton production in e^+e^- collisions [158]. A value of $M = 1TeV$ was assumed in those calculations. The signature for such a process would be a large missing mass in the reaction. In the heavy ion case this is hard to realize experimentally and the authors conclude that "*a definite experimental signature cannot*

be predicted". For further details we refer to this paper.

4.4 Search for Heavy Point-like Dirac Monopoles

In [34] it was proposed to search for heavy magnetic monopoles in $\gamma\gamma$ collisions at hadron colliders like the Tevatron and LHC. The idea is that photon-photon scattering $\gamma\gamma \to \gamma\gamma$ below the monopole production threshold is enhanced due to the strong coupling of magnetic monopoles to photons. The magnetic coupling strength g is given by $g = \frac{2\pi n}{e}$ where $n = \pm 1, \pm 2, ...$ Since $\frac{e^2}{4\pi} = 1/137$ the magnetic coupling strength is indeed quite large. In this reference differential cross sections for $\gamma\gamma$ scattering via the monopole loop are calculated for energies below the monopole production threshold. The result depends strongly on the assumed value of the spin of the monopole. With this elementary cross section as an input, the cross section for the process $pp \to \gamma\gamma$+anything is calculated. Elastic, i.e., anything= pp and inelastic contributions are taken into account. The signature of such a process is the production of two photons where the transverse momentum of the pair is much smaller than the transverse momentum of the individual photons. At the Tevatron such a search was performed. They looked at a pair of photons with high transverse energies. No excess of events above background was found [159]. Thus a lower limit on the mass of the magnetic monopole could be given. A mass of 610, 870, or 1580 GeV was obtained, for the assumed values of a monopole spin of 0, 1/2, or 1 respectively.

4.5 Tightly Bound States

One can also speculate about new particles with strong coupling to the $\gamma\gamma$-channel. As seen in Sec. 3.6 above, large $\Gamma_{\gamma\gamma}$-widths will directly lead to large $\gamma\gamma$ production cross sections. The two-photon width of quarkonia, for example, is proportional to the wave function squared in the center of the system, see Table 3. Thus we can expect, that if a system is very tightly bound it should have a sufficiently large two-photon width due to the factor $|\Psi(0)|^2$ which is large in these cases. Examples for such tightly bound systems are discussed, e.g., in [160,161]. Composite scalar bosons at $W_{\gamma\gamma} \approx 50$ GeV are expected to have $\gamma\gamma$-widths of several MeV [160,161]. The search for such kind of resonances in the $\gamma\gamma$-production channel will be possible at LHC. In Part 3 (p. 110ff) of the TESLA Design Report [134] the reader can find some interesting remarks about the "agnostic" approach to compositeness. From Eq. (68 and Fig. 14 one can easily obtain a value for the production cross-sections of such states and the corresponding rates in the various collider modes. Of course, such ideas are quite speculative. However due to the high

flux of equivalent photons such searches seem worth- while, and a possible discovery would be quite spectacular.

Certainly, many aspects in the present section are quite speculative, and one will have to wait for the future e^+e^- and $\gamma\gamma$ colliders to do the physics in the region of several 100 GeV. However, it may be possible to have a glimpse into this region with the very peripheral collisions at LHC which will be taking data in a few years from now.

5 Photon-Nucleus and Photon-Hadron Interactions

Let us start this section with a few rather qualitative remarks which may serve as a guideline. Two-photon processes in relativistic ion collisions have a relatively simple nature: both ions interact by means of the quasireal photons, which they both emit. Theses photons can be thought of as being away, well separated from the nuclei ($b > R_1 + R_2$, $b_i > R_i$). The nuclei remain almost intact after such a collision. The coherence of the ion interaction is taken into account in terms of ion form factors, see Chap. 2. And thus we have virtually pure $\gamma\gamma$-interactions and the rich $\gamma\gamma$-physics as discussed above.

Photon-nucleus processes in relativistic ion collisions are in general more complicated. The photon radiated by one ("spectator") ion interacts with the other ("target") ion in a wide range of photon energies. Besides interacting electromagnetically it can also have a hadronic component, due to its fluctuation into a vector meson ("vector meson dominance", etc.). This leads to quite different interaction mechanisms in photon-ion reactions. If the photon is of low energy we observe the excitation of the giant dipole or other multipole resonances. As these are relatively low energy excitations, they can occur at rather large distances. When the photon (being a non-strongly interacting particle) interacts inside the target ion with a single nucleon we observe the excitation of nucleon resonances and related phenomena.

When the photon fluctuates either to a $q\bar{q}$-pair or a vector meson before interacting with the nucleons of the target, diffractive processes are possible. These can also be called "photon-Pomeron" processes. This signature is similar to the photon-photon or Pomeron-Pomeron processes. An important case is the diffractive vector meson production. Due to the production with a nuclear target, both the coherent and incoherent production can take place. As the vector meson produced inside the nucleus has to go through the nuclear medium, new phenomena will appear. They are widely discussed in the literature in terms of color transparency of the ions, of formation- and coherence-lengths of hadrons etc., see, e.g., the review [162].

Below we give an overview of all these quite interesting phenomena, we present basic formulae and discuss also practical aspects, which are — as it appears now — important for experiments at ion colliders.

5.1 Photonuclear Processes: Giant Dipole Excitation, Beam Loss and Luminosity Monitor

At relativistic heavy ion accelerators in the region up to several AGeV the study of the electromagnetic excitation of the giant dipole resonance (GDR)

and other multipole resonances has been a subject of considerable physics interest. Even the excitation of the double phonon giant dipole resonance (DGDR) was observed and studied. This is made possible due to the strong electromagnetic fields in these collisions, for recent reviews see [163–165]. In the fixed target experiments at SPS/CERN with energies in the 100 AGeV region, fragmentation processes have been investigated like the fission of Pb in PbPb interactions observed by the NA50 collaboration [166]. Such experiments also help to extrapolate to the collider energies (A similar situation is also present in the case of bound-free electron-positron production, see Sec. 7.6 below). While in general a good agreement with theoretical expectations is found [167], a puzzling discrepancy still exists. In [168] a measurement of the total dissociation cross section of Pb for different targets was done. Beside the dominant electromagnetic interaction (proportional to Z_T^2) and the nuclear interaction, a component proportional to Z_T was found. This contribution is in addition to the contribution due to the target electrons, which is sometimes called "incoherent". The size of this extra contribution in the case of a Pb target is 9.74 barn, larger than the hadronic/nuclear cross section of 7.86 barn. This large value precludes explanations in terms of purely nuclear effects. A possible interpretation in terms of incoherent electromagnetic processes on protons in the target nucleus was investigated in [15]. But the size of this effect was found to be too small to explain the results.

The dominant contribution to the electromagnetic excitation of the ions comes from the excitation of the giant dipole resonance (GDR). This is a strongly collective nuclear state which exhausts the Thomas-Reiche-Kuhn sum rule to a very large extent. The impact parameter dependent probability of the one-phonon GDR excitation is given to a good approximation by

$$P_{GDR}(b) = S/b^2 \exp\left(-S/b^2\right) \tag{79}$$

for $b > R_{min} = R_1 + R_2$. The quantity S denotes an area which is given by [10]

$$S = 5.45 \times 10^{-5} Z_1^2 N_2 Z_2 A_2^{-2/3} \mathrm{fm}^2. \tag{80}$$

The total cross section is obtained by integrating over the impact parameter from a minimum value of R_{min} up to the adiabatic cutoff radius $R_{max} \sim \gamma_{ion} c/\omega$. The energy of the GDR is given phenomenologically by $\hbar\omega = 80\ MeV/A^{1/3}$. This and the assumption that the classical Thomas-Reiche-Kuhn sum rule is exhausted to 100% by the GDR enter into the expression for S given above. To lowest order in S/R_{min}^2 the cross-section is given by

$$\sigma_{GDR} = 2\pi S \ln\left(\frac{\gamma_{ion} c}{\omega R_{min}}\right). \tag{81}$$

The interest in these (low energy) excitations at the heavy ion colliders is mainly motivated by more practical considerations: the huge cross section for electromagnetic interaction (of the order of 100's of barn) leads to beam loss and — as was only noticed very recently [169] — to a local beam pipe heating, with the possible danger of quenching of the superconducting magnets. This is due to the effect that most of the nuclear excitations (to the GDR) are followed by the emission of a few neutrons. The remaining nucleus (with a change in the Z/A ratio) will hit the beam pipe and deposit its energy in a rather small area. An even more serious problem is the formation of one-electron atoms in bound-free electron-positron pair creation (see below, Sec. 7.6).

On the other hand it was noticed also that the neutrons coming from the GDR decay can conveniently be detected in the zero degree calorimeter (ZDC). These low energy neutrons in the rest frame of the nucleus are high energy neutrons in the collider frame (with energies in the TeV range in the case of the LHC). This leads to the possibility of using them as a luminosity monitor. Especially the use of mutual GDR excitation has been studied in detail as a possible luminosity monitor for RHIC, as well as, LHC [170].

The mutual excitation probability is to a good approximation given by the product of the probabilities for the single excitations [30]. For symmetric collisions ($Z_1 = Z_2$, $A_1 = A_2$) we have

$$P_{\text{mutual}}(b) = P^2_{\text{GDR}}(b) = \frac{S^2}{b^4} \exp\left(-2S/b^2\right) \tag{82}$$

and the total cross section is given by the integration over the impact parameter from R_{min} to ∞:

$$\sigma_{\text{mutual}} = \frac{\pi S}{2}\left[1 - \exp\left(-2\frac{S}{R^2_{min}}\right)\right] \approx \frac{\pi S^2}{R^2_{min}}, \tag{83}$$

where the last equation is valid if S/R^2_{min} is small.

This formalism can be extended to include also the excitation of the double giant dipole resonance (DGDR) and even higher phonon states with phonon numbers N_1 and N_2 respectively. Taking into account the Bose character of these excitations one obtains

$$P_{N_1,N_2}(b) = \frac{1}{N_1!N_2!}\left(\frac{S}{b^2}\right)^{N_1+N_2} \exp\left(-2S/b^2\right). \tag{84}$$

The total cross section is found again by integration over the impact parameter

from R_{min} to ∞:

$$\sigma_{N_1,N_2} = \frac{(N_1+N_2-2)!\pi S}{N_1!N_2!2^{N_1+N_2-1}} \left[1 - \exp(-2S/R_{min}^2) \sum_{k=0}^{N_1+N_2-2} \left\{ \frac{2S}{R_{min}^2} \right\}^2 \frac{1}{k!} \right]$$
$$\approx \frac{\pi S}{N_1!N_2!(N_1+N_2-1)} \left[\frac{S}{R_{min}^2} \right]^{N_1+N_2-1},$$

where again the last equation is valid to lowest order in S/R_{min}^2. Even for the heaviest systems S/R_{min}^2 is less than one, but not very much: with $R_{min} = 2R_A$) we obtain $S/R_{min}^2 = 0.53$ and 0.48 for the system PbPb ($A = 208$) and AuAu ($A = 197$), respectively. The probability to excite a one phonon GDR in close collisions is thus of the order of 30%. Detailed calculations using photonuclear data (instead of the gross properties of the GDR as discussed above) as an input were performed by Vidovic et al. [171] and Baltz et al. [172]. An improved value of $S = (17.4\ \mathrm{fm})^2$, including photonuclear excitation beyond the GDR, was given in [173] for the PbPb collisions at LHC, based on [172].

Close collisions of ions contribute most to the mutual excitation. This leads to a stronger dependence of the mutual excitation cross section on the detailed form of the cutoff, as compared to the single neutron production, with its rather weak logarithmic dependence on the cutoff radius. On the other hand the measurement of the mutual excitation process is less affected by possible background processes — like beam-gas interactions — than the single GDR excitation. This makes it more suitable as a luminosity monitor. Mutual excitation is sensitive to some extent to nuclear effects. The theoretical calculations [170] and especially [174,167] show that nevertheless a good accuracy can be achieved. In [167] it is concluded that "*Good description of CERN SPS experimental data on Au and Pb dissociation gives confidence in the predictive power of the model for AuAu and PbPb collisions at RHIC and LHC*". This method to monitor the luminosity is currently used at RHIC and plans are also underway to use it at LHC/CERN. In [175] it was concluded that this method is possible also for the ALICE experiment, see also the discussion in Chap. 8 below.

Very recently the first experimental results have become available from the ZDC at RHIC [176]. The ratio of the total cross section (mutual Coulomb plus nuclear interaction) and nuclear interaction alone was measured to be 0.64 in good agreement with the expected theoretical result of 0.66. Also ratios of cross sections for the emission of different numbers of neutrons from each ion were compared with theoretical predictions. The energy spectrum in the ZDC measured in the experiment at RHIC is shown in Fig. 19, taken from [177], where the dominant peak is caused by high-energy neutrons in the ZDC. At LHC energies a clear structure due to multiple-neutron emission of the

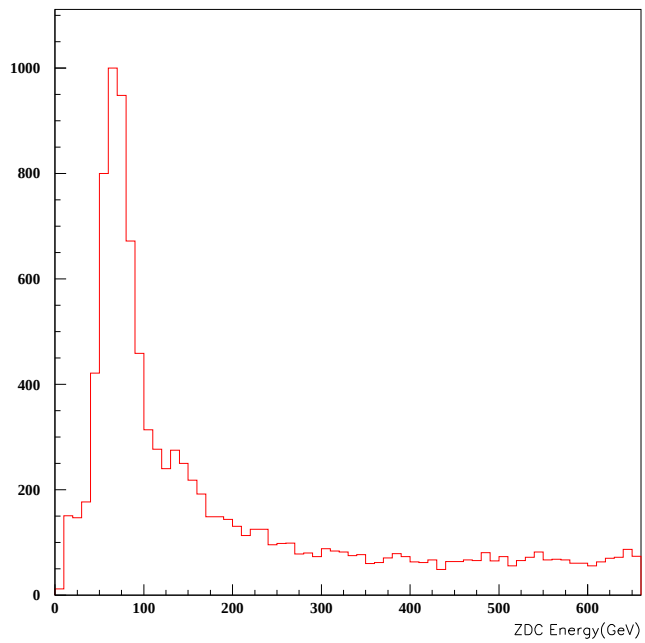

Fig. 19. Online ZDC energy distribution of neutrons obtained during RHIC colliding beam operation with beam energy 65 GeV per nucleon. Extracted from [177].

ions is predicted, see Fig. 20 [178], where the expected energy distribution for neutrons in the ZDC for the ALICE experiment is shown. Another application

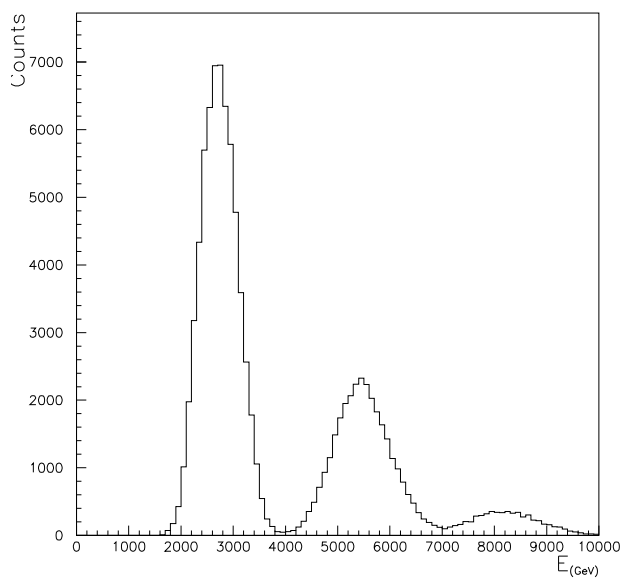

Fig. 20. Expected ZDC energy distribution of neutrons from e.m. of giant dipole resonance in the ALICE experiment at LHC. The ZDC energy resolution is included in the calculations. Extracted from [178].

of the neutron emission processes in heavy ion collisions is to use them as a trigger for the electromagnetic interaction (only) of the ions in the collisions by observing neutrons in both of the ZDC's. This opens the possibility to

select $\gamma\gamma$-processes and suppress other peripheral processes in ion collisions — like photon-Pomeron and Pomeron-Pomeron processes in experiments with an open geometry, i.e., where it is impossible to identify the $\gamma\gamma$-processes by measuring directly the very small P_t of the system produced in $\gamma\gamma$-processes. This will be discussed in more detail in Chap. 8 below.

For both of these purposes the cross section needs to be known very well. Especially the different decay channels resulting in a different number of neutrons emitted have therefore been studied in a detailed investigation in [174,167]. For the simulation the internuclear cascade in the excited nucleus was used.

5.2 Excitation of Nucleon Resonances

The electromagnetic excitation of the Δ resonance in peripheral heavy ion collisions was already observed at the SPS [179]. Cross sections for the electromagnetic excitation of the nucleon resonances are sizeable at the collider energies. This was first studied in [41], where the following values are given: 17 b for UU collisions at RHIC and 25 b for PbPb collisions at LHC. These numbers are based on the folding of the equivalent photon spectra with an experimental input for the γ-nucleon cross-sections up to $E_\gamma = 2$ GeV (in the nucleon rest frame). For further details we refer to that reference. These resonances predominantly decay by the emission of mesons, mainly pions. These pions will be emitted in a rather narrow cone in the beam direction. Maybe they are useful? The cross section for nucleon resonances is 25 b for PbPb collisions at LHC, compared to 8 b for the total nuclear cross section. With the branching ratio of about 33% for the decay of the Δ to $n\pi^+$ and of about 66% for the decay to $p\pi^0$, and relatively small decay energy, a beam of pions with a narrow energy range will be produced. For a recent reference of photoproduction of mesons we refer to [180]. Some time ago the production of beams of pions and other strongly interacting particles by photons was considered by Drell in [181]. A detailed study of the pion emission in heavy ion collisions is performed in [182]. Various mechanisms are considered along with their characteristics. The electromagnetic excitation of nucleon resonances is found to be one of the important channels.

5.3 Photonuclear Reactions to the Continuum above the Nucleon Resonances

The continuum above the nucleon resonances is also strongly excited at collider energies. A first estimate of this effect was given in [41]. In this exploratory calculation a constant value (independent of the photon energy) of $\sigma = 100\mu$b was assumed for photon energies above 2 GeV (in the nucleon rest frame). This gives a value of 2.6 b for UU at RHIC and 19 b for PbPb at LHC. More detailed

calculations were done in [43] and [171]. In this last work experimental values of photonuclear cross-sections for Pb up to 80 GeV were used as an input into the calculations. For PbPb collisions at LHC a cross section of 53.7 b was given for the region between 40 MeV and 2 GeV. From 2 GeV to 80 GeV the cross section is 18.7 b in good agreement with the estimate above. For AuAu collisions at RHIC the corresponding experimental photonuclear data points only exist up to 9.5 GeV. Scaling the experimentally known cross section for Pb to the case of Au a value of 5.6 b was given for the region of 2–80 GeV. For the region above 80 GeV, where no experimental data were available, several parameterizations have been used. Only a small cross section of 0.7 barn was found for AuAu at RHIC, in contrast to 16.3 barn for PbPb collisions at LHC. This is due to the much harder equivalent photon spectrum at the higher beam energies at the LHC.

As has been mentioned already before, the electromagnetic breakup of the nuclei is one of the main loss processes in PbPb collisions at LHC. Therefore a precise knowledge of these cross sections also at higher photon energies is of interest.

5.4 Coherent Vector Meson Production in Photon Diffraction

A lot of theoretical studies of coherent, as well as, incoherent photoproduction of vector mesons in nuclei exist. With the hard equivalent photon spectra present at the relativistic heavy ion colliders new experimental perspectives are opened up for these studies. As was emphasized above the photon virtuality Q^2 is essentially restricted to zero, as opposed to the situation in electron scattering, where this quantity can be varied. Let us mention here some basic concepts of this vast field, where we essentially stick to the case of quasireal photons.

Among the many possible channels, the coherent production of vector mesons (that is, when the nucleus stays in the ground state), as well as, other C-odd mesons in photon-Pomeron processes is a very interesting one to be studied in peripheral heavy ion collisions. From an experimental point of view these processes are quite similar to the two-photon processes discussed above. The main difference lies in the quantum number of the produced system, which in a photon-Pomeron collisions corresponds to $C = -1$. The low value of the transverse momentum $P_\perp$ of the mesons is a very clear experimental signature for this, comparable to the similar one in the photon-photon case. In fact the production of ρ^0 mesons was already observed at STAR/RHIC [50] by looking for its decay into $\pi^+\pi^-$ pairs, see Sec. 8.3.2 below. The invariant mass distribution for pairs with $P_t < 0.1$ GeV shows a clear peak at the ρ mass.

Let us describe the main ideas to treat coherent vector meson production, where we follow essentially the work of [183] and [19]. The calculation is done in the rest frame of one of the nuclei. The minimum momentum transfer is given to a good accuracy by $t_{min} = (M_V^2/2k)^2$, where M_V is the vector meson mass and k the photon momentum. This quantity (it corresponds to the minimal q_L^2 defined in Eq. (92) below) is very small (essentially zero) for high photon momenta. The coherence length $l_c = 1/q_L$ is larger than the size of the nucleus. This means that the photon will fluctuate into a vector meson pair already outside the nucleus and this virtual meson is then put on-shell in the interaction with the nucleus.

We are interested in the total cross section for the reaction $\gamma A \to VA$. To get to this several steps have to be done. One starts with the experimentally known cross section for $\gamma p \to Vp$ as an input. This cross section can usually be parameterized in the Regge form [184]

$$\left.\frac{d\sigma(\gamma p \to Vp)}{dt}\right|_{t=0} = b_V \left(XW^{\epsilon} + YW^{-\eta}\right), \tag{85}$$

where W is the center-of-mass energy and the constants b_V, X, Y, ϵ and η are determined from fits to the data (compare also with the parameterization of the total $\gamma\gamma$ cross section Eq. (57)). A major simplification comes from the use of vector meson dominance [185], which allows to relate this photoproduction cross section to the cross-section for forward elastic $Vp \to Vp$ scattering:

$$\left.\frac{d\sigma(\gamma p \to Vp)}{dt}\right|_{t=0} = \frac{2\pi\alpha}{f_V^2} \left.\frac{d\sigma(Vp \to Vp)}{dt}\right|_{t=0}, \tag{86}$$

where f_V denotes the vector-meson–photon coupling. The further calculations are simplified if one assumes that $\mathrm{Re}f(0)/\mathrm{Im}f(0) \ll 1$, i.e., the Vp scattering is mainly absorptive. This assumption is, e.g., relaxed in [186] at the expense of having to introduce a new parameter. This assumption is certainly better fulfilled for the ρ meson than for the J/Ψ. With this the forward scattering cross section is proportional to the square of the imaginary part of the forward scattering amplitude. The optical theorem can be used to relate this forward elastic scattering cross section to the total cross section σ_{Vp} for vector meson nucleon scattering:

$$\sigma_{Vp}^2 = 16\pi \left.\frac{d\sigma(Vp \to Vp)}{dt}\right|_{t=0}. \tag{87}$$

Using this elementary cross section σ_{Vp} and the nuclear density distribution $\rho_A(r)$ we can obtain in a Glauber calculation [183] the total elastic scattering

cross section as well as the total cross section for VA scattering:

$$\begin{aligned}\sigma_{\text{elastic}}(VA) &= \int d^2b\,[1-\exp\left(-\sigma_{Vp}T_A(b)/2\right)]^2 \\ \sigma_{\text{total}}(VA) &= 2\int d^2b\,[1-\exp\left(-\sigma_{Vp}T_A(b)/2\right)]\,,\end{aligned} \tag{88}$$

where T_A is the nuclear thickness function

$$T_A(b) = \int dz\rho_A(\sqrt{b^2+z^2}). \tag{89}$$

VMD allows us now to relate the cross section for elastic VA scattering back to the coherent production cross section

$$\sigma(\gamma A \to VA) = \frac{2\pi\alpha}{f_V^2}\sigma_{\text{elastic}}(VA). \tag{90}$$

This expression allows us to discuss the dependence of the cross section on A in two limiting cases. In the transparent limit, we expand the exponent to first order. Using a nuclear density distribution corresponding to a homogeneous charged sphere, integration of Eq. (88) gives us $\sigma(\gamma A \to VA) \sim A^{4/3}$. In the black disc limit on the other hand we find $\sigma(\gamma A \to VA) \sim R^2 \sim A^{2/3}$. If only a finite range of t needs to be taken into account, the differential scattering cross section $d\sigma/dt$, see [183] can be used.

A slightly different path is used in [19]. The optical theorem for nucleus A and vector meson dominance is used to get

$$\left.\frac{d\sigma(\gamma A \to VA)}{dt}\right|_{t=0} = \frac{\alpha\sigma^2_{\text{total}}(VA)}{4f_V^2}. \tag{91}$$

From this equation one can directly see the A-dependence of the coherent forward photoproduction amplitude for the two limiting cases: in the transparent limit there is a A^2 behavior (typical for coherent processes) and in the black disc limit we have an $A^{4/3}$ rise with nucleon number A.

The t-dependence of the coherent photoproduction is modeled by the nuclear form factor $F_{el}(t)$. A convenient parameterization of this form factor is given in Eq. (14) of [19]. This form factor falls off very fast with t, the angular distribution is peaked very much in the forward direction (up to a t_{max} of the order of $1/R^2$). Integration over t in order to obtain the total coherent cross section yields a factor of $A^{-2/3}$. Thus the total coherent photoproduction scales as $A^{4/3}$ for the transparent and as $A^{2/3}$ for the black nucleus case, in agreement with the discussion above. The above description illustrates an important idea,

which goes back to the work of Drell and Trefil [187]: using the nucleus as a laboratory, one can determine otherwise unaccessible vector-meson–nucleon scattering cross sections. Several groups studied such processes already in the 1960s and 1970s. This is reviewed in [185]. More recent experiments using virtual photons from muon or electron scattering are less comparable because the photons are more virtual (compared to $1/R_A$). There are some experimental results on coherent cross sections: older data exist from DESY and Cornell. In Figs. 5,6,7 and 9 of [186] there are good fits to the Cornell data. Photons of $E_\gamma = 6.1$ and 8.8 GeV were scattered on complex nuclei like C, Mg, Cu, Ag, Pb and U. At RHIC and LHC one has the possibility to study these processes in great detail, for vector mesons up to the Upsilon and over a much wider energy range. With the forthcoming new detailed results, the theoretical analysis can be improved, for a detailed formalism see, e.g., [183] or [186].

Further interesting ideas are advanced in [19,20,188]. Since either nucleus can emit the photon, there is an interference between these two indistinguishable processes. Such interference effects are discussed theoretically in [20,188]. We refer the reader to this work for further details. Interference effects are sensitive to amplitudes. Therefore it will be interesting to see whether such effects can tell us more about the real and imaginary parts of the amplitudes involved.

Another possibility is multiple vector meson production. There is an analogy to the double phonon giant dipole excitation, see, e.g., [10,163]: in both cases identical bosons are produced and symmetrisation has to be done. This is very important in the case of the double phonon states, since the dipole phonons are only labeled by their spin-projection quantum numbers $M = 0, \pm 1$. On the other hand for the produced vector mesons, there is in addition a continuous quantum number — namely their momenta — which can be quite different in general. Therefore one can expect that boson effects are less important in this case. However, it would be most interesting to observe the production of two identical vector mesons with close enough momenta and study such Boson effects. For details and further references, see [20].

It is noted in [20] and [188] that coherent vector meson production cross sections are huge. E.g., the ρ production in AuAu collisions at RHIC is 10 % of the total hadronic cross-section, in PbPb collisions at LHC it is about equal to the total hadronic cross-section. So heavy ion colliders can act as vector meson factories with rates comparable to those of e^+e^- vector meson machines. Up to 10^{10} Φ mesons will be produced in 10^6 s with Ca beams at LHC. This can be compared to the expected rates at the dedicated Φ-factory DAΦNE [189]: at the beginning, a number of 2.2×10^{10} yearly produced Φ is expected. This will allow for searches of rare decay modes, CP violation and the like. Also there is the possibility to do vector meson spectroscopy: mesons like the $\rho(1450)$, $\rho(1700)$ and $\Phi(1680)$ will be copiously produced. The current

situation of vector meson spectroscopy is outlined in [190]. It is concluded there that many interesting questions are still not understood. Hopefully relativistic heavy ion colliders can contribute to these QCD studies. Of course, it will have to be seen how well such experiments can be done in the hostile environment of the violent central collisions with their extremely high multiplicities.

5.5 Incoherent Production of Vector Mesons

In the incoherent vector meson production process the photon interacts with a nucleon to produce a vector meson leaving the nucleus in an excited state. We follow here mainly the formalism of [191].

The coherence length is defined as $l_c = 1/q_L$, where q_L is the difference between the longitudinal momenta of the photon and the produced vector meson. It is given by:

$$q_L = \frac{M_V^2 + p_T^2}{2\omega}, \tag{92}$$

where p_T denotes the transverse momentum of the produced vector meson with mass M_V, and ω is the photon energy. The incoherent cross section for the production of a vector meson in a reaction, where the nuclear state changes from $|0\rangle$ to $|f\rangle$ $(f \neq 0)$ in Glauber theory is given by:

$$\frac{d\sigma_{inc}^{\gamma V}(0 \to f)}{d^2 p_T} = \left| \int \frac{d^2 b}{2\pi} \ \exp(-i\ \vec{p}_T\ \vec{b}) \ \left\langle f \left| \Gamma_A^{\gamma V}(\vec{b}) \right| 0 \right\rangle \right|^2, \tag{93}$$

where the transition operator $\Gamma_A^{\gamma V}(\vec{b})$ is defined as

$$\begin{array}{l} \Gamma_A^{\gamma V}(\vec{b}; \{\vec{s}_j, z_j\}) = \\ \sum_{j=1}^{A} \Gamma_N^{\gamma V}(\vec{b} - \vec{s}_j)\ e^{i q_L z_j}\ \prod_{k(\neq j)}^{A} \left[1 - \Gamma_N^{VV}(\vec{b} - \vec{s}_k)\ \Theta(z_k - z_j) \right] \end{array} . \tag{94}$$

It consists of the vector-meson production amplitude $\Gamma_N^{\gamma V}$ and an amplitude Γ_N^{VV}, which describes the elastic scattering of the vector meson on the nucleon. By taking $|f\rangle = |0\rangle$, we can treat also the elastic/coherent case, above. Of course the equations there are related to the one here by making use of the "cumulant expansion" [192].

Because of the phase factor $e^{i q_L z_j}$ in this equation, the photon production amplitude on two nucleons with positions $|z_i - z_f| < l_c$ adds up coherently. E.g., with $M_V = 0.8\ GeV$ and $\omega = 8\ GeV$ we have $l_c = 4$ fm (for $p_T \approx 0$).

The equivalent photon spectrum at RHIC extends up to several hundred GeV (as viewed from an orbiting nucleus), therefore this coherence condition will be fulfilled in many cases.

The low and high energy limits of incoherent photoproduction are given in Eq. (12) of [191] as

$$\sigma_{inc}^{\gamma V} = \sigma(\gamma^* N \to VN) \int d^2b \int_{-\infty}^{\infty} dz\ \rho(b,z)\ \times \\ \times \left\{ \begin{array}{ll} e^{-\sigma_{in}^{VN} T_z(b)} & \text{(low energy)} \\ e^{-\sigma_{in}^{VN} T(b)} & \text{(high energy)} \end{array} \right\}. \tag{95}$$

This formula contains the elementary vector meson production cross section and a shadow correction factor. In the low energy limit, with $l_c \ll R$, the attenuation of the outgoing vector meson is governed by the thickness $T_z(b)$, which is the thickness experienced by the vector meson from its point of creation $(\vec{b}, z)$ till its exit from the nucleus. In the high energy limit the attenuation is governed by $T(b) = T_{z\to-\infty}(b)$, the thickness of the nucleus along the total path. This corresponds to the interpretation already given above, that at high energies the photon has already converted to a virtual vector meson long before hitting the nucleus. The meson is then put on the mass shell by the interaction with a target nucleon. This interpretation is familiar from the vector dominance model.

An interesting quantity is the nuclear transparency. It is defined as the ratio of the incoherent production cross section on a nucleus A to A times the elementary photoproduction cross section on a nucleon. In Fig. 21 we show the cross sections for incoherent vector meson production at the LHC. A nuclear transparency of 1 was assumed. This should (of course) be scaled with some realistic value of the transparency factor, which can, e.g., be read off from Fig. 1 of [191]. For a Pb nucleus those authors find a value of about 0.1 for $\omega > 10$ GeV ($Q^2 = 0$).

Both the coherent and incoherent production of vector mesons have been studied at HERMES/HERA in eA collisions [193]. The photon virtuality was $0.4\ GeV^2 < Q^2 < 5\ GeV^2$which is much larger than the $Q^2 < 1/R^2$ in AA collisions. A theoretical discussion is given in [194] where a systematic multiple scattering formalism is developed for vector meson electroproduction from nuclei. Also formation-, propagation-, and hadronization-scales for quark-gluon fluctuations of the virtual high-energy photon are considered.

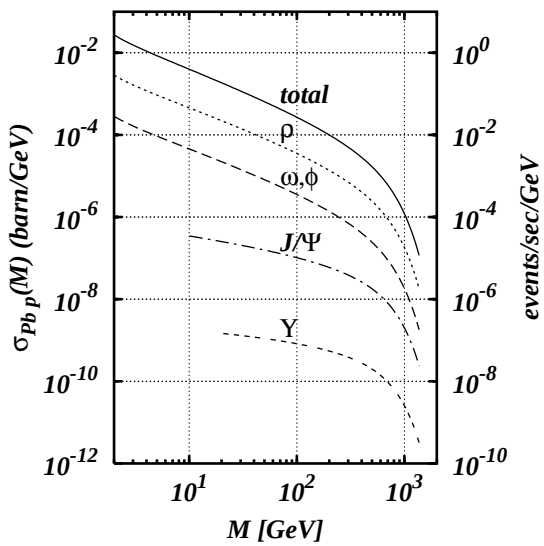

Fig. 21. The cross sections for the diffractive vector meson production of ρ,ω,J/Ψ, and Υ, as well as, the total diffractive cross section is shown for the collision of a virtual photon coming from a Pb ion at LHC energies with a proton as a function of the invariant mass M of the photon-proton system. For the completely incoherent cross section, this cross section needs to be multiplied by A. Parameter for the different cross section are taken from [184].

5.6 Photon-Gluon Fusion and the Gluon Structure Function in a Nuclear Environment

The production of $c\bar{c}$ and $b\bar{b}$ pairs in photon-gluon processes has been suggested as a method to measure the gluon distribution in a nucleon by Frixione et al. [195]. Such processes are under study experimentally at HERA [57] (especially [196]), and [58] (especially [197]). Also there has been much progress in the theoretical study of these processes and the investigation of higher order effects. A recent reference is [198]. With the high photon fluxes at relativistic heavy ion colliders such studies will also be possible for nuclei instead of nucleons. This is reviewed in [16] and we give only a brief update here.

In these photon-gluon fusion processes, one of the ions provides the photon, which hits the gluon of the other ion to produce a $q\bar{q}$ pair. Such processes are coherent for one ion and incoherent for the other. This leads to a special kind of event topology: there is one nucleus, which remains intact (or at least almost, the "spectator", which provides the equivalent photons), and the "target" (which provides the gluon), will be broken up (often called the "remnant") plus a $q\bar{q}$ jet.

The first estimate of the production of heavy quarks in such collisions was done in [199]. Central collisions were not excluded in their approach. More refined calculations focusing on the production of $c\bar{c}$ and $b\bar{b}$ quarks were done

in [42–44,16].

The flavour content of the quark jets can be determined by detecting the corresponding D or B mesons. This of course needs to be included in the specification of the triggering. In this context the study of inclusive processes with heavy flavour production is also of interest. We mention the measurement of inclusive $D_s^{\pm}$ photoproduction at HERA [200]. The photon-proton c.m. energies were in the range of $130 < W < 280$ GeV. Photoproduction events were selected by the requirement that no scattered positron was identified. The c.m. energies of the photon-proton system can therefore not be determined directly from the momentum of the scattered positron, but needs to be extracted from the transverse momentum of the jet from the two produced quarks. They were determined with the Jacquet-Blondel estimator of W, see also Sec. 7.4 and especially Eq. (116).

Modification of parton distribution functions inside the nucleus is one of the interesting topics of QCD [201–203]. These modifications are expected to be present especially at small value of x, where the partons distributions of the individual nucleons start to overlap with each other. In a recent work [204] the gluon distribution in this low-x region was assumed to be given by the "color glass condensate". In this model, the photoproduction of a $q\bar{q}$ pair in very peripheral AA collisions was calculated. The authors conclude that "*it appears that this process is very sensitive to the properties of the gluon distribution in the region where saturation might play an important role*".

Quite recently the production of top quarks at the LHC was studied in [45]. It was found there that 210 $t\bar{t}$ pairs will be produced in a 10^6s OO run at LHC (with an assumed luminosity of $1.4 \times 10^{31}\mathrm{cm}^{-2}\mathrm{s}^{-1}$). Top quark production has been studied before in [199]. In [45] the photon spectrum excluding central collisions and a more modern version of the gluon distribution function is used. The results are sensitive to the large Q^2 behavior of the distribution function. Shadowing is also included. For more details we refer to this work. It will be an interesting channel to be studied at the forthcoming LHC.

6 Diffractive Processes

Diffractive processes are of interest in pp and AA collisions for their own sake and as a possible background to $\gamma\gamma$ collisions. At HERA diffractive photon-proton interactions have been studied in great detail, see [205–207]. The processes of diffractive photoproduction of vector mesons on nuclei were discussed in subsections 5.4 and 3.5. Elastic proton proton scattering will be studied at RHIC [208].

In this subsection we discuss double diffractive (or double Pomeron) processes in ion-ion collisions. This case is certainly even more difficult than the diffraction in the $\gamma\gamma$ and γp interactions, as discussed above. The double diffractive processes have been studied already at the ISR in pp-collisions and at the TEVATRON in $p\bar{p}$ collisions [209–211]. These processes are also one of the main topic in the current COMPASS experiment at the SPS [212].

Generally one could define diffractive processes as hadronic or ion interactions by means of exchange of one or several Pomerons. The Pomeron itself is regarded in QCD as a colorless object consisting of 2 (correlated) gluons gg. Also discussed now are three-gluon objects ggg, i.e., Odderons. The simplest diffractive process meeting this definition is the elastic scattering and there are several special experimental programs devoted to this question in pp collisions [213,214,36]. For the elastic scattering in AA collisions, see also Chap. 2 in [15].

We are interested in diffraction mainly as a possible background for photon-photon and photon-hadron processes. We will therefore look only at those processes where particles are produced in the central region together with no breakup of the two ions, as they correspond to the tagging conditions for photon-photon and photon-hadron processes, see Chap. 8. Experimentally these double diffractive processes ("double Pomeron exchange") have been studied for alpha-alpha collisions already at the ISR in 1985 [215]. Results for double diffraction in $p\bar{p}$ collisions at the TEVATRON have also been studied recently [210]. Diffractive photon-nucleus processes could also be studied with nuclear targets in a future option at HERA [136]. For an overview of diffractive processes we refer to [216,217,24].

These double diffractive processes are characterized by hadrons produced in a region of rapidity y well separated by so-called "rapidity gaps" from the rapidity of the initial ions, see Fig. 22. If a colored object (e.g., a single quark or gluon) would be transfered from one of the ions, the probability for the existence of such a gap is suppressed exponentially with y [216,36], therefore these events will be mainly due to the exchange of colorless objects. This characteristics coincides also with the condition for finding the two ions in

the ground state ("coherent case"). This process will therefore be due to the exchange of either neutral mesons or Pomerons, where these two contributions were already present in the total cross section $\gamma\gamma \to$ hadrons, discussed in Chap. 3 above. At high energies, as it takes place in relativistic ion collisions, only the Pomeron exchanges are dominant in the cross sections.

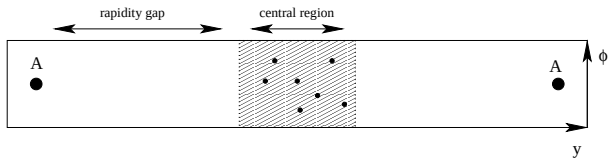

Fig. 22. Coherent double diffractive processes are characterized by particles produced in the central rapidity region and the two ions leaving the interaction with almost the initial rapidity. Between them is a large empty region, defining the "rapidity gap". Adapted from [216]
.

In the phenomenological approach of Donnachie and Landshoff [218–221] the Pomeron is described as a single Regge pole with a "propagator"

$$D_{\mathbb{P}}(t,s) = \frac{(s/m^2)^{\alpha_{\mathbb{P}}(t)-1}}{\sin\left(\frac{1}{2}\pi\alpha_{\mathbb{P}}(t)\right)} \exp\left(-\frac{i}{2}\pi\alpha_{\mathbb{P}}(t)\right), \tag{96}$$

where s is the square of the total c.m. energy, $t = -q^2$ the square of the momentum transfer and the Regge trajectory of the Pomeron given by

$$\alpha_{\mathbb{P}}(t) = 1 + \epsilon + \alpha'_{\mathbb{P}} t, \tag{97}$$

with $\epsilon = 0.085$ and $\alpha'_{\mathbb{P}} = 0.25\ \mathrm{GeV}^{-2}$ (see also the parameterization mentioned above for $\gamma\gamma \to$ hadron). The coupling of the Pomeron to the proton is given by

$$\beta_{p\mathbb{P}}(t) = 3\beta_0 F_1(-t), \tag{98}$$

with $\beta_0 = 1.8\ \mathrm{GeV}^{-1}$ and F_1 is taken as the isoscalar electromagnetic form factor, for which the usual dipole parameterization is assumed. How the Pomeron couples with the whole nucleus is an interesting question. Very little seems to be known about this at present. This will introduce some uncertainty into the calculations discussed here. In general it is assumed to be of the form

$$\beta_{A\mathbb{P}}(t) = 3A\beta_0 F_A(-t), \tag{99}$$

that is, a coherent coupling to all nucleons $\sim A$ with the elastic form factor guaranteeing that the Pomeron emission does not lead to a breakup of the

ion. The coherence will be destroyed rather quickly with increasing t, t being restricted essentially by $|t| \lesssim 1/R^2 \approx (60\ \mathrm{MeV})^2$, compared to the "natural range" given by Regge theory $|t| \lesssim 1/r_0^2 \approx (500\ \mathrm{MeV})^2$ with $r_0^2 = \alpha'_{\mathbb{P}} \ln(s/m^2)$.

The use of the elastic form factor corresponds to taking into account the finite size of the nucleus, see the discussion in Chap. 2. The additional hadronic "initial state interaction" between the other nuclei need to be taken into account. Whereas their effect was small in most cases in the photon-photon collisions, it will be much more severe here, due to the short range nature of the Pomeron. Also the "final state interaction", the third effect discussed in Chap. 2, will be more important in this case. Whereas the electromagnetic field decreases inside the nucleus and therefore the number of equivalent photons there is small, this is not the case for the equivalent Pomerons inside the nucleus. Both the finite size and the initial state interaction effects are assumed to lead to a considerable decrease of the (effective) coupling so that we finally expect only an increase of the cross section with A^δ, where $\delta < 1$.

This model for the Pomeron has been used as the basis in a number of studies within the "equivalent Pomeron approximation" [222]. The inclusive production of the Higgs boson ($\mathbb{P}\mathbb{P} \to H$+anything) was studied for pp collisions in [223], see Fig. 23(a). It was assumed that the major contribution for the Higgs boson production comes from the gluon-gluon fusion via a heavy-quark loop into the Higgs. The gluon distribution function inside the Pomeron is not fully settled, but it was assumed that the Pomeron consists mainly of gluons. A gluon distribution of the form

$$G_{\mathbb{P}}(x) = 6/x(1-x)^5 \tag{100}$$

was used.

This approach was extended to AA collisions in [222]. Also an estimate for the exclusive Higgs boson production ($\mathbb{P}\mathbb{P} \to H$, where the Higgs boson alone without any other hadronic particles is produced, see Fig. 23(b)) was given. The Pomeron-Pomeron-Higgs coupling was modeled by assuming that the Pomeron is a correlated two gluon exchange [218], and the coupling to the Higgs boson was then done again via a heavy quark loop, see Fig. 23(b). In contrast to the photon the Pomeron, being not a real particle but a phenomenological description, has a finite size. Therefore the exclusive production of some heavy mass resonances (corresponding to an object with a small size) is highly suppressed.

Central collisions were excluded in [222] by using only the impact parameter range $b > R_1 + R_2$. This exclusion of the central collisions leads to a suppression of the inclusive production cross section by six orders of magnitude. It was concluded that both the exclusive and inclusive production are small compared

to the photon-photon case. The exclusive production of η mesons was studied similarly in [224]. Again it was found to be only a small background compared to the dominant photon-photon process.

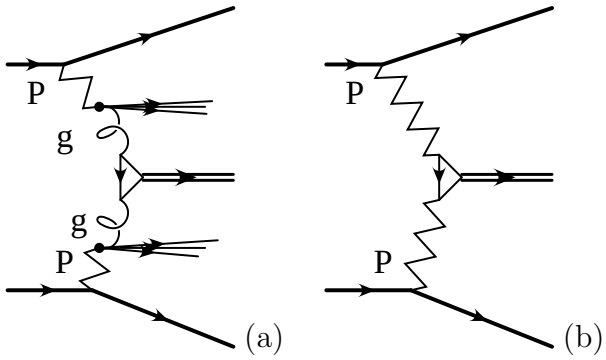

Fig. 23. The inclusive (a) and exclusive (b) production of, e.g., a Higgs boson through Pomeron-Pomeron interaction. The dominant process in both cases comes from the coupling of the Higgs boson with the two Pomerons or gluons through a heavy quark loop.

The calculation of the production of a central cluster of hadrons with a given invariant mass was done in [21] within the Dual Parton Model [225]. By assuming that only one of the nucleons produces a central cluster and all other nucleons scatter only elastically, central collisions were removed. Within a Glauber-like calculation of this, the dependence of the cross section on A is given by $\sigma \sim A^{1/3}$. This $A^{1/3}$ can be understood by assuming that there is only a "ring zone" surrounding each ion, which is active for Pomeron-Pomeron interactions, see Fig. 24, corresponding to the black disc limit. It was concluded that the cross-section for Photon-Pomeron and Pomeron-Pomeron interactions for this case are larger than the cross section for photon-photon events for almost all ion species except for the very heavy ones (Pb), were they are comparable.

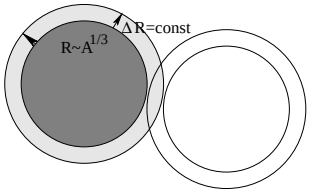

Fig. 24. Due to the strong interaction of the nucleons in both ions and the short range of the Pomeron, essentially only a narrow ring around the nuclear radius, contributes to the diffractive interactions without nuclear breakup. As the nuclear radius increases with $R \sim A^{1/3}$ this explains the increase of the Pomeron-Pomeron cross section with $A^{1/3}$.

Whereas the central collisions were effectively removed in [21], the coherence condition, which essentially guarantees that the ion does not break up due to the Pomeron emission, was not included in this approach. As mentioned

above the Pomeron is a short ranged object, it would normally give a large momentum transfer of the order of 500 MeV to the nucleus. Therefore it is very likely that the nucleus will break up. An elastic form factor for the whole ion was not taken into account in this approach. Some estimates were made [226], indicating that including this would lead to a further suppression of the diffractive events, favoring again the photon-photon case.

This further decrease of the diffractive production cross section due to coherence effects was confirmed also in [227] within the equivalent Pomeron approach, see above. Three different types of final states were considered and compared to the photon-photon case: the exclusive production of resonances (mainly different η mesons) was studied, as well as, the (continuum) production of a π pair. The contribution of Pomeron-Pomeron interaction compared to photon-photon collisions in these cases is found to be only 1% or less for both RHIC and LHC for all ions. This is again due to the fact that the exclusive process is highly suppressed. As a third type of reaction the production of a central hadronic cluster is studied. Here it is found that for light ions (Ca,Ag) at LHC diffractive processes can become of the same size and even dominate at an invariant mass of the cluster below 5 GeV. Also at RHIC the diffractive processes will dominate over the photon-photon processes. No results are given for the photon-Pomeron interactions in [227].

A useful expression for the production of a central cluster of hadrons in Pomeron-Pomeron processes is given in the framework of the simple Regge model, see, i.e., [228,24]. The cross section of these processes are given approximately by

$$d\sigma_{PP}/dm_X^2 = \frac{\sigma_0}{m_X^2}\ (A^{1/3}+\delta)\ \ln\frac{s_{NN}}{(m_X m_N R)^2}, \tag{101}$$

where $\sigma_0 = 1.3\ \mu b$, m_X is the mass of the produced hadron cluster in a central rapidity region, s_{NN} is the square of the c.m. energy of the nucleon-nucleon collisions, R the radius of the nucleus, m_N is the nucleon mass and δ is the width of the nuclear surface. After integration of Eq. (101) over dm_X^2 an estimate of the cross section for Pomeron-Pomeron processes can be obtained. One sees again that this cross section roughly increases with $A^{1/3}$, that is, also with $Z^{1/3}$. This should be compared with the factor Z^4 in the cross section for two-photon processes. Thus in heavy ion collisions we can expect the predominance of two-photon processes, whereas in light ion- and especially in *pp*-collisions the contribution of Pomeron-Pomeron processes will be much more essential. These more qualitative cross section estimates are fully confirmed by detailed calculations, see above and Sec. 8.2.1.

Due to strong shadowing of the Pomeron inside the nucleus only the surface region will contribute to peripheral diffractive processes. Photon-photon and

Pomeron-Pomeron processes will therefore scale approximately with the ion species as Z^2 and $A^{1/3}$, respectively [24]. Thus for heavy ions, like Pb, we may expect dominance of the photon-photon processes whereas, say in *pp* collisions, the Pomeron-Pomeron processes will dominate in coherent collisions.

Diffractive processes are an additional field of studies in peripheral ion collisions. They essentially have the same triggering conditions and therefore one should be able to record them at the same time as photon-photon and photon-hadron events. One may think also about going beyond the coherent case ("no breakup"). Processes with a large rapidity gap have been proposed [229,230] as an interesting physics topic and many interesting questions, like the probability for a gap as a function of its width y have been posed.

As a potential background for coherent photon-photon and photon-hadron collisions in very peripheral collisions we conclude that they are in most cases only a small background for the heaviest ions. Without the triggering on "no breakup" for the two ions, they dominate the production of hadrons in the central region. The same is also the case for *pp* collisions at the LHC.

7 Special Aspects of Dilepton Pair Production

Due to their small mass, electrons (positrons) and to some extent also muons play a special role in very peripheral heavy ion collisions. They are produced much more easily than other heavier particles, and — especially in the case of e^+e^- pair production — some new phenomena, like multiple pair production, will occur. A small mass means that the Compton wave length — for electrons this is $\lambda_C = \frac{1}{m_e} \approx 386$ fm — is large, larger than the nuclear radius R of several fm. The equivalent photon approximation has to be modified when applied in this case. The cutoff radius is not given by the nuclear radius anymore but by the Compton wavelength of the particle. The reason is that in the cross section for the $\gamma\gamma \to e^+e^-$ subprocess the dependence on the virtualities Q_1^2 and Q_2^2 of the (quasireal) photons can no longer be neglected. As was explained in Chapter 2 the photon virtuality in heavy ion collisions is limited by the nuclear radius up to $Q^2 \lesssim 1/R^2$, which is much larger than m_e^2. Especially for invariant masses of the order of several m_e — which contribute mostly to the total cross section — the photon-photon cross section deviates from the one for real photons for virtualities Q_1^2 and/or $Q_2^2 \gtrsim m_e^2$, (see App. E and Eq. (6.25) of [59]). For the muon — with a Compton wavelength of about 2 fm — we expect the standard equivalent photon approximation (EPA) to be applicable with smaller corrections. For e^+e^- pair production using EPA together with the cutoff radius equal to the electron Compton wave length gives a fair approximation for the total cross section. On the other hand EPA completely fails for certain regions of the phase space and also for the calculation of pair production probabilities at small impact parameters (as discussed in detail below).

The calculation of pair production in heavy ion collisions dates back to the work of Landau & Lifschitz [25] and Racah [26] in the thirties, as already mentioned in the introduction. In connection with the relativistic heavy ion colliders there has been some renewed interest and cross section calculations have been done using the semiclassical approximation in [10] and using Feynman Monte Carlo techniques in [231]. For lower energies (about 1–2 GeV per nucleon) coupled channel calculations have been done also by a number of groups [232,233].

The total cross section for pair production is huge (about 200 kbarn for PbPb at LHC, 30 kbarn for AuAu at RHIC [234]). Electron-positron pairs therefore present a possible background. The differential cross section show that most of the particles are produced at low invariant masses (below 10 MeV) and into the very forward direction, see Fig. 25. The highly energetic electrons and positrons tend to be even more concentrated along the beam pipe, therefore most of them remain unobserved. On the other hand, the cross section for highly energetic electrons and positrons is still of the order of barns. These QED

pairs constitute a potential hazard for the detectors, see below in Chap. 8. On the other hand they can also be useful as a possible luminosity monitor, as is discussed, e.g., in [24,35].

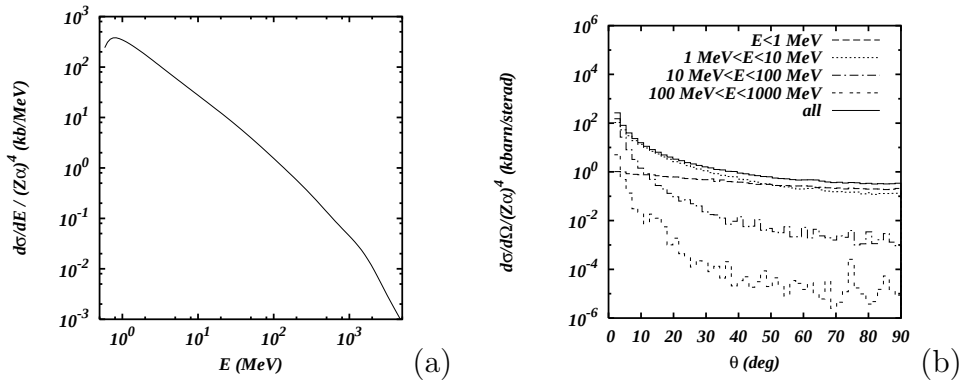

Fig. 25. Single differential cross sections for the e^+e^- pair production at LHC as a function of the energy (a) of either electron or positron and as a function of the angle of the electron or positron with the beam axis (b). Most pairs are produced with energies between 2–5 MeV in the Lab frame and in the very forward or backward direction.

Due to the strong electromagnetic fields of short duration new phenomena, especially multiple pair production, but also Coulomb-corrections, will appear in relativistic heavy ion collisions. They are of interest for the study of QED of strong fields. This will be discussed in the next two sections. In addition there are also a number of processes related to pair production, like bremsstrahlung from produced pairs, or the production of electrons and muons not only as free particles but either produced into an atomic state bound to one of the ions ("bound-free pair production") or as a bound state of the pair ("positronium", "dimuonium", or even "ditauonium" production). This will be discussed then in the rest of this chapter. For an introduction to aspects of atomic physics of relativistic heavy ion collisions, we refer the reader to [235,236].

7.1 Strong Field Effects in Electron Pair Production: Multiple Pair Production

The special situation of the electron pairs can already be seen from the formula for the impact parameter dependent probability for (single) pair production $P^{(1)}$ in lowest order. (For heavy nuclei the semiclassical approximation is valid and the impact parameter b can be considered to be an observable quantity, see, e.g., Chapter 2 of [15] and further references given there.) Using the double equivalent photon approximation (valid for $1/m_e \ll b \ll \gamma/m_e$) with the cutoff radius set to $1/m_e$ one obtains [237,238]

$$P^{(1)}(b) \approx \frac{28}{9\pi^2}\frac{Z_1^2 Z_2^2 \alpha^4}{m_e^2 b^2}\left[2\ln\gamma_{lab}^2 - 3\ln(m_e b)\right]\ln(m_e b) \quad \text{for } 1 \ll m_e b \ll \gamma_{lab}$$
$$\approx \frac{28}{9\pi^2}\frac{Z_1^2 Z_2^2 \alpha^4}{m_e^2 b^2}\left[\ln\frac{\gamma_{lab}^2}{m_e b}\right]^2 \quad \text{for } \gamma_{lab} \ll m_e b \ll \gamma_{lab}^2 \tag{102}$$

As this calculation underestimates the probability in the range of small impact parameters, one might expect that also probabilities larger than one are possible. As mentioned already in the introduction, the use of the equivalent photon approximation is not justified here. Therefore (more) exact calculations need to be done.

The impact parameter dependent probability in lowest order was calculated numerically in [239,240]. The quantity $P^{(1)}(b)$ found there is larger than the one given by Eq. (102), and values larger than one are possible at RHIC and LHC. As an example $P^{(1)}(b=0) = 3.9$ (1.6) [79], and $P^{(1)}(1/m_e) = 1.5$ (0.6) [239] for LHC (RHIC) are found. It means that a new class of phenomena appears here.

The fact that the cross section for the electron-pair production in lowest order rises too quickly with beam energy and will eventually violate unitarity at very high energies was already mentioned by Heitler in [241], and speculations about possible remedies were made there. Whereas it was assumed to be an *"academic problem"* at that time, the fact that unitarity is violated in the lowest order calculations at RHIC and LHC energies for the heavy systems has generated some renewed interest [10]. It led to a series of studies starting almost a decade ago. It was found that the production of multiple pairs in a single collision restores unitarity [242].

For $Z\alpha \sim 1$ the interaction of the leptons with several photons coming from the external field will be much more likely than the exchange of photons among the singly charged leptons, see Fig. 26. Therefore we will neglect the lepton-lepton interaction, treating it as a pure external field problem.

This was first studied in [242,243]. Hereby, the e^+e^- pair was treated as a "quasiboson". Neglecting rescattering terms a closed expression was obtained to all orders. A similar approach was also followed in [244]. In [245] another approach was used, starting from a description within the Dirac sea picture. All studies essentially make use of the "quasiboson" approximation, that is, treating the pair as an "unbreakable unit". All find the probability to produce N pairs $P(N,b)$ to be given by a Poisson distribution:

$$P(N,b) = \frac{P^{(1)}(b)^N}{N!}\exp\left[-P^{(1)}(b)\right], \tag{103}$$

where $P^{(1)}(b)$, the probability for pair production calculated in lowest order

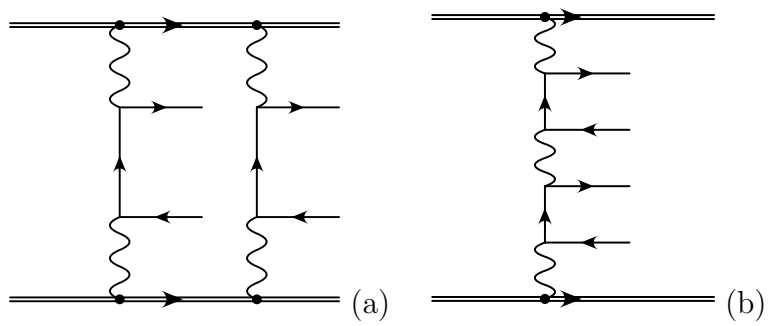

Fig. 26. The dominant two pair production process at the energies of RHIC and LHC is shown in (a). Due to $Z\alpha \sim 1$ this process is favored, giving a cross section of $\sim Z^8\alpha^8 \ln^2 \gamma_{lab}^2$. On the other hand the process of (b) is proportional to $\sim Z^4\alpha^6 \ln^4 \gamma_{lab}^2$. It will therefore take over at extremely high γ_{lab}.

(which, as shown before, can become larger than one), is actually the "average number of e^+e^- pairs" produced in a single ion collision:

$$\langle N(b)\rangle = \sum_N NP(N,b) = P^{(1)}(b). \tag{104}$$

One should keep in mind that the two-pair production process as shown in Fig. 26(a) is rising approximately with $\sim Z^4\alpha^8 \ln^2(\gamma_{lab}^2)$, whereas the one shown in Fig. 26(b) rises with $\sim Z^4\alpha^6 \ln^4(\gamma_{lab}^2)$ [246,247,59] and will finally take over at extremely high values of γ_{lab}. We are still far away from this regime. On the other hand, as mentioned in [59] the multiple pair production at large invariant masses is again dominated by Fig. 26(b).

The use of the Poisson distribution Eq. (103) allows us to interpret the lowest order calculation as a calculation of multiple pair production. Multiple pair production cross sections can be defined by integrating Eq. (104) over b, for example:

$$\sigma_T = \int d^2b\, \langle N(b)\rangle = \sum_N N\sigma(N). \tag{105}$$

It was shown in [248,234] that the matrix element for N-pair production S_N factorizes quite generally into an antisymmetrized product of individual pair production amplitudes s^{+-} (corresponding to individual fermion lines) and the vacuum-vacuum amplitude (corresponding to all closed fermion loops), see also Fig. 27:

$$S_N = \langle 0|\, S\, |0\rangle \sum_\sigma \mathrm{sgn}(\sigma) s^{+-}_{k_1 l_{\sigma(1)}} \cdots s^{+-}_{k_N l_{\sigma(N)}}, \tag{106}$$

where k_i,l_i are the quantum numbers (momenta and spin projection) of electron and positron, respectively, and σ denotes a permutation of $\{1,\cdots,N\}$.

The vacuum-vacuum amplitude is present in all QED calculations, but whereas it is of absolute value one without external fields or for static fields (and is therefore factored out and dropped in the calculation), it is < 1 here, as pair creation occurs out of the initial vacuum state and the probability for no-pair production $|\langle 0| S |0\rangle|^2$ has to be smaller than one. This result was confirmed recently in [249]. The amplitude s^{+-} corresponds to the one of single pair production neglecting the vacuum-vacuum amplitude; it is the one that is calculated, for example, in lowest order Born approximation.

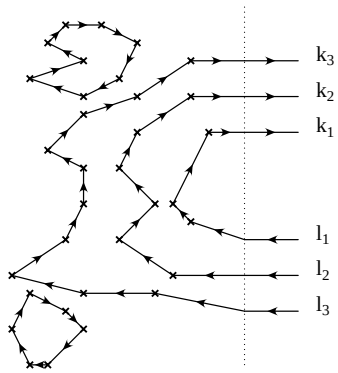

Fig. 27. Graphical illustration of the general form of the N-pair production process. The interaction with the external field is shown as crosses. The production of a pair is described by a fermion line coming from and leaving to the future, interacting an arbitrary number of times with the external field. Such a line corresponds to s^{+-} in Eq. (106). The vacuum-vacuum amplitude $\langle 0| S |0\rangle$ corresponds to the sum of all closed fermion loops. For details we refer to [248].

Calculating the total N pair probability

$$P(N,b) = \frac{1}{(N!)^2} \sum_{k_1,\cdots,k_N,l_1,\cdots,l_N} |S_N|^2 \tag{107}$$

one gets two different types of contributions. In the first type — see Fig. 28(a) — the same permutation σ is present in S_N and S_N^+, whereas different ones are used in the second type — see Fig. 28(b). Neglecting this second class — and therefore the antisymmetrization in the final state — one recovers again the Poisson distribution Eq. (103).

The fact that the second class of diagrams gives in general a small contribution as compared to the first one can be understood due to the correlation of the electron and positron momenta. They are not produced completely independently of each other. Especially their transverse momenta are correlated; this is obvious in the equivalent photon approximation where the sum of the transverse momenta is close to zero, which is also true in the exact calculation in lowest order. Therefore the "quasiboson" approximation, that has been used in the early studies is justified. In addition the deviation from the Poisson

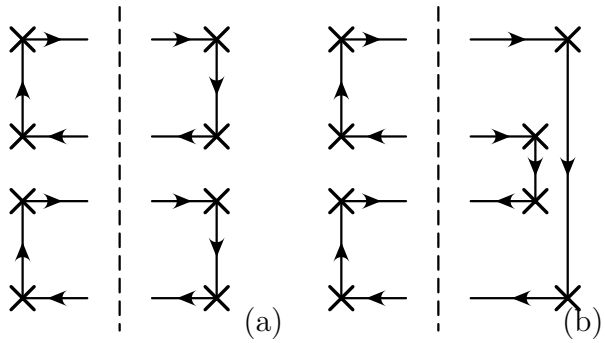

Fig. 28. The two pair production probability consists of two types of diagrams. The class of diagrams (a), where electron and positron are always matched in S_N and S_N^+ leads to the Poisson distribution. Diagrams of type (b) are assumed to be small due to the correlation of the momenta of electrons and positrons.

distribution in the case of two pair production was calculated explicitly for small impact parameters $b \approx 0$ [248,250]. Figure 29 shows the contribution from the two diagrams of Figure 28. At LHC energies the deviation is found to be only of the order of 1%.

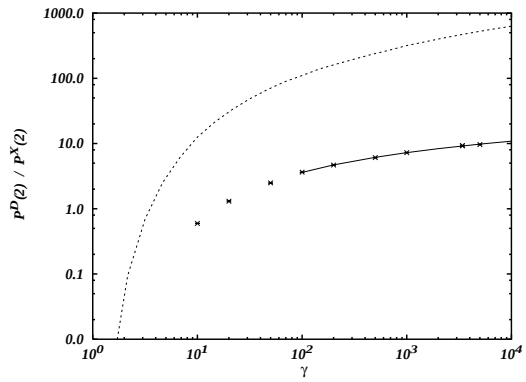

Fig. 29. The contribution of diagram (a) and (b) of Fig. 28 to the two-pair production probability at impact parameter $b \approx 0$ is shown as a function of the Lorentz factor γ_{lab} of the collision. The dotted line shows contributions from the diagram of Fig. 28(a), the numerical data points and solid line those of Fig. 28(b). Taken from [250].

Using Eq. (103) one can use the impact parameter dependent probability $P(b)$ of [239,240] to obtain the probabilities for N-pair production $P(N, b)$, see Fig. 30. One can see that for impact parameters $b \approx 2R$ up to about $1/m_e$ on the average 3–4 pairs will be produced in PbPb collisions at the LHC. This means that each photon-photon event — especially those with high invariant mass, which occur predominantly at impact parameters close to $b \gtrsim 2R$ — is accompanied by the production of several (low-energy) e^+e^- pairs (most of them however will remain unobserved experimentally). Integrating over the impact parameter the total multiple pair production cross section were given in [234]. The single pair production probability $P(b)$ falls off essentially as

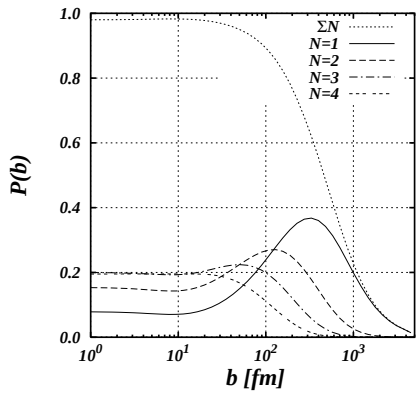

Fig. 30. The impact parameter dependent probability to produce N e^+e^--pairs ($N = 1, 2, 3, 4$) in one collision is shown for the LHC ($\gamma_{lab} = 2950$,PbPb). Also shown is the total probability to produce at least one e^+e^--pair $\sum_N P(N, b) = 1 - P(0, b)$. One sees that at small impact parameters multiple pair production dominates over single pair production.

$1/b^2$. The total cross section is dominated by large impact parameters and not very sensitive to the multiple pair production effects at small b. In [238] the reduction of the exclusive one-pair production cross section $\sigma(N = 1)$ was estimated to be -6.4% for RHIC and -4.7% for LHC, using the numerical results of [248,234]. Multiple pair production cross section on the other hand are dominated by impact parameters, around $b \approx \lambda_c = 1/m_e$. Measuring them would be of interest. At the SPS (CERN) the effect was looked for, see [251], but only an upper bound could be given, which is still above the theoretical prediction.

7.2 Strong Field Effects in Electron Pair Production: Coulomb Corrections

The calculation of the impact parameter dependent probabilities described above have been done in lowest order perturbation theory, even though $Z\alpha \approx 0.7$ is not small. One could therefore ask how reliable these calculations are. Higher order effects (in addition to multiple pair production discussed in the previous section) could become important. This will be discussed now.

For low beam energies (around 1–2 GeV per nucleon) coupled channel calculations have been made by a number of people [232,233]. They found a rather large increase of the cross section. For the higher energies at RHIC and LHC such an approach is no longer viable due to the large number of channels to consider [252] (For a calculation at $\gamma = 200$, see [253]). Since the review in [15] a number of papers appeared treating higher order effects in ultrarelativistic heavy ion collisions in the high energy limit.

In the following we are concerned only with higher order corrections to the

single fermion line, that is to s^{+-} of Eq. (106), assuming that the Poisson distribution can then be used to account for multiple pair production. These effects are generally called "Coulomb corrections", as they mostly deal with the Coulomb distortion of both the electron and positron wave functions due to additionally exchanged photons. Formally two kinds of classes can be distinguished. In the first one only Coulomb rescattering will be considered, that is, only one pair will be present at all intermediate time steps. The second one, which we call "multiple particle corrections", are those processes, where more than one pair is present at an intermediate time step, with an electron and a positron from two different pairs annihilating at a later step. Such a distinction is less useful in the usual Feynman approach, as intermediate lines describe both electrons and positrons, but it is well defined in a retarded boundary condition approach, corresponding to the Dirac sea picture.

The second class of diagrams was studied in [248] for small impact parameters $b \approx 0$ within the framework of the Magnus theory and neglecting all Coulomb rescattering terms. The effect was found to be rather small, at most 5% for PbPb collisions at LHC. As these effects are expected to be largest for the small impact parameters, one has to conclude that their effects will be rather small in the cross section. We therefore consider the first class in the following.

A classical result for this first class of higher-order effects can be found in the Bethe-Heitler formula for the process $\gamma + Z \to e^+ + e^- + Z$ (corresponding to the highly asymmetric case $Z_1\alpha \to 0$, $Z_2\alpha \approx 1$): one obtains for an unscreened nucleus

$$\sigma = \frac{28}{9}\frac{(Z\alpha)^2}{m_e^2}\left[\ln\frac{2\omega}{m_e} - \frac{109}{42} - f(Z\alpha)\right], \tag{108}$$

with the higher-order term given by

$$f(Z\alpha) = (Z\alpha)^2 \sum_{n=1}^{\infty} \frac{1}{n(n^2 + (Z\alpha)^2)} = \gamma + \mathrm{Re}\psi(1 + iZ\alpha) \tag{109}$$

with the Euler constant $\gamma \approx 0.57721$ and ψ the Psi (or Digamma) function. As far as total cross sections are concerned the higher-order contributions tends to a constant for $\omega \to \infty$.

This is used as the basis for a detailed calculation of higher order effects on the (single pair) cross section in [254]. The higher order effects were classified according to the number of photons n and n' exchanged with each ion, see Fig. 31. The dominant term is given by the $n = n' = 1$ contribution (Fig. 31(a)), due to the $1/b^2$ behavior of the single photon exchange. It leads to the famous $ln^3\gamma$ rise of the (total one pair production) cross section. The next important terms are those with $n = 1$, $n' > 1$ and $n > 1$, $n' = 1$ (see

Fig. 31(b) and (c)). They are enhanced proportional to $\sim \ln^2 \gamma$. The last class of diagrams will only be $\sim \ln \gamma$ and is therefore neglected in [254]. A systematic way to take the leading terms into account in e^+e^- pair production was used in [255,254], leading to a result which corresponds to the Bethe-Heitler result above and is therefore in accord with the Bethe-Maximon corrections [256–258]. The authors find corrections to the total Born cross sections, which are negative and equal to -25% and -14% for RHIC and LHC. Therefore the Coulomb corrections in the single pair production cross section (better σ_T as defined in Eq. (105), as this is what is really calculated) seem to be well understood. A negative correction was also found in the work of [10]. These

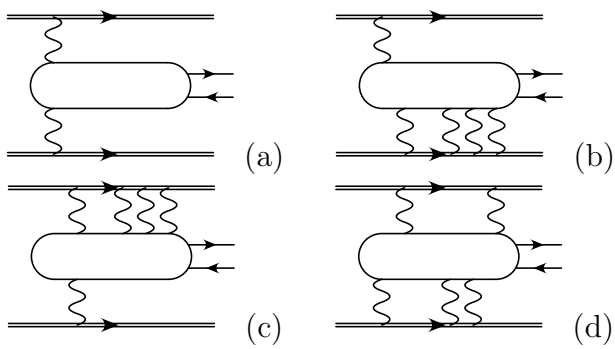

Fig. 31. Contributions to the single pair production cross section can be classified by the number of photons that is emitted by each ion. If each ion emits only one photon (a) the cross section has a $\ln^3 \gamma$ dependence. If only one of the ions emits only one photon ((b) and (c)), only a $\ln^2 \gamma$ dependence is found. Finally with both ions emitting several photons (d), only a $\ln \gamma$ dependence is expected.

theoretical developments are further supported in [237].

Please note that such a classification according to n and n', resulting in different powers of $\ln \gamma$ is not helpful for multiple pair production, as at least two photons must be emitted from each nucleus in this case (corresponding always to the case $n > 1, n' > 1$ above) and one will not have a cross section proportional to $\ln^3 \gamma$ from the beginning. A different approach, which is good in the small impact parameter region, is therefore needed.

In a series of papers the exact solution of the Dirac equation of an electron in the field of the two nuclei in the limit of the Lorentz factor $\gamma_{lab} \to \infty$ was studied. The interest started after an article showed how the summation to all orders in the high energy limit can be done in the related problem of bound-free pair production [259], see also below. In a first article [260] it was shown that also in the free pair production case the summation to all orders can be done analytically. Due to the form of the electromagnetic field of the two ions in the high energy limit — both of them being essentially localized on two different sheets corresponding to $z = \pm t$, where z is the direction of the beams — only a certain class of diagrams was found to be dominant in this case, see Fig. 32. The sum of the interactions with one of the ions in the

highly energetic case gives the typical eikonal phase. It was shown that this leads to a matrix element very similar to the one in lowest order, but where the photon propagator is replaced with

$$\frac{1}{q_\perp^2 + q_l^2} \to \frac{1}{(q_\perp^2 + q_l^2)^{1-iZ\alpha}}. \tag{110}$$

The authors of [261] come to the same conclusion; they also show that by integrating over the impact parameter the cross section becomes identical to the lowest order Born result, as only the absolute values squared of the modified photon propagators Eq. (110) are needed. The same result is also found in [262]. In [263] the scattering of electrons is studied, which is then related via crossing invariance to the pair production process.

A numerical calculation of the impact parameter dependent probability was done in [264] and also in [265] (see also the two comments following [265]). Calculating the impact parameter dependent probability in this approach a reduction of up to 50% was found for small impact parameters, leading to the same reduction for the multiple pair cross section. Therefore Coulomb corrections are expected to be important also at small impact parameters.

The fact that the cross section to all orders corresponds to the lowest order Born result is obviously in contradiction to the Bethe Maximon corrections, as described above. This can be seen from Eq. (7.4.3) of [10] and it was pointed out in [254] and later also in [237,266]. In [266] it was noted that in the limit of $\gamma \to \infty$, different types of diagrams are of importance in the electron scattering case and in the pair production case, that is, taking only the dominant diagrams in both cases will violate crossing symmetry. In [237] the question of how to do this limit is studied in more detail. By making a careful transition to $\gamma \to \infty$ the Bethe Maximon corrections were found to be present also in this case. The failure of the eikonal technique to reproduce the Bethe Maximon results was already noted in [267].

The equality of the nonperturbative cross section to all orders with lowest order result can therefore be seen as an artifact of the regularization of the modified photon propagator. Eq. (110) is found by taking the limit $\gamma \to \infty$ first; in this limit the modified photon propagator is $1/(q_\perp^2)^{1-i\eta}$. Taking this limit — which essentially corresponds to the sudden approximation — is justified only for small impact parameters. In fact integrating this expression over b would lead to a diverging cross section, essentially due to the singular behavior of the propagator for $q_\perp \to 0$. Therefore in [261] the form of the propagator Eq. (110) was suggested. It is mainly this form of the propagator which in the end leads to the equality of the two cross sections. A more careful regularisation of the propagator would lead to an expression in agreement with the Bethe Maximon theory [268]. On the other hand this means that

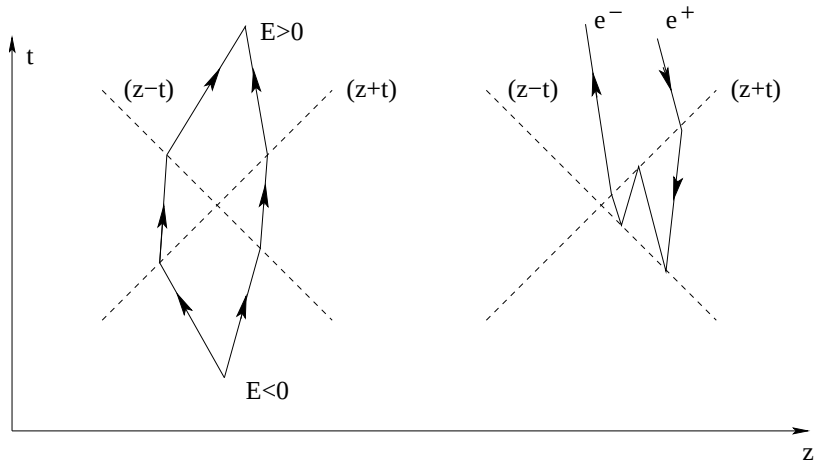

Fig. 32. The special structure of the electromagnetic interaction can be seen in this t-z plot. Due to the Lorentz contraction the electromagnetic fields are localized in two sheets corresponding to $z = \pm t$. In the "retarded" or "Dirac sea" approach (left) an electron with negative energies comes from $t = -\infty$, crosses the field of each ions only once before leaving as an electron with positive energy. In the "Feynman" approach, the positron comes from $t = +\infty$ and can go forward and backward in time therefore interacting a number of times with the ions.

the probabilities for small impact parameter, which get a large part of their contribution from large $q_\perp$ should be expected to be reliable.

In all derivations of the pair production in the high energy limit [260,261,263] the pair production are not calculated using Feynman boundary conditions, that is, treating the positrons as particles going backward in time [269–272]. Instead a retarded approach, that is, essentially the "Dirac sea" picture is used: the problem is treated as the scattering of a negative energy electron into a positive energy state, see, e.g., [269,272]. In this approach the structure of the interaction with the external field can be exploited easily, see Fig. 32.

This has two consequences: the total cross section as well as the differential cross section with respect to either the electron or the positron should be reliable, but not the differential cross section with respect to both leptons, as the "rescattering of the hole" is not taken into account [237]. In addition in [249] it is shown that the cross section calculated in this way does not correspond to the exclusive one-pair production σ_1 but to σ_T, as defined in Eq. (105). This result was already found there to be true for the calculation of the single-pair production cross section, neglecting the vacuum-vacuum amplitude. But whereas the Poisson distribution was needed there, it is found in [249] to be exact in the general case as well.

Single and multiple pair production in charged particle (heavy ion) collisions without nuclear contact is a QED process and should in principle be calculable precisely with the methods of QED. Although the calculations in detail

are quite complicated, the theoretical concepts are well understood by now. Especially the importance of higher order corrections due to the multiple pair production cross section would be an interesting test. First experimental observations of e^+e^- pairs has been reported already by STAR at RHIC [273]. A comparison with experiments will hopefully be possible soon.

7.3 Electromagnetic Production of Electron Pairs and Other Particles in Central Collisions

Differential production probabilities for dileptons from $\gamma\gamma$ processes in central relativistic heavy ion collisions are calculated using the equivalent photon approximation in an impact parameter formulation and are compared to Drell-Yan and thermal ones in [87,274,275]. The very low $p_\perp$ values and the angular distribution of the pairs give a handle for their discrimination to those coming from other sources, e.g., from meson decay.

In [80] it is shown that particle production in central collisions via the $\gamma\gamma$-mechanism is so small that it can be neglected in practice. The probability to produce a final state with invariant mass M and rapidity Y is given by

$$\frac{d^2P}{dMdY} = \frac{Z_1 Z_2 \alpha^2}{\pi^3 R^2} \left(1 - a^2 \exp(-2\,|Y|)\right) \frac{2\sigma_{TT}(M^2)}{M}, \tag{111}$$

where σ_{TT} is the corresponding $\gamma\gamma \to f$ fusion cross-section and $a = \frac{RM}{2\gamma}$ (R is the larger one of the nuclear radii). This probability is very small, since we typically have $\sigma_{TT} \ll R^2$. Electromagnetically produced electrons were also measured in distant $S - Pt$ collisions in the CERES/NA45 experiment [276]. The authors also conclude that "*the rate of e^+e^- pairs from QED production in collisions with nuclear overlap for the CERES acceptance is negligible compared to e^+e^- pairs from meson decays*". For further details we refer to [80,276].

7.4 Electrons and Muons as Equivalent Particles, Equivalent Electron (Muon) Approximation

The equivalent photon approximation can be generalized to other particles [277,278]. A light or zero mass particle moving with high energy splits into a pair of light or zero mass particles. The constituents of this daughter pair subsequently react as "equivalent beams" with the target system. This subprocess is easier to describe than the original reaction. Here we are interested in those processes, where the (equivalent) photon splits into a lepton pair and

the (equivalent) leptons induce reactions with the target, e.g., deep inelastic lepton scattering. (The discussion here has some similarity to the more general one in Chap. 3 above, where also vector mesons and quark pairs are considered.)

The production of lepton pairs from (real or virtual) photons producing a pair by inelastic scattering from a nuclear target was first studied in [279], see also [69], where it was mostly regarded as an additional contribution to the (elastic) pair production. Now we suggest that the equivalent photons may also be used as a lepton beam to study deep inelastic lepton scattering from a nucleus.

Up to now only the production of dileptons in heavy ion collisions was considered, for which the four-momentum Q^2 of the photons was less than about $1/R^2$ (coherent interactions). There is another class of processes, where one of the interactions is coherent ($Q^2 \leq 1/R^2$) and the other one involves a deep inelastic interaction ($Q^2 \gg 1/R^2$), see Fig. 33. These processes are much rarer than the events with two coherent interactions. But they may also be of interest in the future. They are readily described theoretically using the equivalent electron– (or muon–, or tau–) approximation, as given, e.g., in [277,278]. They are characterized by the fact that the lepton is almost on-shell (i.e. the propagator of the virtual particle will become very large, since its momentum squared $|p^2| \simeq m^2$). In the following we will speak of muons, but the same considerations apply also to electrons.

The equivalent photon can be considered as containing muons as partons. The equivalent muon number is given by [277]:

$$f_{\mu/\gamma}(\omega, x) = \frac{\alpha}{\pi} \ln\left(\frac{\omega}{m_\mu}\right)\left[x^2 + (1-x)^2\right], \tag{112}$$

where m_μ denotes the muon mass. The energy E_μ of the equivalent muon is given by $E_\mu = x\omega$, where ω is the energy of the equivalent photon. This spectrum has to be folded with the equivalent photon spectrum given approximately by, see Eq. (11):

$$f_{\gamma/Z}(u) = \frac{2\alpha}{\pi}\frac{Z^2}{u} \ln\left[\frac{1}{u m_A R}\right]. \tag{113}$$

For $u < u_{max} = \frac{1}{R m_A}$ we then get:

$$f_{\mu/Z}(x_1) = \int_{x_1}^{u_{max}} du f_{\gamma/Z}(u) f_{\mu/\gamma}(u E_A, x_1/u). \tag{114}$$

The energy of the heavy ion is denoted by E_A, the photon energy is given by $\omega = uE_A$,and the muon energy by $E_\mu = x_1 E_A = uxE_A$. This expression can be calculated analytically.

The deep inelastic lepton-nucleon scattering can now be calculated in terms of the structure functions F_1 and F_2 of the nucleon. It would be interesting to see how the nucleon structure functions F_1 and F_2 are modified in the nuclear medium. (It remains however unclear at present how accurate such measurements could be.) The inclusive cross section for the deep-inelastic scattering of the equivalent muons is given by

$$\frac{d^2\sigma}{dE'_\mu d\Omega} = \int dx_1 f_{\mu/Z}(x_1) \frac{d^2\sigma}{dE'_\mu d\Omega}(x_1), \tag{115}$$

where $\frac{d^2\sigma}{dE'_\mu d\Omega}(x_1)$ can be calculated from the usual invariant variables in deep inelastic lepton scattering (see, e.g., Eq. (35.2) of [280]). Here the scattering angle of the lepton is θ and its energy E'. The accompanying muon of opposite charge, as well as the remnants of the struck nucleus, will scatter to small angles and generally remain unobserved, see Fig. 33. The hadrons scattered

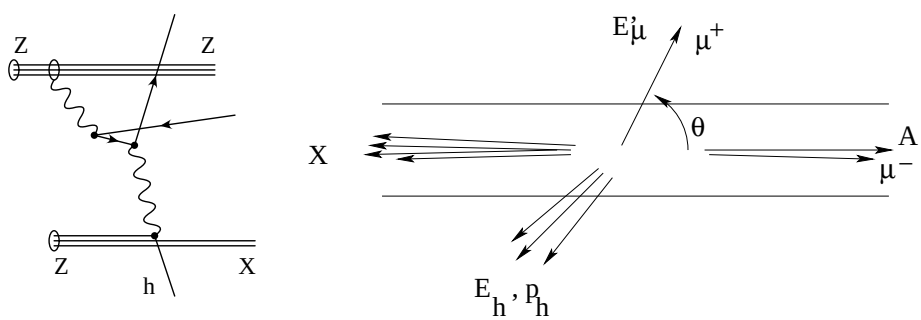

Fig. 33. Events where the "equivalent muon" is scattered deep inelastically on the other ion are characterized by one muon being emitted with a large transverse momentum, whereas the other muon escapes unobserved (together with the remnants of the struck ion) in the forward direction. Energy and momentum of the struck parton can be used to infer the energy of the (initial) equivalent muon.

to large angles can be observed, with total energy E_h and momentum in the beam direction of p_{zh}. One can use the Jacquet-Blondel variable y_{JB} defined as

$$y_{JB} = \frac{E_h - p_{zh}}{2E_\mu}. \tag{116}$$

The missing hadrons which do not enter the detector (which we assume to be almost 4π) have a small p_T, and thus their contribution to the numerator $E_h - p_{zh}$ is small (ultrarelativistic particles are assumed). One gets a good

estimate of y using this method. Combining this with Eq. (3.27) of [207] the initial energy of the equivalent muon E_μ can in principle be reconstructed as

$$E_\mu = \frac{1}{2}\left[E_h - p_{zh} + E'_\mu(1-\cos\theta)\right]. \tag{117}$$

This is quite similar to the situation at HERA, with the difference that the energy of the lepton beam is continuous, and its energy has to be reconstructed from the kinematics (How well this can be done in practice remains to be seen). Of course the struck parton also has to go through the nucleus, and there is the possibility of FSI with it. This could introduce some uncertainty in the reconstruction.

Quite similar also the excitation of individual nuclear states is possible in this way. As these states can decay electromagnetically, they are a possible source of high energetic photons. Recently this excitation was discussed [281] for a related process, where pairs are produced first and then excite the nuclear levels in a second step. It is astonishing that the authors found a quite large cross section of 5.1 barn for this process in the case of CaCa collisions at the LHC.

7.5 Radiation from e^+e^--Pairs

The bremsstrahlung in very peripheral relativistic heavy ion collisions was found to be small, both for real [10] and virtual [282] bremsstrahlung photons. This is due to the large mass of the heavy ions. Since the cross section for e^+e^- pair production is so large, one may expect to see sizeable effects from the radiation of these light mass particles. For e^+e^- colliders it was found that *"at large values of s the photon emission process in electroproduction of the e^+e^- pair ... becomes very important (and in a number of cases, decisive)"* [283].

In the soft photon limit (see, e.g., [284]) one can calculate the cross section for e^+e^- pair production accompanied by soft photon emission

$$Z + Z \to Z + Z + e^+ + e^- + \gamma \tag{118}$$

as

$$d\sigma(k, p_-, p_+) = -e^2\left[\frac{p_-}{p_-k} - \frac{p_+}{p_+k}\right]^2 \frac{d^3k}{4\pi^2\omega} d\sigma_0(p_+, p_-), \tag{119}$$

where $d\sigma_0$ denotes the cross section for the e^+e^- pair production in heavy ion

collisions (without soft photon emission). The corresponding Feynman graphs are given in Fig 34(a)+(b). An alternative approach is to use the double equivalent photon approximation and calculate the (lowest order) matrix element for the QED subprocess

$$\gamma + \gamma \to e^+ + e^- + \gamma.$$

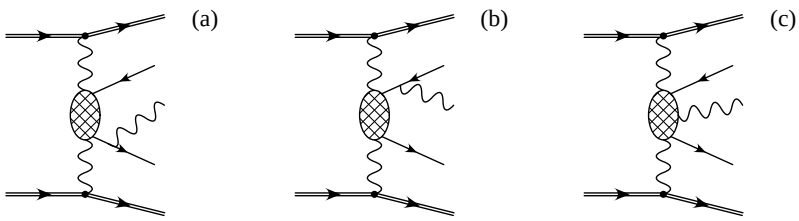

Fig. 34. Emission of a bremsstrahlung photon from pairs produced electromagnetically. Process (a) and (b) are dominant in the infrared regime. For the calculation either the IR approximation together with a full calculation of the pair production was used or a full calculation of all three diagrams together with photon spectra from double equivalent photon approximation (DEPA). Similar diagrams, where the photon line is attached to the ions are generally small due to the heavy mass of the ions. They are neglected here.

In Fig. 35 we show results of calculations for soft photon emission. The cross section for the QED process (Eq. (7.5) above) in lowest order was used and folded with the corresponding (double) equivalent photon spectra [285].

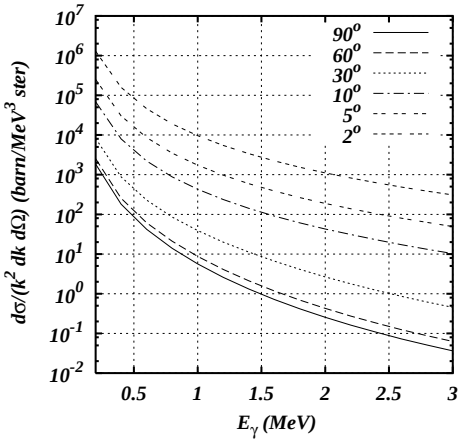

Fig. 35. The energy-dependence of bremsstrahlung-photons from e^+e^- pair production is shown for different angles. We show results for PbPb collisions at LHC.

These low energy photons might constitute a background for the detectors. Unlike the low energy electrons and positrons, they are not bent away by the magnets. The angular distribution of the photons also peak at small angles, but again a substantial amount is still left at larger angles, even at 90°. The

typical energy of these low energy photons is of the order of several MeV, i. e., much smaller than the expected level of the energy equivalent noise in the CMS ECALs [286].

7.6 Bound-free Pair Production

The bound-free pair production, also known as "electron-pair production with capture", is a process which is also of practical importance for relativistic heavy ion colliders. An electron-positron pair is produced, where the electron is not free but bound in an atomic state of one of the ions:

$$Z_1 + Z_2 \rightarrow (Z_1 + e^-)_{1s_{1/2},\dots} + e^+ + Z_2. \tag{120}$$

As this changes the charge state of the nucleus, it is lost from the beam in the collider. Together with the electromagnetic dissociation of the nuclei (see Sec. 5.1 above) these two processes are the dominant loss processes for heavy ion colliders. It has only been realized recently [169], see also [92,287], that this process can also result in a localized beam-pipe heating: the atomic states are produced with a perpendicular momentum of the order of m_e, which is rather small and therefore leads to a narrow singly-charged ion beam. These beams with altered magnetic rigidity will deposit their energy in a localized region of the beam pipe and cause a localized heating. This can lead to the quenching of the superconducting magnets. The energy deposited per unit time is of the order of Watts. This limits the luminosity of the PbPb collider at LHC [92]. Due to the lower beam energy at RHIC, the energy deposit there is smaller and therefore less important.

From a simple kind of coalescence model, a scaling law for the cross-section σ_n for bound-free pair production of the form

$$\sigma_n \sim \frac{Z_1^5 Z_2^2}{n^3} \tag{121}$$

can be derived, where n is the principal quantum number of the bound state and only s-states are populated [288,289]. It is easiest to see this in a system where the nucleus Z_1 is at rest.

A typical graph is shown in Fig. 36. An atom $(Z_1 + e^-)$ with momentum $\vec{k}$ is produced. The bound state wave function is a strongly peaked function of the relative momentum $\vec{\kappa}_{rel} = \vec{l} - (M_{Z_1}/M_{(Z_1+e^-)})\vec{k} \sim \vec{l} - \vec{k}$ where $\vec{l}$ is the three-momentum of the photon exchanged with the target. This momentum is of the order of m_e, while the momentum κ_{rel} is of the order of $Z_1 \alpha m_e$ (i.e. Z_1 times the Bohr momentum $p_{Bohr} = \alpha m_e$.). Since this momentum l is

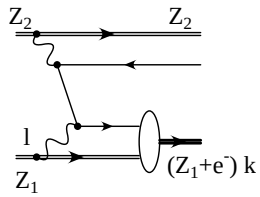

Fig. 36. A typical graph describing the bound-free pair production process, see [288].

usually much larger than κ_{rel} the loop integration over the relative momentum factors out and the factor $\Psi(0) \sim Z^{3/2}$ is found, where Ψ is the bound state s-wave function in coordinate space. The cross section to produce free pairs is proportional to $Z_1^2 Z_2^2$; so the scaling law Eq. (121) above is obtained directly from the scaling properties of the hydrogen-like wave-functions.

The calculations to be discussed in the following are not done along these lines. Instead the matrix elements involving the full wave functions of the bound and free lepton in the field of nucleus Z_1 are evaluated directly. As will be seen below, these scaling rules still hold to a good degree of accuracy. Not unexpectedly deviations are found for the large values of Z_1 , where $Z_1\alpha \lesssim 1$. In these cases the argument given above is not so well fulfilled ($\kappa_{rel} \lesssim m_e$ but not $\ll m_e$). But still, the $1/n^3$ scaling is also very well fulfilled in this case, see below (and Fig. 37).

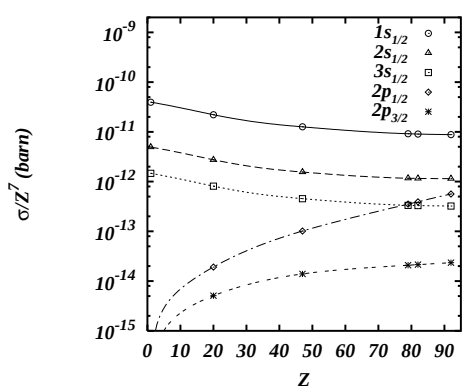

Fig. 37. The cross section for the bound-free pair production process are shown for LHC energies (using $\gamma = 3400$) as a function of the charge of the ion Z. The cross sections for capture to a given state with quantum numbers n_f, κ_f are scaled by the factor Z^7, see Eq. (121).

Recently, the cross-section for the process Eq. (120) was calculated in PWBA using exact Dirac wave functions for a point nucleus [290]. The formalism of [291] was extended in a straightforward way to the heavy ion case. The cross-section for capture to the n, κ state can be written as

$$\sigma_{n_f,\kappa_f}^{(bfpp)} = 16\pi^2 \left(\frac{Z_P \alpha_{em}}{\beta_{ion}}\right)^2 \sum_{\kappa_i} \int_{m-E_i}^{\infty} d\omega \int_0^{\infty} \frac{d(k_\perp^2)}{k_\perp^2 + k_z^2}$$
$$\times \left\{ \frac{1}{k_\perp^2 + k_z^2} T_l + \frac{\beta_{ion}^2}{2} \frac{k_\perp^2}{\left[k_\perp^2 + (k_z/\gamma_{ion})^2\right]^2} T_\perp \right\}. \tag{122}$$

Here β_{ion} and γ_{ion} are the velocity and the Lorentz factor of the projectile ion in the rest frame of the target ion, $k_\perp$ denotes the perpendicular momentum of the exchanged photon, $k_z = \omega/\beta_{ion}$ is its component in the beam direction and the energy is given by ω. The quantities $T_\perp$ and T_l are functions of ω and Q^2, independent of γ. For the integrations over $k_\perp$ and ω a logarithmic grid in ω and $k_\perp$, with energies and momenta up to 500 m_e and angular momenta up to $l = 200$ was used.

In addition to $1s_{1/2}$ capture the capture to the $2s_{1/2}$, $2p_{1/2}$, $2p_{3/2}$ and $3s_{1/2}$ states was also calculated explicitly. The only approximation in these calculations is the neglection of higher order effects (in Z_2). In Fig. 37 we show the dependence of the cross-section (divided by the approximate scaling factor Z^7) as a function of Z for various bound states (We consider the symmetric case $Z_1 = Z_2 = Z$; as the dependence on the projectile charge (in lowest order) is given by Z_2^2 — see the scaling law Eq. (121) — the asymmetric cases can be found as well.) We especially note the rise of the cross-section for $p_{1/2}$ states. This is due to the s-wave character of the small component of the bound-state wave-function. We also see a deviation from the Z^7 scaling, which is due to the behavior of the Dirac wave functions for small values of r [292]. While the bound state wave function is further increased as compared to the nonrelativistic Z^3 rise, the Coulomb repulsion of the positron causes the $s_{1/2}$ curves in Fig. 37 to decrease with increasing Z. The $1/n^3$ scaling with the principal quantum number n for the s-states is very well fulfilled in these calculations for all values of Z.

The cross section per target in Eq. (122) can be shown to be of the form

$$\sigma = A \ln \gamma_{lab} + B = C \ln \gamma_{ion} + D. \tag{123}$$

This form has been found to be a universal one at sufficient high values of γ. The constant A and B (and alternatively C and D) then only depend on the Z value of the target. Parameterizations for A and B [290] for typical cases are given in Table 5.

The calculation of bound-free pair production has a long history. Let us mention here the papers [293–298]. Most of these calculations have either not been done at the high beam energies relevant for RHIC and LHC or are based on the EPA. In [10] an analytical formula for bound-free pair production was

Ion	A	B	σ,$\gamma_{lab} \approx 100$	σ, $\gamma_{lab} \approx 3400$
Pb	35.5barn	-22.1barn	146 barn	272 barn
Au	28.7barn	-17.8barn	114 barn	212 barn
Ca	4.46mbarn	-2.88mbarn	18.7 mbarn	33.9 mbarn

Table 5
Parameters A and B (see Eq. (123)) as well as total cross sections for the bound-free pair production per target for RHIC and LHC. The parameters are taken from [290]. Capture to the $1s$-, $2s$-, $2p1/2$-, $2p3/2$-, and $3s$-states are taken into account.

given, starting from approximate wave functions for electron and positron. For large values of Z this formula underpredicts the cross-section. The reason for this was recently discussed in [299]. All other results were found to be in agreement with each other [290].

Most calculations were done in first order in the interaction with the projectile only. For a long time the effect of higher order processes have been under investigation. Such higher order processes would violate the Z_2^2 scaling in Eq. (121). At lower beam energies, in the region of a few GeV per nucleon, coupled channel calculations have indicated, that these give large contributions, especially at small impact parameters, increasing the cross section by orders of magnitude. Newer calculations tend to predict considerably smaller values at higher energies, indicating that the number of channels used in the original calculations was not sufficiently large enough [252]. In a recent calculation such effects were studied at high beam energies [259] in the high energy limit $\gamma \to \infty$. In these calculations the higher orders were found to be quite small (less than 1%) and even tend to reduce the cross section. Higher order effects are more important for the smaller impact parameters $b \sim 1/m_e$, where the fields are largest. It seems interesting to note that very large (almost macroscopic) impact parameters contribute: for $\omega = 1$ MeV $\sim 2m_e$ and $\gamma_{ion} = 2 \times 10^7$ (relevant for PbPb collisions at LHC) one has $b_{max} = \frac{\gamma_{ion}}{\omega} \sim 4\mu m$.

There are experimental results of bound-free pair production for fixed targets at the Bevalac, AGS, and SPS/CERN. At Bevalac energies, the experimental results [300–302] are not quantitatively reproduced by lowest order theories. Higher order effects are present for the systems with $Z\alpha \lesssim 1$, see the conclusion of [302]. At the higher AGS energies [303,304], higher order effects become smaller and there is good overall agreement with theory. A cross-section of 8.8 b was found for AuAu collisions at $\gamma_{ion} = 12.6$, in agreement with the theoretical results of [290,295,298]. Screening effects due to the target electrons will be small, since only small impact parameters contribute appreciably. At the even higher SPS energies, the effects of the target electrons (screening, as well as, "antiscreening") should be taken into account [305–307]; for further details see the references given above. The bound-free pair production was measured at the SPS for $\gamma = 168$ with a fixed target [308,309]. There is an

overall agreement with theoretical expectations, for details we refer to these papers.

In principle the same process is also possible for muon-production. Due to their larger mass and therefore smaller Bohr radii, muon-capture is much more sensitive to the finite size of the nucleus. But the cross section for this process are rather small.

The process corresponding to Eq. (120) with one of the ions replaced by an antiproton $\bar{p}$ was used to produce fast antihydrogen [288,310,311]. In [311] a value of $1.12 \pm 0.14 \pm 0.09$ pb was given for the cross section for $Z_2 = 1$. The momentum of the antiproton beam was in the range between 5203 and 6323 MeV. Due to experimental limitations all capture into the $1s$-state and 98% of those into the $2s$-state but no higher states were measured. This experimental value is in agreement with the theoretical ones of 0.89 pb [291] and 1.02 pb [312] for $\gamma_{ion} = 6$. (The contribution of the capture to the $2s_{1/2}$-state is given by the $1/n^3$ scaling law, as discussed above.)

Finally we discuss a practical aspect. When passing through the magnetic fields in the collider, it is possible in principle that the atom formed in the interaction region will be subsequently ionized in the magnetic fields of the system. Since this would alleviate the problems related to beam pipe heating (see the discussion above) we give now a simple estimate, which shows that this effect will be negligible in practice. Let us assume that the $(Z + e^-)$ atom moves through a constant magnetic field of strength B. In its rest-frame this corresponds to an electric field of strength $E = \gamma_{lab}\beta_{lab}B$, i.e., a linear term eEx is added to the Coulomb potential of the electron in the field of nucleus Z. This could cause ionization by tunneling through this barrier, see, e.g., [292]. For a given binding energy $E = 1\text{Ry}\,\frac{Z^2}{n^2}$, with $1\text{Ry} = 13.6eV$, this escape of the electron from the Coulomb barrier is even allowed classically for a certain critical field. For a given Z and electric field E a critical value n_{crit} is found, above which the atom ionizes in this classical approach. Such field ionization is well known for the case of the loosely bound Rydberg atoms. This ionization will happen very fast, it is of the order of the classical orbiting time of an electron in the corresponding state with principal quantum number n. We find

$$n_{crit}^4 = 3.2 \times 10^8 Z^3/E, \tag{124}$$

where E is the field strength given in units of V/cm. See also Eq. (54.2) of [292]. As an example we take $Z = 82$, $E = 10^{10}V/\text{cm}$ which corresponds to a magnetic field of $B = 1$ Tesla and $\gamma = 3000$. We have $n_{crit} \sim 12$, i.e. only states with very high principal quantum number will be ionized. According to the $1/n^3$ scaling law, their contribution can safely be neglected.

Finally we note that the electron and the positron can also form a bound state: positronium. This is in analogy to the $\gamma\gamma$-production of mesons ($q\bar{q}$ states) discussed in Sec. 3.6. With the known width of the parapositronium,

$$\Gamma^{(0)}(n^1 S_0) = \frac{\alpha^5 m_e}{2\, n^3}\,, \tag{125}$$

the photon-photon production of this bound state was calculated in [313]. The production of orthopositronium, $n = 1\ ^3S_1$ was calculated recently [314] and [315], see also [316] where the three-photon production of vector mesons is treated. In [317] an effective parameter ρ is introduced, which controls the relative importance of two- and three-photon- processes (see also p. 1677 of [15]):

$$\rho = \left(\frac{Z\alpha\Lambda}{m_{\mu\mu}}\right)^2, \tag{126}$$

with $1/\Lambda^2 = 1/6\,\langle r^2\rangle$ and $\langle r\rangle^2$ is the mean square radius of the charge distribution and $m_{\mu\mu}$ is the mass of dimuonium (or any other produced particle). This factor ρ is always much smaller than 1 except for positronium, where ρ is given by $Z\alpha$ (in this case $\Lambda \approx 1/R$ should be replaced by $\Lambda \approx 1/m_e$, see the discussion at the beginning of this chapter). Therefore the production of orthopositronium is only suppressed by the factor $(Z\alpha)^2$ as compared to the two-photon production of parapositronium. Since $(Z\alpha)^2 \sim 0.5$ for the heavy systems like Au or Pb, one expects that both kinds of positronium are produced in similar numbers. Detailed calculations show that the three-photon process is indeed not much smaller than the two-photon process [314,318].

The bound $\mu^+\mu^-$ system ("dimuonium") is an interesting example of a pure electromagnetic bound state, which can be effectively studied in heavy-ion collisions. Dimuonium has a mass of about two muon masses, $m_{\mu\mu} \approx 211$ MeV and the binding energy in the ground state is of the order of 1.4 keV. Although this system is well known theoretically, see [319–324], dimuonium has not been observed experimentally up to now. Like in the case of positronium, one should distinguish para- and ortho- dimuonium with $S^C = 0^+$ and 1^- respectively, which can be produced in electromagnetic decays of light mesons, i.e. orthodimuonium in radiative decays of η- [322,325] and K_L- mesons [323], while paradimuonium in decays of ω- and ϕ- mesons. The hyperfine structure and the decay rate of dimuonium are influenced by the electronic vacuum polarization in the far time-like asymptotic region, which does not yield any contribution in any other bound states [326,327]. In particular, a relative contribution

of 1.6 % to the decay rate of orthodimuonium is predicted in [320,321] and this would allow a test of QED in a previously unexplored kinematic region.

Dimuonium production in heavy ion collisions is studied in [328] in detail. Below we will mainly follow this paper. Paradimuonium is produced dominantly in two-photon processes, orthodimuonium in three-photon processes while its production by bremsstrahlung is suppressed, see Fig.38. The paradimuonium

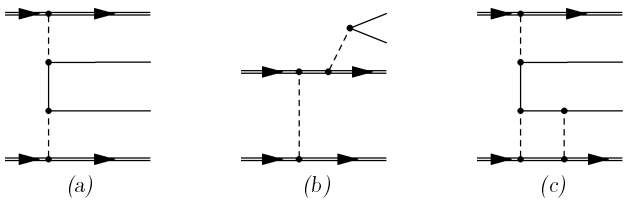

Fig. 38. Diagrams for two-, one- (bremsstrahlungs) and three- photon production mechanism of a dimuon bound state in heavy ion collisions [328].

production cross-section is determined according to Eqs. (67) and (68) by the $\gamma\gamma$-width, which in the leading order approximation is given by Eq. (125) with m_u instead of m_e. Orthodimuonium cross section is suppressed compared with that of paradimuonium by more than an order of magnitude see Eq. A1 of [328]. The production cross sections are given in Table 6. The main decay

	$\sigma(AA \to AA + PDM)$, μb	$\sigma(AA \to AA + ODM)$, μb
AuAu, RHIC	0.15	0.021
PbPb, LHC	1.35	0.089
CaCa, LHC	6.6×10^{-3}	6.9×10^{-5}

Table 6
Production cross sections for paradimuonium (PDM) and orthodimuonium (ODM) in heavy ion collisions, as predicted in [328].

channels are the annihilation processes into two photons for paradimuonium and e^+e^- for orthodimuonium. Dimuonium can therefore be observed via these decay channels. Further details, especially concerning background processes, can also be found in [328].

One might even think of the production of ditauonium (DT). With the ditauonium mass $m_{DT} = 3554\ MeV$, its width $\Gamma_{\gamma\gamma}$ (see Eq. (125)) is given by 0.018 eV. From these values we can immediately obtain the cross section of ditauonium production in $\gamma\gamma$-interactions in heavy ion collisions. For example, in PbPb collisions at the LHC we obtain from Eq. 68 and Fig. 14 the production cross section $\sigma_{DT} = 0.7\ nb$. We note that the lifetime of the τ of 291×10^{-15}s corresponds to the width of τ-lepton $\Gamma_\tau = 0.00226$eV, i.e., the ditauonium $\gamma\gamma$-width is about 5 times larger than the width of its weak decay given by $2\Gamma_\tau$ and thus the ditauonium can be really produced as a bound state of two τ-leptons.

8 Methods of Detecting Very Peripheral Collisions in Experiments at Heavy Ion Colliders

In this chapter we discuss the study of $\gamma\gamma$-events in heavy ion collisions from an experimental point of view. We discuss the general characteristics of these kind of events and how they can be used as basic signatures for the triggering and off-line selection of these events. We discuss further various background sources for $\gamma\gamma$-processes, including single-photon, photon-Pomeron and double Pomeron processes, their corresponding cross sections and expected trigger rates. We also give an overview of the experimental methods used for the selection of different final states produced in $\gamma\gamma$ interactions, based on the experience of current e^+e^--collider experiments, as well as, on the first studies of very peripheral events in heavy ion collisions at RHIC and Monte-Carlo simulations done for the future heavy-ion experiments at LHC.

8.1 Signatures of $\gamma\gamma$-Processes in Heavy Ion Collisions

The experimental technique for the detection of $\gamma\gamma$-processes is based on special observables (signatures) which make the $\gamma\gamma$-processes different from other very peripheral processes, as well as, from strong peripheral interactions of the ions. In particular one of the main features of coherent electromagnetic interactions of relativistic ions is the small transverse momentum transfer from the ions. As a result the ions remain intact after such an interaction and in general they will be kept for some time in the beam pipes and thus cannot be detected in an experimental setup. Therefore very clean events will be detected with particles produced mostly in the central rapidity region. (In Sec. 2.5 we already mention the interesting possibility to tag the scattered protons in pp collisions studied in [76]. In the case of ions this is probably impossible to achieve, due to the low limits on x, see Sec. 1 above.)

It is useful to mention in this context also the excitation of the Giant Dipole (GDR) and other higher Multipole and/or Multiphonon Resonances (MR), which lead in their decay to the emission of one or several low-energy neutrons in the nucleus rest frame, see Sec. 5.1. In the laboratory frame — due to the very high Lorentz factor of ions and the low momenta of the neutrons in the ion frame — one has almost monoenergetic neutrons, which can be detected in the very forward hadron calorimeters commonly called the Zero Degree Calorimeters (ZDC) of the experimental setup by the deposit of multiples of the energy $\gamma_{lab} m_n$ for each detected neutron. These almost monoenergetic signals in the ZDCs, see Figs. 19 and 20, and their small number are therefore a good signature of the electromagnetic nature of the interaction between the two ions.

Another feature of $\gamma\gamma$-processes in heavy ion collisions is a relatively low multiplicity of secondary particles compared to those in strong ion interactions. Fig. 39 shows the average charged particle multiplicity for the process $\gamma\gamma \to X$ as a function of the effective $\gamma\gamma$-mass as predicted by PYTHIA [329]. This should be compared with the multiplicity expected in strong peripheral ion collisions. As an example the expected average charged particle multiplicity distribution vs. pseudorapidity $dN_{\rm ch}/d\eta$ in PbPb collisions with a large impact parameters b between $1.8 \times R_{Pb} < b < 2 \times R_{Pb}$ is shown in Fig. 40 for LHC energy. This multiplicity distribution has been calculated using HIJING [330]. The total charged particle multiplicity in hadronic peripheral collisions is much higher than that in $\gamma\gamma$-processes; even if one is using a restricted aperture, let's say, $|\eta| < 1$, the multiplicity is still expected to be of the order of hundreds and therefore remains very high. The most important signature

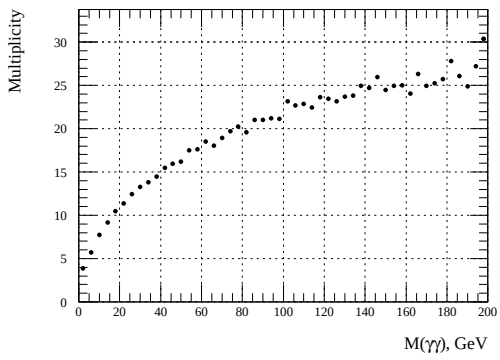

Fig. 39. The average charged particle multiplicity in $\gamma\gamma$-interactions vs. the effective $\gamma\gamma$-mass predicted by the PYTHIA model [329].

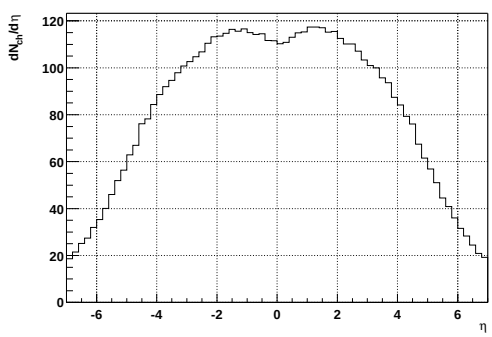

Fig. 40. Charged particle multiplicity $dN_{\rm ch}/d\eta$ in hadronic peripheral PbPb collisions with impact parameter $1.8 \times R_{Pb} < b < 2 \times R_{Pb}$ calculated with the HIJING generator [330].

of $\gamma\gamma$ processes in coherent ion-ion collisions is the quite low total transverse momentum $P_\perp$ of the produced system. As discussed in Chap. 1, see Eq. (4), the $\gamma\gamma$ system has a transverse momentum less than about $\sqrt{2}/R$, where R is the nuclear radius. But the average transverse momenta is even smaller than this, namely

$$P_\perp \sim M_{\gamma\gamma}/\gamma_{lab}. \tag{127}$$

For the effective $\gamma\gamma$ mass range at RHIC ($M_{\gamma\gamma} < 3$ GeV), as well as, at LHC ($M_{\gamma\gamma} < 100$ GeV) we have $P_\perp \sim 30\ MeV$. It should be remembered

however that transverse momentum distributions have not yet been calculated explicitly within the semiclassical approximation. The problem is formulated in [88]. In order to use this feature for selecting $\gamma\gamma$-processes the experimental setup has to provide a large enough aperture for the detection of both charged and neutral particles, including also secondary photons. It should provide also a sufficiently good transverse momentum resolution.

Many of the $\gamma\gamma$ reactions, which are planned to be studied, are exclusive processes. In this case the net charge of the detected particles or the number of charged tracks can be taken into account. This leads to one more selection criteria for $\gamma\gamma$-processes, requiring an even number of charged track of opposite signs.

We therefore may formulate the criteria for the selection of the two possible classes of two-photon processes in collisions of relativistic ions:

- *The pure $\gamma\gamma$-processes* are characterized by a small multiplicity of the charged particles in the central detectors, a small total transverse momentum of the produced system and the absence of any signal in both ZDCs;
- *The $\gamma\gamma$-processes with EM excitation of the secondary ions* are characterized as well by a small multiplicity of the charged particles in the central detectors, a small total transverse momentum of the produced system and by neutrons coming from the GDR or MR decay in one or both ZDCs.

Actually these are ideal criteria for the event identification, which in real experiments are often less clear due to different limitations of the experimental setup that lead to distortions and mixtures between the different event classes, as well as, to the contamination of them by background processes.

8.2 Background Processes

In this section we discuss different sources of background for very peripheral processes in relativistic heavy ion collisions. As mentioned already in Chap. 6, one should distinguish between photon-photon, photon-Pomeron and Pomeron-Pomeron processes. All of them are quite interesting in themselves and they also have similar signatures. The physical nature of them is quite different, and each of these processes should therefore be considered as a background for the others. All those processes belong to the class of very peripheral collisions, taking place at impact parameter $b > 2R$. The strong interaction of the ions with impact parameter $b \approx 2R$ is a common source of background for all very peripheral processes and should be taken into account. This is a physical background, as it results from the interaction of the ions with each other.

On the other hand there is background coming from the apparatus, which is then specific for each experimental setup. As potentially important sources of such a background we discuss in the following one-photon processes, the photonuclear excitation of the ions and multiple e^+e^- pair production. Cosmic ray events and beam-gas interaction should be mentioned also in this respect as possible background sources of the apparatus.

8.2.1 Physical Background

Two-photon processes in relativistic ion collisions are discussed in detail in Chap. 3 including the corresponding cross sections and rates. Pomeron-Pomeron processes as a possible background have been discussed in Chap. 6.

As was mentioned there the Pomeron-Pomeron cross section increases with $A^{1/3}$ or equivalently with $Z^{1/3}$, compared to the Z^4 rise of the photon-photon processes. Therefore in heavy ion collisions we can expect the predominance of two-photon processes, whereas in light ion and especially in *pp*-collisions the contribution of Pomeron-Pomeron processes will be much more essential. As shown in Chap. 6 this is confirmed in detailed calculations, see, e.g., [21,227].

The cross section for the photon-Pomeron processes in ion-ion collisions can then be estimated with the help of the factorization relations [115,116], as explained in Sec. 3.5, using the cross section for photon-photon and Pomeron-Pomeron interactions:

$$\sigma^2_{tot}(\gamma\mathbb{P} \to X) = \sigma_{tot}(\gamma\gamma \to X)\ \sigma_{tot}(\mathbb{P}\mathbb{P} \to X), \tag{128}$$

which is valid also for the corresponding differential cross sections. This can be used to estimate the total cross section of the photon-Pomeron processes in relativistic ion-ion collisions using the known cross sections of the photon-photon and Pomeron-Pomeron processes as $\sigma_{\gamma\mathbb{P}} = \sqrt{\sigma_{\gamma\gamma}\sigma_{\mathbb{P}\mathbb{P}}}$.

The cross sections of the three different processes for PbPb, ArAr and *pp* collisions at the LHC, as well as, for AuAu, CuCu and *pp* collisions at RHIC are shown in Table 7.

From this it is seen that at the LHC in the very peripheral PbPb collisions we have dominantly two-photon processes, in *pp* collisions on the other hand double Pomeron processes dominate, while in the ArAr collisions cross sections of all three very peripheral processes are comparable. Similar cross sections ratios for different ion species are valid also at RHIC.

Apart from the different A-dependence of the very peripheral processes the selection of one of the processes can be enforced by using the following additional

signatures:

(1) A different total P_t distributions for very peripheral processes is expected because in the case of Pomeron-Pomeron processes the P_t are in general higher than in the case of photon-Pomeron processes, and these are again higher than those in photon-photon processes, see [24].
(2) The different processes will lead to a different C-parity of the (exclusive) system produced in the different very peripheral processes. C-parity should be even in the two-photon and double-Pomeron processes, while it is odd in the case of photon-Pomeron processes,
(3) The probabilities for the excitation of the GDR and MR of the ions, that is, of the additional electromagnetic excitation of the nuclei should be a good sign for a very peripheral collision, discriminating them against, e.g., grazing collisions or diffractive processes. The probability to excite a GDR or MR in the ions is much higher for an additional photon-induced reaction than for a hadronic collision. The GDR favors neutron over proton emission, whereas a direct hadronic nucleon emission is insensitive to proton/neutron, and thus the emission of a soft proton in the ion rest frame and detection of the almost monoenergetic proton in the charged ZDC could be regarded as a sign of a Pomeron-ion interaction.

	Reaction	$AA \to X$ (nuclear)	$AA \to AAX$ ($\mathbb{P}\mathbb{P} \to$ hadrons)	$AA \to AAX$ ($\gamma\gamma \to$ hadrons)	$AA \to AAX$ ($\gamma\mathbb{P} \to$ hadrons)
L	σ(PbPb), barn	7.8	$8.4 \cdot 10^{-4}$	$1.5 \cdot 10^{-1}$	$1.1 \cdot 10^{-2}$
H	σ(ArAr), barn	2.1	$6.7 \cdot 10^{-4}$	$5.6 \cdot 10^{-6}$	$6.1 \cdot 10^{-4}$
C	$\sigma(pp)$, barn	0.07	$5.2 \cdot 10^{-4}$	$1.5 \cdot 10^{-8}$	$2.8 \cdot 10^{-6}$
R	σ(AuAu), barn	7.5	$2.2 \cdot 10^{-4}$	$1.8 \cdot 10^{-3}$	$6.3 \cdot 10^{-4}$
H	σ(CuCu), barn	3.1	$2.1 \cdot 10^{-4}$	$9.3 \cdot 10^{-5}$	$1.4 \cdot 10^{-4}$
I	$\sigma(pp)$, barn	0.07	$2.2 \cdot 10^{-4}$	$1.7 \cdot 10^{-9}$	$6.1 \cdot 10^{-7}$
C					

Table 7
Cross sections of the nuclear, Pomeron-Pomeron, photon-photon and photon-Pomeron processes ($M > 1\ GeV$) in PbPb, ArAr, pp collisions at the LHC and in AuAu, CuCu, pp collisions at the RHIC.

Please note that in the case of heavy ion collisions, due to the large probabilities for electromagnetic excitations, see Sec. 5.1, additional electromagnetic processes, which we illustrate for the case of ρ^0-production in AuAu collisions at RHIC in Fig.41, are very likely. In heavy ions, the probability for the excitation of the GDR is large for small impact parameter, but this is not essential for the selection of $\gamma\gamma$-processes because for heavy ions $\gamma\gamma$-processes dominate over the processes involving the Pomeron. The signature 3 above could

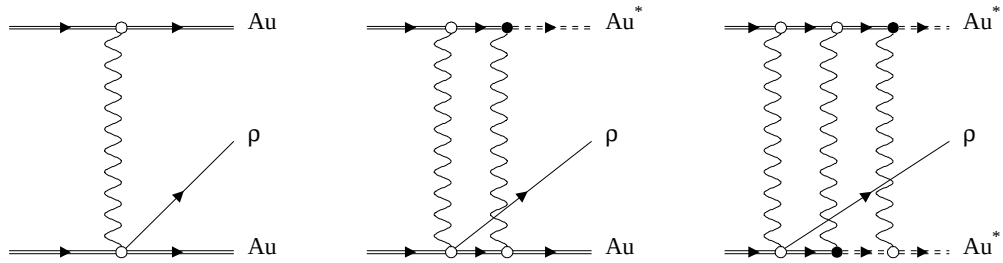

Fig. 41. Diagrams of ρ^0 production in heavy ion collisions when neither, one or both nuclei are excited electromagnetically. Diagrams are show up to vertex permutations.

become important in the case of intermediate ion collisions, where on the one side the cross sections of photon-photon, photon-Pomeron and Pomeron-Pomeron processes are comparable, but on the other side the cross section of GDR excitation is low as well, and thus the analyzing power of signature 3 becomes very high.

Concerning the strong interaction of the two ions, these events in general are quite different in their properties from the very peripheral ones discusses above, compare, for example, Figs. 39 and 40. Nevertheless in the case of detectors covering only a small aperture range, like the central detector and especially the ZDC, the background from these processes should be taken into account.

8.2.2 Apparatus Backgrounds

Since the cross sections of the interesting coherent processes in relativistic very peripheral ion-ion collisions are much smaller than the total cross sections, the key point in all experiments to study very peripheral ion-ion collisions is the organization of the primary or "Level Zero" (L0) trigger, which is needed in order to start the Data Acquisition System (DAQ) of the experiment.

The Higher Level (HL) triggers are used then further only to stop or continue the data taking by the DAQ of the triggered event from the detectors. The main aim of the HL-triggers is to prevent storage of the physically uninteresting events. Due to the finite dead time of the DAQ the L0 trigger rate cannot be too high, otherwise the data taking in the experiment will be fully blocked. Thus processes, which give a too high a load on the L0 trigger detectors, should be considered as a most important source of background.

The first trigger on coherent processes in relativistic heavy ion collisions was developed for the STAR experiment at the RHIC [331]. The L0-trigger is based on the charged particle multiplicity in the pseudorapidity interval $|\eta| < 1$,

measured in the Central Trigger Barrel (CTB) and Multi-Wire Chambers (MWC) at the endcaps of the TPC. The information from the trigger detectors is divided into 4 bins in azimuthal angle which can be used to apply cuts on event topology to select events with tracks lying in opposite ϕ-sectors. At the L1 and L2 trigger levels the improved multiplicity information is available after refining kinematics. At the L3-level the tracking information is available to apply momentum cuts and use the charge of the tracks. The decision time of the trigger levels 0, 1/2 and 3 were given by the authors as 1.7 μs, 100 μs and 10 ms respectively. Besides these triggers STAR also used a minimum bias trigger to select events when both nuclei were dissociated [50]. This trigger is based on zero-degree calorimeters (ZDC). The presence of a signal in each of the ZDCs corresponding to one or more neutrons with the full beam energy defines events when the nuclei are electromagnetically dissociated.

The positioning of the main trigger detectors of an experiment is highly sensitive to the background processes. In this connection the low mass single and multiple e^+e^--pair production in heavy ion collisions has to be considered as one of the major background processes, because its cross section is really huge (200 kbarn for PbPb at LHC and 30 kbarn for AuAu at RHIC), the rapidity distribution is rather flat (and thus covers all detectors) and all other signatures are quite similar to those of the photon-photon processes, because the e^+e^--pair production is also just a photon-photon process, see Sec. 7.1 above. Electrons and positrons are produced preferably in the very forward or backward directions, see Fig. 25(b), but these pairs do not constitute a background for the ZDCs as their energy is rather small, Fig. 25(a), compared to the typical hadron energy in this pseudorapidity interval. But the central trigger detectors (i.e., the CTB in the case of the STAR experiment) can be essentially loaded by these pairs. Due to their low transverse momentum $P_\perp$ an essential reduction of this background can be done, if one uses the central trigger detector at a sufficiently large radius, a strong solenoidal magnetic field, or both. (In the case of the CTB at STAR its radius, 2.2 m and $B = 0.2$ T, is sensitive to charged particle with $P_\perp > 130$ MeV [331], which reduces the background from soft e^+e^--pair significantly). On the other hand if the central trigger detectors are too large, we may expect some background from cosmic ray events. As was shown in [331] the rate of cosmic rays entering the TPC is due to the large size of the TPC (16 m^2) almost 3 kHz, which is rather high. In [49] the cosmic ray flux through the STAR trigger detectors was estimated to give an important percentage of all background processes.

Another possible trigger detector, the ZDC, can be contaminated by the electromagnetic excitation of the ions alone to the Giant Dipole and other resonances, see Sec. 5.1. We are studying here the following two types of processes: one-photon exchange with the electromagnetic excitation of one of the ions and no particle detected in the central rapidity region and the production of one or more low mass e^+e^--pair together with the electromagnetic excitation of

one of the ions. The cross sections of these processes in heavy ion collisions at RHIC and LHC are equal to $\sigma_{AuAu\to AuAu^*} = 58$b, $\sigma_{AuAu\to AuAu^*(e^+e^-)_{N>0}} = 13$b, and $\sigma_{PbPb\to PbPb^*} = 114$b, $\sigma_{PbPb\to PbPb^*(e^+e^-)_{N>0}} = 22$b, respectively, using for the GDR excitation Eq. (79) and for the e^+e^- pair production Eq. (103). The similar process but with the mutual excitation of both ions have almost the same order of magnitude, as the probability for excite the GDR is not much smaller than one, see Sec. 5.1. For intermediate ions (CuCu at RHIC and ArAr at LHC) the exchange of additional soft photons leading to electromagnetic excitation is suppressed by a factor of about $A^{10/3}$, see Eq. (79). Therefore the background load on the ZDC as a potential trigger detector by electromagnetic excitation of the ions alone is important only in the case of heavy ion collisions, but it is negligible small for the intermediate and low mass ions.

8.2.3 Trigger for Very Peripheral Processes

In this subsection we briefly summarize the most essential aspects, which should be taken into account for a trigger to study the very peripheral ion collisions.

The central trigger barrel (like the CTB in STAR) with endcups have to be considered as the major detectors for the L0-trigger to select very peripheral ion collisions. The trigger requirement is a low charged particle multiplicity n_{ch} in the central trigger detectors, let's say $1 < n_{ch} < 20$. The solenoidal magnet is an obligatory part in such type of experiments, because it prevents the overloading of the trigger barrel by background processes. Two background processes should be taken into account for an optimization of the trigger detector parameters: the processes of low mass multiple e^+e^- production and the background from cosmic events. The basic parameters are the magnetic field in the solenoid B and the trigger barrel radius R_{bar} or the inner radius of endcups, R_{inn}. For the optimization of the trigger one increases the value of BR (where $R = \min\{R_{bar}, R_{inn}\}$) to reduce the background from low mass multiple e^+e^--pair production up to a value, at which the background from cosmic ray events is still not too high. The optimal detector parameters correspond probably to a detector configuration, when the background rates from the e^+e^--pair production and from cosmic events are comparable. The signals from the ZDCs are not so important, due to their contamination with processes of the electromagnetic excitation of the heavy ions. But it could be useful for the suppression of Pomeron-Pomeron processes in the case of intermediate ion collisions.

Another possibility for a very peripheral trigger in ion-ion collisions is the barrel Electromagnetic Calorimeter (ECAL). This is one of the most popular detectors used in experiments at e^+e^- and hadron colliders, see, for example, [286]. The requirement that the total deposited energy in the ECAL is suf-

ficiently low compared with the one in strong interaction of the ions, allows an effective selection of very peripheral events at a L0 trigger level. Because the energy in the ECAL from the low mass multiple e^+e^--pairs is quite small, these events do not provide any background. The strong ion interactions in peripheral collisions as a background process can be effectively suppressed by using additional signals from the ZDCs, which for these events are very high as was discussed in Chap.5. Only cosmic ray events provide in this case some background, which can be suppressed at the HL trigger level, based on general event topology, see [50].

8.3 Detection of Some $\gamma\gamma$-Processes

Two-photon processes in heavy ion collisions have not yet been widely studied experimentally with the first heavy ion collider RHIC starting its operation only a year ago. However, a group of experimentalists at the STAR detector have studied the possibility to observe $\gamma\gamma$-processes during the last six years. Earlier $\gamma\gamma$-physics has been studied at e^+e^--colliders by almost all collaborations. The experience gained of these e^+e^--experiments to detect $\gamma\gamma$ processes can be applied now to the heavy ions experiments. Below we give an overview of the major experimental observations of $\gamma\gamma$-processes at e^+e^--colliders and the studies done for heavy ion experiments.

8.3.1 Experiments at e^+e^--Colliders

All e^+e^--collider experiments which have been running so far, have accumulated a large experience for the detection of $\gamma\gamma$ processes. Although the signatures of two-photon processes in electron-position collisions differ from those in heavy-ion collisions, they still have many common features which allows to take over their experience to the future heavy ion collider experiments. Many recent experimental data from e^+e^--colliders (LEP-II, CLEO, KEKB) are for quasi-real photon interactions, like those in heavy-ion collisions. Here we give a review of the $\gamma\gamma$ processes detected by those experiments.

$\gamma\gamma \to$ hadrons. This reaction was studied by the L3 collaboration at LEP [101] to measure the total cross section for the scattering of two real photons into hadrons. The two-photon cross section $\sigma(\gamma\gamma \to \text{hadrons})$ was measured in the invariant mass range of $5 < W_{\gamma\gamma} < 185$ GeV. Hadronic two-photon events were selected by the following criteria:

- Events with the scattered beam electrons detected were rejected. This restricts the virtuality of the interacting photons to $Q^2 < 8$ GeV^2 with an average value of $\langle Q^2 \rangle \sim 1.5 \times 10^{-2}$ GeV^2.

- The total energy in the electromagnetic calorimeter was required to be between 0.5 and 50 GeV to suppress beam backgrounds and exclude radiative events.
- The detected multiplicity should be greater than six to exclude events containing τ-pairs.

After the selection the visible effective mass of the event, $W_{\rm vis}$ was measured. An unfolding procedure based on the Monte Carlo event generators PHOJET and PYTHIA was used to calculate the two-photon mass $W_{\gamma\gamma}$. The systematic uncertainties due to the Monte Carlo generators were estimated to be negligible for $W_{\gamma\gamma} < 65$ GeV, but are important for higher $\gamma\gamma$-masses.

Production of light resonances. The L3 collaboration studied also light resonance production in $\gamma\gamma$-collisions [332]. The resonances were studied in the $K^0_S K^\pm \pi^\mp$ and $\eta\pi^+\pi^-$ final states. The $\eta(1440)$, $f_1(1420)$, $f_1(1285)$ were observed. The mass region between 1200 and 1500 MeV is expected to contain several states. The pseudoscalar state $\eta(1440)$ was observed in hadron collisions and in radiative J/Ψ decay, but not in $\gamma\gamma$-collisions. Only a very low upper limit of its two-photon width was measured, which supports the interpretation of $\eta(1440)$ as a glueball candidate. Axial-vector states $f_1(1420)$, $f_1(1285)$ are also present in this mass region.

Since these are exclusive processes, their selection criteria differ from those for the process $\gamma\gamma \to X$ above:

- The $K^0 \to \pi^+\pi^-$ was identified by the secondary vertex separated from the interaction point, the effective invariant mass of the two pions and the angle correlation between the K^0 momentum and the two final tracks.
- $K^\pm\pi^\mp$ was identified by the two tracks coming from the interaction point and their dE/dx measurement being consistent with a $K\pi$ hypothesis.
- The final state $\eta\pi^+\pi^-$ was identified by the presence of two photons and two tracks of opposite charge and the $\gamma\gamma$ invariant mass.

$\gamma\gamma \to K^+K^-$, $\gamma\gamma \to K^0_S K^0_S$. These reactions were studied by the L3 collaboration at LEP [333], by the BELLE collaboration at KEKB [334] and by the CLEO at CESR [335]. The events were selected according to usual criteria for exclusive reactions, i.e., the requirement of two or four charged tracks for the K^+K^- and $K^0_S K^0_S$ final states respectively, with a net charge of zero. K^0_S mesons were identified by secondary vertex reconstruction and the invariant mass of the secondary track pairs. The vector sum of the transverse momenta of all tracks should be small. These experiments aimed to study the resonances in the mass region from 1.3 to 2.3 GeV, where glueballs are expected to be found. A tensor state $f_J(2220)$ was observed in the radiative decays of J/Ψ

and was considered a good candidate for a glueball. Since gluons do not couple to photons they cannot be produced directly in $\gamma\gamma$ collisions. The e^+e^- experiments did not observe any resonance around the mass 2220 MeV, thus they support the glueball interpretation of the $f_J(2220)$ state.

$\underline{\gamma\gamma \to c\bar{c}X,\ \gamma\gamma \to b\bar{b}X.}$ Open charm and beauty production was measured by the L3 collaboration [336,337]. The event selection was performed in two steps. The first one selects hadronic states and the second one identifies c and b quarks by their semileptonic decays. The hadronic final states were selected by requiring at least 5 tracks and a visible energy below $\sqrt{s}/3$. The visible mass of the events was restricted to $W_{\rm vis} > 3$ GeV. Then the unfolding procedure based on either PYTHIA or PHOJET was applied to obtain the $\gamma\gamma$ c.m. energy.

$\underline{\gamma\gamma \to D^{*\pm}X.}$ The inclusive production of D^*-mesons was measured by L3 [338] and OPAL [339]. $D^{*\pm}$ mesons were detected via their decay chains $D^{*\pm} \to D^0\pi_s^+$ and $D^0 \to K^-\pi^+$, $D^0 \to K^-\pi^+\pi^0$. The reconstruction of these decay chains requires a sample of events containing hadronic final states. The hadronic events were selected by cuts on the energy measured in the electromagnetic and hadronic calorimeters and using tracing information.

$\underline{\gamma\gamma \to \eta_c,\ \chi_{c0},\ \chi_{c2}.}$ Charmomium production was studied by CLEO [340,341] and L3 [342]. The $\gamma\gamma$ and total widths of these states were measured. CLEO searched for η_c meson in the $K_S^0K^\mp\pi^\pm$ decay mode, and χ_{c0} and χ_{c2} via their decay into $\pi^+\pi^-\pi^+\pi^-$. The L3 collaboration detected η_c in various decay modes with $\pi^\pm$, $K^\pm$, π^0, K^0, η' and $\rho^\pm$ in the final state. Therefore the selection criteria were the usual ones for exclusive events with such type of particles.

Summarizing the experience collected by e^+e^- experiments to study $\gamma\gamma$ interactions, one can see typical event selection criteria, which can be adapted to heavy ion collisions. The $\gamma\gamma$ events are characterized by the absence of the scattered beam particles, a low (or fixed in the case of exclusive reactions) multiplicity in the final state, low transverse momentum of the final state, zero net charge of the tracks, low (compared to the annihilation processes) energy deposited in the detectors. Depending on the reaction to be studied, different topology cuts can be applied. In the case of inclusive reactions a Monte Carlo based unfolding procedure is used to obtain the $\gamma\gamma$ mass from the visible event mass.

8.3.2 Experiments at Heavy Ion Colliders

The STAR collaboration is the first one to study $\gamma\gamma$-processes in heavy ion collisions in the AuAu collisions at 100–250 A GeV at RHIC [47,46,343,331]. The scope of their interest is lepton pair production, meson pair production, meson spectroscopy, baryon pair production, and possibly charmonium production. They studied background processes, trigger and experimental techniques to select $\gamma\gamma$-processes.

Background. STAR studied several major sources of background for the two-photon processes: peripheral hadronic nuclear collisions, beam-gas interactions, cosmic rays, photon-nucleus collisions and Pomeron processes. Cosmic rays and beam gas reactions are a problem mainly at the trigger stage, because the more precise data analysis at the later stage rejects such kind of events via track and vertex information. Detailed Monte Carlo simulation has been performed to separate signal from background [343]. Peripheral hadronic nuclear collisions were simulated with two standard nuclear event generators, FRITIOF [344] and VENUS [345] with impact parameters from 12 to 20 fm. Beam-gas interactions were simulated by the same event generators as Aup and AuN collisions where hydrogen p and nitrogen N represent the beam-gas content. Photonuclear reactions were studied by DTUNUC [346]. Only γAu collisions with photon energies larger than 10 GeV were simulated. Cosmic rays were simulated with a flux of 1.8×10^2 m^{-2}s^{-1} and the trigger rates in the TPC were estimated. The most important cuts, which discriminate $\gamma\gamma$ events from background, were found to be:

- Multiplicity: many two-photon reactions, which can be detected at RHIC, have two or four charged particles in the final state;
- the sum of the transverse momentum of the final state particles should be small, of the order $\sqrt{2}\hbar c/R$; in the analysis a cut $|\Sigma \vec{p_T}| \leq 40$ MeV was used;
- the c.m. rapidity distribution of the $\gamma\gamma$ system is centered around zero with a narrow width; the cut $|y_{\gamma\gamma}| \leq 1.0$ was applied; this cut is realized automatically by the detector acceptance and reduces also the beam-gas and photonuclear interactions since these are characterized by an asymmetric particle emission.

Monte Carlo simulation performed by the STAR collaboration [343] showed that these cuts are able to separate the signals from background.

First experimental results from STAR. RHIC had a first AuAu run in 2000, and the first reports on observation of coherent interactions in nuclear collisions appeared at the beginning of 2001. In [50] the first observation of exclusive ρ^0 production is presented. The ρ^0 are produced with small perpendicular

momentum, as expected, if they couple coherently to both nuclei. Here we pay special attention to the event selection used.

The production of ρ^0s were studied in the decay channel $\rho^0 \to \pi^+\pi^-$. The data on AuAu collisions at $\sqrt{s_{NN}} = 130$ GeV was collected during the Summer 2000 run. The ρ production was studied with two separate triggers. The topology trigger was designed to trigger ρ^0 decays detected in the central trigger barrel (CTB). The topology trigger divided the CTB into 4 azimuthal quadrants as shown in Fig. 42. This trigger selects events with at least one hit in the North

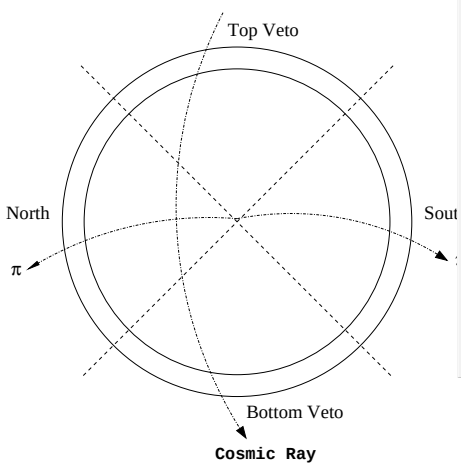

Fig. 42. Topology trigger on coherent interactions at STAR. Figure taken from [50].

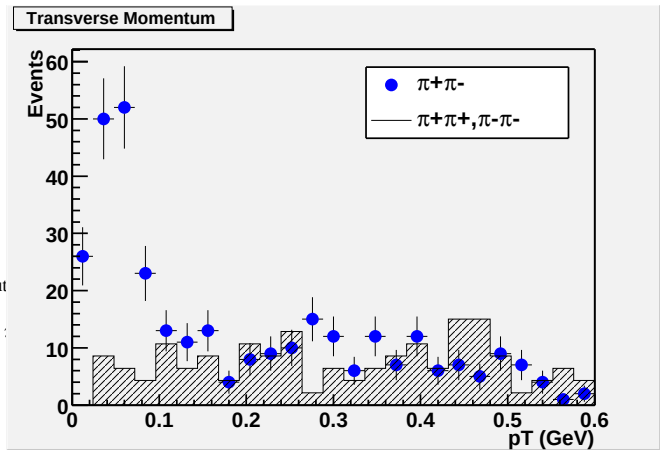

Fig. 43. The transvers momentum $P_\perp$ of the two pions triggered with the topological trigger. The enhancement at small transverse momentum, coming from the very peripheral collisions, is clearly seen. Figure taken from [50].

and the South sectors. The top and bottom quadrants were used to reject most cosmic rays. The selected events were then passed through a level-3 trigger, which rejects events with more that 15 tracks or a vertex far outside the interaction point. These cuts rejected 95% of the events and rejected events from central collisions, beam-gas interactions and cosmic rays.

A minimum bias trigger used both zero degree calorimeters (ZDC) to select events, where both nuclei dissociated. This trigger required a coincidence between the two ZDCs with a single (or more) neutron depositing their energy in each ZDC.

In the analysis STAR selected events with exactly two tracks with a vertex within 2 cm of the center of the TPC in the transverse plane, and within 2 m along the beams. A slightly acoplanarity of the track pairs was required to reject the remaining cosmic rays. The sum of the transverse momentum of the track pairs has a peak at low p_T, which shows that they are coming from coherent collisions, see Fig. 43. The invariant mass spectra of the $\pi^+\pi^-$-pairs in events selected by both kind of triggers shows a peak around the ρ^0 mass.

The STAR collaboration was the first one who studied experimentally the coherent interaction of heavy ions. In 2001, STAR has upgraded the detectors and the trigger, which will allow to increase the data taken by several orders of magnitude. Also it allows to study other reactions in coherent heavy ion interactions.

8.4 Perspectives of ion experiments

As was discussed before, $\gamma\gamma$ processes have been studied thoroughly at e^+e^--experiments up to the $\gamma\gamma$-invariant masses of about 3 GeV. Recently the B-factory at KEK, the e^+e^--collider KEKB started operating, and a few papers have already appeared concerning the detection of $\gamma\gamma$-processes in the experiment BELLE at KEKB. These recent reports have attracted some attention of the physics community towards KEKB as a new facility to study two-photon physics. Actually KEKB provides an "*unprecedented luminosity*" [347] of 4.49×10^{33} cm^{-2}s^{-1}. Thus the $\gamma\gamma$-luminosity achieved at KEKB is several orders of magnitude higher than that at RHIC in the whole range of $\gamma\gamma$ invariant masses possible in both colliders. So far the BELLE collaboration has reported only on a few measurements of $\gamma\gamma$ processes [334,348], based on the first run stored in 2000, but one expects that a lot of high-statistics results will appear from BELLE soon and the low-mass $\gamma\gamma$-physics will be exhausted there on the level of femtobarn cross sections. However the physics domain of photon-Pomeron and Pomeron-Pomeron processes at RHIC is out of the competition with any lepton collider.

For the experiments at LHC, the possibilities to study very peripheral ion collisions are currently discussed by the CMS and ALICE collaborations. The effective $\gamma\gamma$-luminosity at LHC is large enough due to the high collision energy. In addition the $\gamma\gamma$ mass range, that can be achieved in ion collisions there, allows to study $\gamma\gamma$ processes well beyond the mass range studied at LEP, see Fig. 6.

CMS considers an extensive heavy ion program, which includes also the physics of very peripheral ion collisions [22,349]. This program is quite attractive, especially as CMS provides a detector with a rather wide aperture and allowing thus to study various $\gamma\gamma$-reactions. The physics of very peripheral ion collisions at ALICE has been discussed in a number of papers, see [350,55,351]. Although ALICE is a quite promising setup for studies of this kind of physics a trigger configuration for very peripheral events has not been developed up to now. Nevertheless some possible options were proposed, see, i.e., [352], and problem is still under discussion.

9 Conclusion

In this report we describe the basic properties of very peripheral ion-ion collisions. Due to the very strong electromagnetic fields of short duration, new possibilities for interesting physics arise. The study of these electromagnetic processes, that is, photon-photon and photon-ion collisions is an interesting option, complementing the program for central collisions. It is the study of events characterized by relatively small multiplicities and a small background (especially when compared with the central collisions). These are good conditions to search for new physics. The method of equivalent photons is a well established tool to describe these kinds of reactions. Reliable results of quasi-real photon fluxes and $\gamma\gamma$-luminosities are available. Unlike electrons and positrons heavy ions and protons are particles with an internal structure. Effects arising from this structure are well under control and minor uncertainties coming from the exclusion of central collisions and triggering can be eliminated by using a luminosity monitor from μ– or e–pairs.

The high photon fluxes open up possibilities for photon-photon as well as photon-nucleus interaction studies up to energies hitherto unexplored at the forthcoming colliders RHIC and LHC. Heavy ion colliders are a unique tool to study (quasi-real) photon-nucleus collisions in a hitherto inaccessible energy range. First experimental results at RHIC on coherent ρ production on Au nuclei are forthcoming, as well as, pion- and electron-pair production in very peripheral collisions. A wealth of new data is to be expected. Interesting physics can be explored at the high invariant $\gamma\gamma$-masses, where detecting new particles could be within range. Also very interesting studies within the standard model, i.e., mainly QCD studies will be possible. This ranges from the study of the total $\gamma\gamma$-cross section into hadronic final states up to invariant masses of about 100 GeV to the spectroscopy of light and heavy mesons. The production via photon-photon fusion complements the production from single timelike photons in e^+–e^- collider and also in hadronic collisions via other partonic processes.

A good trigger for very peripheral collisions is essential in order to select photon-photon events. As it was shown in this report, such a trigger will be possible based on the survival of the nuclei after the collision and the use of the small transverse momenta of the produced system. A problem, which is difficult to judge quantitatively at the moment, is the influence of strong interactions in grazing collisions, i.e., effects arising from the nuclear stratosphere and Pomeron interactions. With the pioneering experiments of the (Ultra)Peripheral Collisions Group at STAR at RHIC this field has definitely left the area of theoretical speculations and entered the area to be experimental feasible.

Very peripheral collisions with Photon-Pomeron and Pomeron-Pomeron interactions, that is, diffractive processes are an additional interesting option. They use essentially the same triggering conditions and therefore one should be able to record them at the same time as photon-photon events.

This review is written in a time of rapid progress, both from an experimental and theoretical point of view. A few theorists are studying various aspects of very peripheral collisions, many study the field of γ-hadron processes with, e.g., the interactions of vector mesons in the nuclear medium and the vast field of $\gamma\gamma$ collisions ranging from QCD studies to possible new physics. On the experimental side, experiments on very peripheral collisions are presently performed and analyzed at RHIC. With these experiments the field has left the area of purely theoretical ideas and entered into the reality of experiments. The first heavy ion beams are expected at LHC in 2007 and experiments are in a construction stage. Certainly, the experience at RHIC will help to plan (even) better for LHC. The future is coming and one thing is clear: with all the new forthcoming experimental results the next review of the field of very peripheral collisions will be very different from this one.

9.1 Acknowledgments

We are grateful to very many people for their collaboration, their discussions, encouragements and suggestions at various stages on the present subject. We thank them all. We especially wish to thank N.N. Achasov,A. Alscher, A. Aste, M. Bedjidian, C.A. Bertulani, D. Brand, D. Denegri, O. Drapier, V.V. Ezhela I.F. Ginzburg, S. Datz, K. Eggert, R. Engel, M. Greiner, Z. Halabuka, D. Haas, B. Jeanneret, S.R. Klein, H. Meier, N.N. Nikolaev, J. Norbury, J. Nystrand, A.P.Samokhin, L.I. Sarycheva, V. Serbo, W. Scheid, Ch. Scheidenberger, R. Schuch, G.N. Shestakov, G. Soff, S. White, U. Wiedemann, and P. Yepes.

References

[1] Proceedings of the Quark Matter QM2001, Brookhaven, January 2001, available from `http://www.rhic.bnl.gov/qm2001/`.

[2] A. Angelis *et al.*, J. Phys. G **23**, 2069 (1997).

[3] A. A. Anselm, Phys. Lett. B **217**, 169 (1989).

[4] J. D. Bjorken, Acta Phys. Polon. **B28**, 2773 (1997).

[5] E. Fermi, Z. Phys. **29**, 315 (1924).*

[6] C. A. Bertulani and G. Baur, Physics Today, March, 22 (1994).

[7] J. D. Jackson, *Classical Electrodynamics* (John Wiley, New York, 1975).*

[8] A. Krasnitz and R. Venugopalan, Small x physics and the initial conditions in heavy ion collisions, e-print hep-ph/0104168, 2001.

[9] S. Klein and E. Scannapieco, in *Photon '97, Egmond aan Zee*, edited by (World Scientific, Singapore, 1997), p. 369, e-print hep-ph/9706358.

[10] C. A. Bertulani and G. Baur, Phys. Rep. **163**, 299 (1988).***

[11] G. Baur and H. Rebel, Topical Review, J. Phys. G **20**, 1 (1994).

[12] G. Baur and H. Rebel, Annu. Rev. Nucl. Part. Sci. **46**, 321 (1996).

[13] H. Primakoff, Phys. Rev. **31**, 899 (1951).*

[14] R. Moshammer *et al.*, Phys. Rev. Lett. **79**, 3621 (1997).

[15] G. Baur, K. Hencken, and D. Trautmann, Topical Review, J. Phys. G **24**, 1657 (1998).***

[16] F. Krauss, M. Greiner, and G. Soff, Prog. Part. Nucl. Phys. **39**, 503 (1997).***

[17] G. Baur, K. Hencken, and D. Trautmann, in *Proceedings of the Lund workshop on photon interactions and the photon structure, Lund, September 10-13, 1998*, edited by G. Jarlskog and T. Sjostrand (Dep. of Physics and Theoret. Physics, Lund University, Lund, Sweden, 1998).

[18] K. Hencken, P. Stagnoli, D. Trautmann, and G. Baur, Nucl. Phys. B **82**, 409 (2000).

[19] S. Klein and J. Nystrand, Phys. Rev. C **60**, 014903 (1999).***

[20] S. R. Klein, Nonlinear QED Effects in Heavy Ion Collisions, LBNL-47144, e-print physics/0012021, Talk presented at the 18th Advanced ICFA Beam Dynamics Workshop on Quantum Aspects of Beam Physics, October 15-20, 2000, Capri, Italy, 2000.*

[21] R. Engel *et al.*, Z. Phys. C **74**, 687 (1997).*

[22] G. Baur *et al.*, Photon-Photon Physics with heavy ions at CMS, CMS Note 1998/009, available from the CMS information server at http://cmsserver.cern.ch, 1998.

[23] G. Baur *et al.*, Coherent Interactions with heavy ions at CMS, e-print hep-ph/9904361, 1999.*

[24] K. Eggert *et al.*, FELIX Letter of Intent, CERN/LHCC 97–45, LHCC/I10, to appear in J. Phys. G, 1997.***

[25] L. D. Landau and E. M. Lifshitz, Phys. Z. Sowjet. **6**, 244 (1934).*

[26] G. Racah, Nuovo Cim. **14**, 93 (1937).*

[27] G. Baur and C. A. Bertulani, Z. Phys. A **330**, 77 (1988).**

[28] M. Grabiak, B. Müller, W. Greiner, and P. Koch, J. Phys. G **15**, L25 (1989).**

[29] E. Papageorgiu, Phys. Rev. D **40**, 92 (1989).**

[30] G. Baur, in *CBPF Int. Workshop on relativistic aspects of nuclear physics, Rio de Janeiro, Brazil 1989*, edited by T. Kodama *et al.* (World Scientific, Singapore, 1990), p. 127.

[31] G. Baur and L. G. Ferreira Filho, Nucl. Phys. A **518**, 786 (1990).**

[32] N. Cahn and J. D. Jackson, Phys. Rev. D **42**, 3690 (1990).**

[33] F. Vannucci, in $\gamma\gamma$ *Collisions, Proceedings, Amiens 1980*, Vol. 134 of *Lecture Notes in Physics*, edited by G. Cochard (Springer-Verlag, Heidelberg, Berlin, New York, 1980), p. 238.

[34] I. F. Ginzburg and A. Schiller, Phys. Rev. D **57**, R6599 (1998).

[35] A. G. Shamov and V. I. Telnov, talk by A. Maslennikov, in *Proceedings of the Lund workshop on photon interactions and the photon structure, Lund, September 10-13, 1998*, edited by G. Jarlskog and T. Sjostrand (Dep. of Physics and Theoret. Physics, Lund University, Lund, Sweden, 1998).

[36] A. D. Martin, First Workshop on Forward Physics and Luminosity Determination at the LHC, IPPP/01/13, e-print hep-ph/0103296, 2001.

[37] K. Alder *et al.*, Rev. Mod. Phys. **28**, 432 (1956).

[38] *Coulomb Excitation*, *Perspectives in Physics*, edited by K. Alder and A. Winther (Academic Press, New York, London, 1966).

[39] K. Alder and A. Winther, *Electromagnetic excitation* (North-Holland, Amsterdam, 1975).

[40] A. Winther and K. Alder, Nucl. Phys. A **319**, 518 (1979).

[41] G. Baur and C. A. Bertulani, Nucl. Phys. A **505**, 835 (1989).**

[42] C. Hofmann, G. Soff, A. Schäfer, and W. Greiner, Phys. Lett. B **262**, 210 (1991).**

[43] N. Baron and G. Baur, Phys. Rev. C **48**, 1999 (1993).

[44] M. Greiner *et al.*, Phys. Rev. C **51**, 911 (1995).

[45] S. R. Klein, J. Nystrand, and R. Vogt, Eur. Phys. J. C **21**, 583 (2001).*

[46] S. Klein and E. Scannapieco, Coherent Photons and Pomerons in Heavy Ion Collisions, presented at 6th Conference on the Intersections of Particle and Nuclear Physics, May 1997, Big Sky, Montana, STAR Note 298, LBNL-40495, e-print nucl-th/9707008, 1997.

[47] S. Klein and E. Scannapieco, STAR Note 243, 1995.

[48] S. Klein, in *Photon '95, Sheffield*, edited by D. J. Miller, S. L. Cartwright, and V. Khoze (World Scientific, Singapore, 1995), p. 417.

[49] J. Nystrand and S. Klein, Talk presented at Workshop on Photon Interactions and the Photon Structure, Lund, Sweden, 10-13 Sep 1998. In Lund 1998, Photon interactions and the photon structure, 263-277; LBNL-42524 1998, e-print nucl-th/9811007, 1998.**

[50] S. Klein and the STAR collaboration, Observation of $Au+Au \to Au+Au+\rho^0$ and $Au + Au \to Au^* + Au^* + \rho^0$ with STAR, LBNL-47723, e-print nucl-ex/0104016, 2001.***

[51] F. Meissner, Contribution to the Schlechting Conference, 2001.

[52] S. R. Klein, Coherent Photonuclear Interactions at RHIC: Theory and Experiment, Talk at the RHIC Winter Workshop, 7-9 January 1999, LBNL, Berkeley, USA, 1999.

[53] S. J. Brodsky, Novel Peripheral Processes at RHIC, talk at the RHIC Winter Workshop, 7-9 January 1999, LBNL, Berkeley, USA, 1999.

[54] K. Hencken *et al.*, TPHIC, event generator of two photon interactions in heavy ion collisions, IHEP-96-38, 1996.

[55] S. Sadovsky, CERN-Note ALICE/92-07, 1993.*

[56] J. D. Bjorken, Nucl. Phys. B (Proc. Suppl.) **71**, 484 (1999).

[57] in *Proceedings of the Photon'99 conference, Freiburg, May 23–27, 1999*, edited by S. Söldner-Rembold (Nucl. Phys. (Proc. Suppl.) 82B, North-Holland, 2000).

[58] Proceedings of the Photon 2000 conference, Ambleside, England August 26–31, 2000, to be published in the AIP Conference Proceeding Series.

[59] V. M. Budnev, I. F. Ginzburg, G. V. Meledin, and V. G. Serbo, Phys. Rep. **15**, 181 (1975).***

[60] K. Hencken, D. Trautmann, and G. Baur, Z. Phys. C **68**, 473 (1995).*

[61] F. Halzen and A. D. Martin, *Quarks & Leptons* (John Wiley & Sons, New York, 1984).

[62] *Tables of Isotopes, 7th edition*, edited by C. M. Lederer and V. S. Shirley (Wiley, New York, 1978).

[63] C. Bertulani, Phys. Lett. B **319**, 421 (1993).

[64] B. Kniehl, Phys. Lett. B **254**, 267 (1991).

[65] J. M. Blatt and V. F. Weisskopf, *Theoretical Nuclear Physics* (Springer-Verlag, New York, 1979).

[66] J. D. Walecka, ANL-83-50, 1983.

[67] T. deForest and J. D. Walecka, Adv. Phys. **15**, 1 (1966).

[68] G. Chanfray, J. Delorme, M. Ericson, and A. Molinari, Nucl. Phys. A **556**, 439 (1993).

[69] Y.-S. Tsai, Rev. Mod. Phys. **46**, 815 (1974).

[70] E. J. Moniz *et al.*, Phys. Rev. Lett. **26**, 445 (1971).

[71] M. Drees, R. M. Godbole, N. Nowakowski, and S. D. Rindami, Phys. Rev. D **50**, 2335 (1994).*

[72] J. Ohnemus, T. F. Walsh, and P. M. Zerwas, Phys. Lett. B **328**, 369 (1994).*

[73] M. Drees, J. Ellis, and D. Zeppenfeld, Phys. Lett. B **223**, 454 (1989).*

[74] M. Drees and D. Zeppenfeld, Phys. Rev. D **39**, 2536 (1989).

[75] B. B. Levtchenko, Higgs Production and other Two-Photon Processes in eA Collisions at HERA Energies, SINP-96-71, e-print hep-ph/9608295.

[76] K. Piotrzkowski, Phys. Rev. D **63**, 071502 (2000).

[77] G. Baur and L. G. Ferreira Filho, Phys. Lett. B **254**, 30 (1991).

[78] N. Baron, Ph.D. thesis, Forschungszentrum Jülich, Institut für Kernphysik Jül-2846, 1994.

[79] K. Hencken, D. Trautmann, and G. Baur, Phys. Rev. A **49**, 1584 (1994).

[80] K. Hencken, D. Trautmann, and G. Baur, Phys. Rev. C **61**, 027901 (2000).

[81] B. Lenkeit for the CERES Collaboration, New results on low-mass lepton pair production in Pb-Au collisions at 158 GeV per nucleon, Paris conference?, 1998.

[82] G. Fäldt and R. Glauber, Phys. Rev. **42**, 395 (1990).

[83] C. J. Benesh, A. C. Hayes, and J. L. Friar, Phys. Rev. C **54**, 1404 (1996).

[84] G. Baur and C. Bertulani, Phys. Rev. C **56**, 581 (1997).

[85] C. J. Benesh, A. C. Hayes, and J. L. Friar, Phys. Rev. C **56**, 583 (1997).

[86] W. F. J. M. Th Rubehn and W. Trautmann, Phys. Rev. C **56**, 1165 (1997).

[87] G. Baur, Z. Phys. C **54**, 419 (1992).

[88] G. Baur and N. Baron, Nucl. Phys. A **561**, 628 (1993).

[89] M. Vidović, M. Greiner, C. Best, and G. Soff, Phys. Rev. C **47**, 2308 (1993).

[90] D. Brandt, K. Eggert, and A. Morsch, CERN AT/94-05(DI), 1994.

[91] Conceptual design of the Relativistic Heavy Ion Collider, BNL-52195, 1989.

[92] D. Brandt, Review of the LHC Ion Programme, LHC Project Report 450, 2000.

[93] A. Morsch, ALICE Internal Note ALICE-INT-2001-10, 2001.

[94] L. R. Evans, in *Particle Accelerator Conference, Washington, DC, USA, 17 - 20 May 1993* (IEEE, New York, 1993), p. 1983.

[95] H. Kolanoski and P. Zerwas, in *High Energy Electron-Positron Physics*, edited by A. Ali and P. Söding (World Scientific, Singapore, 1988).

[96] Ch. Berger and W. Wagner, Phys. Rep. **176C**, 1 (1987).

[97] *$\gamma\gamma$ Collisions, Proceedings, Amiens 1980*, Vol. 134 of *Lecture Notes in Physics*, edited by G. Cochard and P. Kessler (Springer, Berlin, 1980).

[98] D. O. Caldwell and H. P. Paar, *Proc. 9th International Workshop on Photon-Photon Collisions, San Diego (1992)* (World Scientific, Singapore, 1992).

[99] *Photon'95, Xth International Workshop on Gamma-Gamma Collisions and related Processes*, edited by D. J. Miller, S. L. Cartwright, and V. Khoze (World Scientific, Singapore, 1995).

[100] *Photon'97, XIth International Workshop on Gamma-Gamma Collisions and related Processes, Egmond aan Zee*, edited by A. Buijs (World Scientific, Singapore, 1997).

[101] L3 Collaboration, Total Cross Section in gamma gamma Collisions at LEP, CERN-EP/2001-012, L3 preprint 235, to appear in Phys. Lett. B (2001), 2001.

[102] G. Schuler and T. Sjöstrand, Z. Phys. C **73**, 677 (1997).

[103] M. Drees and K. Grassie, Z. Phys. C **28**, 451 (1985).

[104] G. Schuler, Z. Phys. C **68**, 607 (1995).

[105] M. Glück, E. Reya, and A. Vogt, Z. Phys. C **53**, 127 (1992).

[106] Particle Data Group, Eur. Phys. J. C **15**, 1 (2000).

[107] M. E. Peskin, Theoretical Summary Lecture for EPS HEP99, SLAC-PUB-8351, e-print hep-ph/0002041, 2000.

[108] L3 collaboration, Phys. Lett. B **408**, 450 (1997).*

[109] T. Barklow, SLAC-PUB-5364, 1990.

[110] S.J Brodsky, T. Kinoshita, and H. Terazawa, Phys. Rev. Lett. **25**, 972 (1970).

[111] V. M. Budnev, I. F. Ginzburg, G. V. Meledin, and V. G. Serbo, Phys. Lett. B **39**, 526 (1972).

[112] V. M. Budnev, I. F. Ginzburg, G. V. Meledin, and V. G. Serbo, Nucl. Phys. B **63**, 519 (1973).*

[113] M. Katuya, Phys. Lett. B **124**, 421 (1983).

[114] G. Tupper and M. A. Samuel, Phys. Rev. D **23**, 1933 (1981).

[115] V. N. Gribov and I. Y. Pomeranchuk, Phys. Rev. Lett. **8**, 343 (1962).

[116] V. N. Gribov and I. Y. Pomeranchuk, Phys. Rev. Lett. **8**, 412 (1962).

[117] H. Albrecht *et al.*, Phys. Lett. B **332**, 451 (1994).

[118] S. Söldner-Rembold, in *29th International Conference on High-Energy Physics, Vancouver, Canada, 23–29 July 1998*, edited by A. Astbury, D. A. Axen, and J. Robinson (World Scientific, Singapore, 1999), p. 914.

[119] H. Vogt, Nucl. Phys. B (Proc. Suppl.) **79**, 283 (1999).

[120] N. N. Achasov and G. N. Shestakov, Phys. Rev. D **52**, 6291 (1995).

[121] N. N. Achasov and G. N. Shestakov, Phys. Rev. D **60**, 117503 (1999).

[122] C. N. Yang, Phys. Rev. **77**, 242 (1948).*

[123] W. Kwong *et al.*, Phys. Rev. D **37**, 3210 (1988).

[124] Bodwin, Nucl. Phys. (Proc. Suppl.) **42**, 306 (1995).

[125] S. Cartwright *et al.*, J. Phys. G **24**, 457 (1998).

[126] R. Godang *et al.*, Phys. Rev. Lett. **79**, 3829 (1997).

[127] N.N. Achasov and G.N. Shestakov, Sov. Phys. Usp. **34**, (No.6) 471 (1991).

[128] H. Albrecht *et al.*, Z. Phys., C **50** 1 (1991).

[129] F. Wilczek, Nature **404**, 452 (2000).

[130] V. Savinov and CLEO Collaboration, QCD Studies in Two-Photon Collisions at CLEO, Contribution W03 to the SLAC Workshop on e^+e^- Physics at Intermediate Energies, eConf C010430 (2001) W03, e-print hep-ex/0106013, 2001.

[131] V. Telnov, in *Photon '95, Sheffield*, edited by D. J. Miller, S. L. Cartwright, and V. Khoze (World Scientific, Singapore, 1995), p. 369.

[132] I. F. Ginzburg, in *Photon '95, Sheffield*, edited by D. J. Miller, S. L. Cartwright, and V. Khoze (World Scientific, Singapore, 1995), p. 399.

[133] I. Ginzburg, Nucl. Phys. (Proc. Suppl.) **82B**, 367 (2000), contribution to DIFFRACTION 2000.

[134] *Tesla Technical Design Report*, edited by F. Richard *et al.* (DESY, Hamburg, 2001), No. DESY 2001-011, ECFA 2001-209, TESLA Report 2001-23, TESLA-FEL 2001-05, ISBN 3-935702-05-1.

[135] M. Krawczyk, in *Future Physics at HERA*, edited by G. Ingelman, A. De Roeck, and R. Klanner (DESY, Hamburg, 1996), iFT 21/96, hep-ph/9609477.

[136] *Future Physics at HERA*, edited by G. Ingelman, A. De Roeck, and R. Klanner (DESY, Hamburg, 1996).

[137] H. E. Haber and G. L. Kane, Phys. Rep. **117**, 75 (1985).

[138] J. Feng and M. Strassler, Phys. Rev. D **51**, 4661 (1995).

[139] A. I. Achieser and W. B. Berestezki, *Quanten-Elektrodynamik* (Teubner-Verlag, Leipzig, 1962).

[140] B. Müller and A. J. Schramm, Phys. Rev. D **42**, 3699 (1990).

[141] E. Papageorgiu, Phys. Lett. B **352**, 394 (1995).

[142] J. Norbury, Phys. Rev. D **42**, 3696 (1990).

[143] S. M. Lietti, A. A. Natale, C. G. Roldão, and R. Rosenfeld, Phys. Lett. B **497**, 243 (2001).*

[144] D. Choudhury and M. Krawczyk, Phys. Rev. D **55**, 2774 (1997).

[145] G. S. M. Greiner, M. Vidovic, Phys. Rev. C **47**, 2288 (1993).

[146] P. Abrue *et al.*, Phys. Lett. B **499**, 23 (2001).

[147] P. Achard *et al.*, Preprint CERN-EP/2001-049.

[148] G. Abbiendi *et al.*, Phys. Lett. B **499**, 38 (2001).

[149] LEP working group for Higgs boson search, LHWG Note/2001-03, e-print hep-ex/0107029.

[150] N. Cabibbo *et al.*, Nucl. Phys. B **158**, 295 (1979).

[151] I. Y. Pomeranchuk, Yad.Fiz. **11**, 852 (1970).

[152] A. A. Logunov *et al.*, Theor. and Math. Phys. **36**, 147 (1978).

[153] M. Linder *et al.*, Phys. Lett. B **228**, 139 (1989).

[154] M. Sher, Phys. Lett. B **317**, 159 (1993).

[155] M. Sher, Phys. Lett. B **331**, 448 (1994).

[156] G. Altarelli *et al.*, Phys. Lett. B **337**, 141 (1994).

[157] J. A. Casas *et al.*, Phys. Lett. B **342**, 89 (1995).

[158] S. C. Ahern, J. W. Norbury, and W. J. Poyser, Phys. Rev. D **62**, 116001 (2000).

[159] B. Abbott, Phys. Rev. Lett. **81**, 524 (1998).

[160] F. M. Renard, Phys. Lett. B **126**, 59 (1983).

[161] U. Baur, H. Fritzsch, and H. Faissner, Phys. Lett. B **135**, 313 (1984).

[162] P. Jain, B. Pire, and J. P. Ralston, Phys. Rev. **271**, 67 (1996).

[163] H. Emling, Prog. Part. Nucl. Phys. **33**, 729 (1995).

[164] T. Aumann, P. F. Bortignon, and H. Emling, Annu. Rev. Nucl. Part. Sci. **48**, 351 (1998).

[165] C. A. Bertulani and V. Y. Ponomarev, Phys. Rep. **321**, 139 (1999).

[166] M. C. Abreu *et al.*, Phys. Rev. C **59**, 876 (1998).

[167] I. A. Pshenichnov *et al.*, Phys. Rev. C **64**, 024903 (2001).*

[168] S. Datz *et al.*, Phys. Rev. Lett. **79**, 3355 (1997).

[169] S. R. Klein, Nucl. Instrum. Methods **A459**, 51 (2001).**

[170] A. Baltz, C. Chasman, and S. N. White, Nucl. Instrum. Methods **417**, 1 (1998).*

[171] M. Vidović, M. Greiner, and G. Soff, Phys. Rev. C **48**, 2011 (1993).

[172] A. J. Baltz, M. J. Rhoades-Brown, and J. Weneser, Phys. Rev. E **54**, 4233 (1996).

[173] A. J. Baltz and M. Strikman, Phys. Rev. D **57**, 548 (1998).

[174] I. A. Pshenichnov *et al.*, Phys. Rev. C **57**, 1920 (1998).

[175] M. Gallio, in *CMS Heavy Ion Meeting in St. Petersburg*, edited by M. Bedjidian (PUBLISHER, ADDRESS, 2000), p. 329.

[176] M. Chiu *et al.*, Measurement of Mutual Coulomb Dissociation in $\sqrt{s_N N} = 130$ GeV Au+Au collisions at RHIC, e-print nucl-ex/0109018, 2001.

[177] C. Adler *et al.*, The RHIC Zero Degree Calorimeters, Nucl. Instrum. Methods **A461**, 337 (2001).

[178] G. Dellacasa *et al.*, ALICE TRD 3, Zero Degree Calorimeter CERN/LHCC 99-5, 1999.

[179] P. B. Price, R. Guaxiao, and W. T. Williams, Phys. Rev. Lett. **61**, 2193 (1988).

[180] B. Krusche *et al.*, Phys. Rev. Lett. **86**, 4764 (2001).

[181] S. D. Drell, Phys. Rev. Lett. **5**, 278 (1960).

[182] K. A. Chikin *et al.*, Inclusive meson production in peripheral collisions of ultrarelativistic heavy ions, nucl-th/0002028, 2000.

[183] K. S. Koelbig and B. Margolis, Nucl. Phys. B **6**, 85 (1968).

[184] J. A. Crittenden, *Exclusive production of neutral vector mesons at the electron-proton collider HERA*, Vol. 140 of *Springer tracts in modern physics* (Springer, Heidelberg, 1997).

[185] T. H. Bauer, R. D. Spital, D. R. Yennie, and F. M. Pipkin, Rev. Mod. Phys. **50**, 261 (1978).**

[186] A. Pautz and G. Shaw, Phys. Rev. C **57**, 2647 (1998).

[187] S. D. Drell and J. S. Refil, Phys. Rev. Lett. **16**, 552 (1966).

[188] S. Klein and J. Nystrand, Phys. Rev. Lett. **84**, 2330 (2000).*

[189] *The second DAΦNE Physics Handbook Vol. 1*, edited by L. Maiani, G. Pancheri, and N. Paver (SIS Ufficio Pubblicazioni, P.O. Box 13, I-00044 Frascati (Roma) Italy, 19XX).

[190] A. Donnachie, Presented at e+ e- Physics at Intermediate Energies, SLAC, Stanford, California, 30 Apr–2 May 2001; hep-ph/0106197, 2001.

[191] J.Huefner, B.Kopeliovich, and J.Nemchik, Phys. Lett. B **383**, 362 (1996).*

[192] J. Hüfner and M. C. Nemes, Phys. Rev. C **23**, 2538 (1981).

[193] K. Ackerstaff and HERMES Collaboration, Phys. Rev. Lett. **82**, 3025 (1999).

[194] T. Renk, G. Piller, and W. Weise, Nucl. Phys. A **689**, 869 (2001).*

[195] S.Frixione, M.L.Manango, and P. Nason, Phys. Lett. B **308**, 137 (1993).

[196] K. Daum, Nucl. Phys. (Proc. Suppl.) **82B**, 212 (2000), contribution to Photon 1999.

[197] D. Hochman, Talk given at PHOTON 2000: International Workshop on Structure and Interactions of the Photon, Ambleside, Lake District, England, 26-031 Aug 2000; hep-ex/0010050, 2000.

[198] S. Frixione, M. Caccaiari, and P. Nason, hep-ph/0107063, 2001.

[199] S. M. Schneider, W. Greiner, and G. Soff, Phys. Rev. D **46**, 2930 (1992).*

[200] J. Breitweg *et al.*, Phys. Lett. B **481**, 213 (2000).

[201] M. Arneodo, Phys. Rep. **240**, 301 (1994).

[202] K. J. Eskola, V. J. Kolhinen, and P. V. Ruuskanen, Nucl. Phys. B **535**, 351 (1998).

[203] K. J. Eskola, V. J. Kolhinen, and P. V. Ruuskanen, Eur. Phys. J. C **9**, 61 (1999).

[204] F.Gelis and A.Peshier, Probing colored glass via $q\bar{q}$ photoproduction. hep-ph/0107142 v2, 2001.

[205] H. Abramowicz, Nucl. Phys. (Proc. Suppl.) **99A**, 79 (2001), contribution to DIFFRACTION 2000.

[206] N. Cartiglia, Diffraction at HERA, e-print hep-ph/9703245, 1997.

[207] A. Levy, Low-x Physics at HERA, Bantz Lectures, DESY Preprint 97-013, 1993.

[208] PP2PP Collaboration, Roman Pot Detectors for Small Angle *pp* Scattering, Technical Design Report, available from http://www.rhic.bnl.gov/pp2pp/, 1998.

[209] K. Goulianos for the CDF Collaboration, Diffraction in CDF: Run I results and plans for Run II, e-print hep-ex/0107069, 2001, contribution to DIS2001.

[210] T. Affolder for the CDF Collaboration, Double Diffraction Dissociation at the Fermilab Tevatron Collider, Phys. Rev. Lett. **87**, 141802 (2001).

[211] A. Santoro, Nucl. Phys. (Proc. Suppl.) **99A**, 289 (2001), contribution to DIFFRACTION 2000, also available hep-ex/0011023.

[212] G. Baum *et al.*, COMPASS : a proposal for a common muon and proton apparatus for structure and spectroscopy. CERN-SPSLC-96-14; SPSLC-P-297, 1996.

[213] W. Kienzle *et al.*, Total Cross Section, Elastic Scatterinf and Diffraction Dissociation at the LHC. TOTEM Technical Proposal, CERN/LHCC 99-7, LHCC/P5, 1999.

[214] PP2PP Collaboration, Roman Pot Detectors for Small Angle *pp* Scattering, Technical Design Report, http://www.rhic.bnl.gov/pp2pp/, 1998.

[215] V. Cavasinni *et al.*, Z. Phys. C **28**, 487 (1985).

[216] J. D. Bjorken, Int. J. Mod. Physics **A7**, 4189 (1992).

[217] J. D. Bjorken, Phys. Rev. D **47**, 101 (1993).

[218] A. Donnachie and P. V. Landshoff, Phys. Lett. B **207**, 319 (1988).

[219] A. Donnachie and P. V. Landshoff, Phys. Lett. B **303**, 634 (1988).

[220] A. Donnachie and P. V. Landshoff, Nucl. Phys. B **311**, 509 (1988/89).

[221] P. V. Landshoff, Pomerons, e-print hep-ph/0108156, 2001.

[222] B. Müller and A. J. Schramm, Nucl. Phys. A **523**, 677 (1991).

[223] A. Schäfer, O. Nachtmann, and R. Schöpf, Phys. Lett. B **249**, 331 (1990).

[224] A. J. Schramm and D. H. Reeves, Phys. Rev. D **55**, 7312 (1997).

[225] A. Capella, U. Sukhatme, C. Tan, and J. Tran Thanh Van, Phys. Rep. **236**, 225 (1994).

[226] R. Engel, private communication.

[227] C. G. Roldão and A. A. Natale, Phys. Rev. C **61**, 064907 (2000).*

[228] S. U. Chung, D. P. Weygand, and H. J. Willutzki, Preprint BNL-46863, 1991.

[229] S. A. Chatrchyan and P. I. Zarubin, in *Second CMS Heavy Ion Workshop, Dubna, Russia* (PUBLISHER, ADDRESS, 1997), Vol. CMS Document 97-011, p. 257.

[230] G. Alberi and G. Goggi, Phys. Rep. **74**, 1 (1981).

[231] C. Bottcher and M. R. Strayer, Phys. Rev. D **39**, 1330 (1989).

[232] K. Momberger, N. Grün, and W. Scheid, Z. Phys. D **18**, 133 (1991).

[233] K. Rumrich, G. Soff, and W. Greiner, Phys. Rev. A **47**, 215 (1993).

[234] A. Alscher, K. Hencken, D. Trautmann, and G. Baur, Phys. Rev. A **55**, 396 (1997).

[235] J. Eichler, Phys. Rep. **193**, 165 (1990).

[236] J. Eichler and W. E. Meyerhof, *Relativistic Atomic Collisions* (Academic Press, San Diego, 1995).**

[237] R. N. Lee and A. I. Milstein, Phys. Rev. A **61**, 032103 (2000).

[238] R. N. Lee, A. I. Milstein, and V. G. Serbo, Structure of the Coulomb and unitarity corrections to the cross section of e^+e^- pair production in ultra-relativistic nuclear collisions, e-print hep-ph/0108014, 2001.*

[239] K. Hencken, D. Trautmann, and G. Baur, Phys. Rev. A **51**, 1874 (1995).

[240] M. C. Güçlü *et al.*, Phys. Rev. A **51**, 1836 (1995).

[241] W. Heitler, *The Quantum Theory of Radiation* (Oxford University Press, London, 1954).

[242] G. Baur, Phys. Rev. A **42**, 5736 (1990).**

[243] G. Baur, Phys. Rev. D **41**, 3535 (1990).

[244] M. J. Rhoades-Brown and J. Weneser, Phys. Rev. A **44**, 330 (1991).

[245] C. Best, W. Greiner, and G. Soff, Phys. Rev. A **46**, 261 (1992).

[246] V. G. Serbo, JETP Lett. **12**, 39 (1970).

[247] L. N. Lipatov and G. V. Drolov, Sov. J. Nucl. Phys. **13**, 333 (1971).

[248] K. Hencken, D. Trautmann, and G. Baur, Phys. Rev. A **51**, 998 (1995).**

[249] A. Baltz, F. Gelis, L. McLerran, and A. Peshier, Nucl. Phys. A **695**, 395 (2001).

[250] K. Hencken, Electromagnetic Production of Electron Positron Pairs in Relativistic Heavy Ion Collisions, Ph. D. thesis, U Basel, Institut für Physik, available from http://quasar.physik.unibas.ch/∼hencken/Preprints/, 1994.

[251] C. R. Vane *et al.*, Phys. Rev. A **56**, 3682 (1997).

[252] K. Momberger, A. Belkacem, and A. H. Sørensen, Europhys. Lett. **32**, 401 (1995).

[253] J. Thiel, J. Hoffstadt, N. Grün, and W. Scheid, Z. Phys. D **34**, 21 (1995).

[254] D. Y. Ivanov, A. Schiller, and V. G. Servo, Phys. Lett. B **454**, 155 (1999).

[255] D. Ivanov and K. Melnikov, Phys. Rev. D **57**, 4025 (1998).

[256] H. A. Bethe and L. C. Maximon, Phys. Rev. **93**, 768 (1954).

[257] H. Davies, H. A. Bethe, and L. C. Maximon, Phys. Rev. **93**, 788 (1954).

[258] L. D. Landau and E. M. Lifschitz, *Quantenelektrodynamik*, No. IV in *Lehrbuch der theoretischen Physik* (Akademie Verlag, Berlin, 1986).

[259] A. Baltz, Phys. Rev. Lett. **78**, 1231 (1997).

[260] B. Segev and J. C. Wells, Phys. Rev. A **57**, 1849 (1998).

[261] A. J. Baltz and L. McLerran, Phys. Rev. C **58**, 1679 (1998).

[262] B. Segev and J. C. Wells, Phys. Rev. C **59**, 2753 (1999).

[263] U. Eichmann, J. Reinhardt, S. Schramm, and W. Greiner, Phys. Rev. A **59**, 1223 (1999).

[264] K. Hencken, D. Trautmann, and G. Baur, Phys. Rev. C **59**, 841 (1999).

[265] M. C. Güçlü, Phys. Rev. C **63**, 049802 (2000).

[266] U. Eichmann, J. Reinhardt, and W. Greiner, Phys. Rev. A **61**, 062710 (2000).

[267] R. Blankenbecler and S.D. Drell, Phys. Rev. D **36**, 2846 (1987).

[268] R. N. Lee and A. I. Milstein, Coulomb corrections and multiple e+e- pair production in ultra-relativistic nuclear collisions, e-print hep-ph/0103212, Phys. Rev. A in press, 2001.

[269] R. P. Feynman, Phys. Rev. **76**, 749 (1949).

[270] J. Schwinger, Phys. Rev. **93**, 615 (1954).

[271] C. Itzykson and J.-B. Zuber, *Quantum Field Theory* (McGraw-Hill, Singapore, 1980).

[272] I. Bialynicki-Birula and Z. Bialynicki-Birula, *Quantum Electrodynamics* (Pergamon, ADDRESS, 1975).

[273] S. Klein, Ultra-peripheral collisions of relativistic heavy ions, Presented at INPC, July 30–August 3, 2001, Berkeley. e-print nucl-ex/0108018., 2001.

[274] G. Baur and N. Baron, Z. Phys. C **60**, 95 (1993).

[275] G. Baur, Nucl. Phys. A **538**, 187c (1992).

[276] R. Baur *et al.*, Phys. Lett. B **332**, 471 (1994).

[277] M. Chen and P. Zerwas, Phys. Rev. D **12**, 187 (1975).*

[278] V. N. Baier, V. S. Fadin, and V. H. Khoze, Nucl. Phys. B **65**, 381 (1973).

[279] S. D. Drell and J. D. Walecka, Ann. Phys. **28**, 18 (1964).

[280] R. M. Barnett *et al.*, Phys. Rev. D **54**, 1 (1996).

[281] V. L. Korotkikh and K. A. Chikin, γ-radiation of excited nuclear discrete levels in peripheral heavy ion collisions, INPH MSU 2001-1/641, e-print nucl-th/0103018, 2001.

[282] H. Meier *et al.*, Eur. Phys. J. C **2**, 741 (1998).

[283] V. S. Fadin and V. A. Khoze, Sov. Phys.-JETP **17**, 313 (1973).

[284] S. Weinberg, *The Quantum Theory of Fields* (Cambridge University Press, Cambridge, 1997), Vol. 1.

[285] K. Hencken, D. Trautmann, and G. Baur, Phys. Rev. C **60**, 34901 (1999).

[286] CMS Collaboration, CMS, the Electromagnetic Calorimeter Project: technical design report, CERN-LHCC-97-033, 1997.

[287] J. B. Jeanneret, Electron capture in Pb-Pb collisions and quench limit, Beam Physics Note 41, 2000.*

[288] C. T. Munger, S. J. Brodsky, and I. Schmidt, Phys. Rev. D **49**, 3228 (1994).

[289] L. L. Nemenov, Sov. J. Nucl. Phys. **41**, 629 (1985).

[290] H. Meier *et al.*, Phys. Rev. A **63**, 032713 (2001).*

[291] H. Meier *et al.*, Eur. Phys. J. C **5**, 287 (1998).

[292] H. A. Bethe and E. E. Salpeter, *Quantum Mechanics of One- and Two-Electron Atoms* (Springer Verlag, Berlin, 1957).

[293] A. J. Baltz, M. J. Rhoades-Brown, and J. Weneser, Phys. Rev. A **44**, 5569 (1991).

[294] A. J. Baltz, M. J. Rhoades-Brown, and J. Weneser, Phys. Rev. A **48**, 2002 (1993).

[295] U. Becker, N. Grün, and W. Scheid, J. Phys. B **20**, 2075 (1987).

[296] A. Aste, K. Hencken, D. Trautmann, and G. Baur, Phys. Rev. A **50**, 3980 (1994).

[297] C. K. Agger and A. H. Sørensen, Phys. Rev. A **55**, 402 (1997).

[298] M. J. Rhoades-Brown, C. Bottcher, and M. R. Strayer, Phys. Rev. A **40**, 2831 (1989).

[299] C. Bertulani and D. Dolci, Nucl. Phys. A **683**, 635 (2001).

[300] A. Belkacem *et al.*, Phys. Rev. Lett. **71**, 1514 (1993).

[301] A. Belkacem *et al.*, Phys. Rev. Lett. **73**, 2432 (1994).

[302] A. Belkacem *et al.*, Phys. Rev. A **56**, 2806 (1997).

[303] N. Claytor *et al.*, Phys. Rev. A **55**, R842 (1997).

[304] A. Belkacem *et al.*, Phys. Rev. A **58**, 1253 (1998).

[305] A. B. Voitkiv, N. Grün, and W. Scheid, Phys. Lett. A **269**, 325 (2000).

[306] A. H. Sørensen, Phys. Rev. A **58**, 2895 (1998).

[307] R. Anholt and U. Becker, Phys. Rev. A **36**, 4628 (1987).

[308] H. F. Krause *et al.*, Phys. Rev. Lett. **80**, 1190 (1998).

[309] H. F. Krause *et al.*, Phys. Rev. A **63**, 032711 (2001).

[310] G. Baur *et al.*, Phys. Lett. B **368**, 251 (1996).

[311] G. Blanford *et al.*, Phys. Rev. Lett. **80**, 3037 (1998).

[312] C. A. Bertulani and G. Baur, Phys. Rev. D **58**, 034005 (1998).

[313] G. Baur, in *Perspectives on Photon Interactions with Hadrons and Nuclei*, *Lecture Notes in Physics*, edited by M. Schumacher and G. Tamas (Springer Verlag, Berlin, Heidelberg, New York, 1990), p. 111.

[314] I. F. Ginzburg, private communication.

[315] G. L. Kotkin, E. A. Kuraev, A. Schiller, and V. G. Serbo, Phys. Rev. C **59**, 2734 (1999).*

[316] C. Bertulani and F. Navarra, 3photon production of Vector Mesons, e-print nucl-th/0107035, 2001.

[317] I. F. Ginzburg, Phys. Rev. C **58**, 3565 (1998).

[318] S. R. Gevorkyan *et al.*, Phys. Rev. A **58**, 4556 (1998).

[319] A. Karshenboim *et al.*, Phys. Lett. B **424**, 397 (1998).

[320] U. Jentschura *et al.*, Phys. Rev. A **56**, 4483 (1997).

[321] A. Karshenboim *et al.*, Sov. Phys.-JETP **86**, 226 (1998).

[322] L. Nemenov *et al.*, Sov. J. Nucl. Phys. **15**, 582 (1972).

[323] J. Malenfant, Phys. Rev. D **36**, 863 (1987).

[324] S. Bilen'kii *et al.*, Sov. J. Nucl. Phys. **10**, 469 (1969).

[325] G. A. Kozlov, Phys.At Nucl. **48**, 167 (1988).

[326] P. J. Mohr, in *Atomic, Molecular and Optical Physics Handbook.*, edited by G. W. F. Drake (AIP, Woodbury, NY, 1996).

[327] M. G. Boshier *et al.*, Comm. At. Mol. Phys. **33**, 17 (1996).

[328] I. F. Ginzburg *et al.*, Phys. Rev. C **58**, 3565 (1998).

[329] T. Sjöstrand, Computer Phys. Commun. **82**, 74 (1994).

[330] X. N. Wang and M. Gyulassy, HIJING 1.0: a Monte Carlo program for parton and particle production in high energy hadronic and nuclear collisions, Preprint LBL 34246; e-print nucl-th/9502021, 1995.

[331] S. Klein and J. Nystrand, STAR Note 347, 1998.**

[332] M. Acciarri *et al.*, Phys. Lett. **B501**, 1 (2001).

[333] M. Acciarri *et al.*, Phys. Lett. **B501**, 173 (2001).

[334] H.C.Huang, e-print hep-ex/0104024, To appear in the proceedings of 4th International Conference on B Physics and CP Violation (BCP 4), Ago Town, Mie Prefecture, Japan, 19-23 Feb 2001, 2001.

[335] R. Godang *et al.*, Phys. Rev. Lett. **79**, 3829 (1997).

[336] M. Acciarri *et al.*, Phys. Lett. **B514**, 19 (2001).

[337] M. Acciarri *et al.*, Phys. Lett. **B503**, 10 (2001).

[338] M. Acciarri *et al.*, Phys. Lett. **B467**, 137 (1999).

[339] A. Csilling, Charm and bottom production in two-photon collisions with OPAL, Talk given at PHOTON 2000: Ambleside, Lake District, England, 26-31 Aug 2000., 2000.

[340] G. Brandenburg *et al.*, Phys. Rev. Lett. **85**, 3095 (2000).

[341] B. I. Eisenstein, Experimental investigation of the two-photon widths of the χ_{c0} and the χ_{c2} mesons, CLNS 01-1732, 2001.

[342] M. Acciarri *et al.*, Phys. Lett. **B461**, 155 (1999).

[343] J. Nystrand and S. Klein, Two Photons Physics at RHIC: Separating Signals from Backgrounds, talk presented at "Hadron'97", Brookhaven National Laboratory, August 1997, STAR Note 315, LBNL-41111 Nov.97, e-print hep-e/9711021, 1997.

[344] H. Pi, Comp.Phys.Comm. **173**, 71 (1992).

[345] K. Werner, Phys. Rev. **87**, 232 (1993).

[346] R. Engel, J. Ranft, and S. Roesler, Phys. Rev. D **55**, 6957 (1997).

[347] CERN Courier, vol.41, No.7, p.6, 2001.

[348] S. Hou, Plenary talk at the conference HADRON2001, 25 August – 1 September 2001, Protvino, Russia., 2001.

[349] G. Baur *et al.*, CMS Note 2000-060, 2000.

[350] N. Ahmad *et al.*, Alice Technical Proposal, CERN/LHCC 95-71, 1995.

[351] S. A. Sadovsky, in *Proceedings of the 6th Intern. Conf. on Hadron Spectroscopy, Manchester, UK, 10-14 August 1995*, edited by M. C. Birse, G. D. Lafferty, and J. A. McGovern (World Scientific, Singapore, 1996), p. 289.

[352] V. Kolosov *et al.*, ALICE Internal Note 95-45, 1995.